Coordination Chemistry Reviews 557 (2026) 217691

Contents lists available at ScienceDirect

Coordination Chemistry Reviews

journal homepage: www.elsevier.com/locate/ccr

Luminescent metal-organic framework glasses: Challenges in quantum dot integration and rare earth doping

Xiaoqing Pei [a], Lingwei Zeng [b], Daqin Chen [a,c,*]

[a] College of Physics and Energy, Fujian Normal University, Fuzhou 350117, PR China
[b] School of Chemistry and Chemical Engineering, Key Laboratory of Theoretical Organic Chemistry and Functional Molecule of Ministry of Education, Hunan University of Science and Technology, Xiangtan, Hunan 411201, PR China
[c] Fujian Provincial Engineering Technology Research Center of Solar Energy Conversion and Energy Storage, Fujian Normal University, Fuzhou, Fujian 350117, PR China

ARTICLE INFO

Keywords:
MOF glasses
Luminescent materials
PeQDs
Rare-earth ions
Photonic devices

ABSTRACT

Metal–organic framework (MOF) glasses, recognized as the fourth class of inorganic–organic hybrid glasses, provide a versatile platform for developing functional materials due to their hybrid composition and tunable pore architectures. This review provides a comprehensive summary of recent advances in MOF glasses, with particular emphasis on their luminescent applications. The mechanism of glass formation, governed by the breaking and reformation of coordination bonds, as well as the critical role of ligand chemistry in determining the glass-forming ability (GFA), are discussed in detail. The advantages and limitations of key synthetic strategies (including melt-quenching, mechanochemical, and desolvation methods) are comparatively analyzed. The evolution from zeolitic imidazolate frameworks (ZIFs) to carboxylate-based systems is examined, highlighting the distinctive role of MOF glasses as hosts for stabilizing perovskite quantum dots (PeQDs) and enabling efficient luminescence. The review also identifies the opportunities and challenges in effectively incorporating rare-earth (RE) ions into MOF glasses, which remains a critical research gap to be addressed. The discussion is further extended to coordination polymer (CP) glasses, emphasizing their tunable and multimodal luminescent behaviors. Finally, the transformative potential of MOF/CP glasses for next-generation devices (such as flexible photonics, high-energy radiation detection, and intelligent optical sensing) is envisioned

1. Introduction

Luminescent materials play a pivotal role in modern optoelectronics, with widespread applications in light-emitting diodes (LEDs), organic LEDs (OLEDs), lasers, X-ray imaging, and optical sensors [1–4]. By converting electrical, radiative, or other forms of energy into visible or near-infrared (NIR) light [5], these materials have driven rapid advancements in display technology [6], lighting systems [7], optical communication [8], and medical imaging [9]. With the advent of the digital era and the proliferation of smart devices, the performance requirements for luminescent materials (such as high quantum efficiency [10], broad color gamut coverage [11], long-term stability [12], and environmental compatibility [13]) have become increasingly stringent [14]. However, conventional luminescent materials face significant bottlenecks that hinder their broader application. For instance, quantum dots (QDs) such as CdSe [15] and PbS [16], exhibit excellent quantum confinement effects and tunable emission wavelengths but contain heavy-metal elements (e.g., Cd, Pb), raising serious concerns about environmental toxicity and biosafety [17]. Their commercialization is restricted by stringent regulations, such as the EU REACH and RoHS directives [18]. Secondly, rare-earth (RE)-doped inorganic glasses (for example, Eu^{3+}- or Tb^{3+}-doped silicate systems) are well known for their high color purity and chemical stability but require high-temperature melting processes (typically above 1000 °C), leading to considerable energy consumption [19]. Moreover, the rigid structure of the glass host restricts flexibility in energy-level tuning, hindering molecular-level precision design [20]. Furthermore, traditional materials often exhibit poor stability. Exposure to high temperature, humidity, or light can lead to oxidation and aggregation of QDs, increasing nonradiative recombination and reducing their photoluminescence quantum yield (PLQY) [17,21–28]. RE-doped glasses are also prone to efficiency fluctuations induced by defect traps [29]. These limitations not only increase material costs but also constrain their potential in flexible electronics, wearable devices, and biocompatible applications [30]. For example, in

* Corresponding author at: College of Physics and Energy, Fujian Normal University, Fuzhou 350117, PR China.
E-mail address: dqchen@fjnu.edu.cn (D. Chen).

https://doi.org/10.1016/j.ccr.2026.217691
Received 8 December 2025; Accepted 6 February 2026
Available online 16 February 2026

X-ray imaging, conventional scintillators such as CsI: Tl, despite their high resolution, exhibit poor radiation hardness and degradation under high-dose irradiation [31]. In LED lighting, the thermal quenching of conventional phosphors leads to color shifts and reduced operational lifetimes [32]. Overall, these challenges arise from the intrinsic structural rigidity and compositional limitations of conventional materials, which hinder their ability to meet the requirements of multifunctional integration and sustainable development [33].

To address these bottlenecks in traditional luminescent materials, researchers have explored novel material systems, among which metal–organic frameworks (MOFs) and their derivative form (MOF glasses) have emerged as key focal points [34]. Coordination polymers (CPs), a broader class that encompasses MOFs, inherently possess the potential to transform from crystalline to amorphous states owing to their coordination-driven network structures [35]. In 2007, Yaghi and co-workers systematically reviewed the design and synthesis of MOFs, which significantly accelerated progress in this research field [36]. MOFs are constructed through the self-assembly of metal ions or clusters

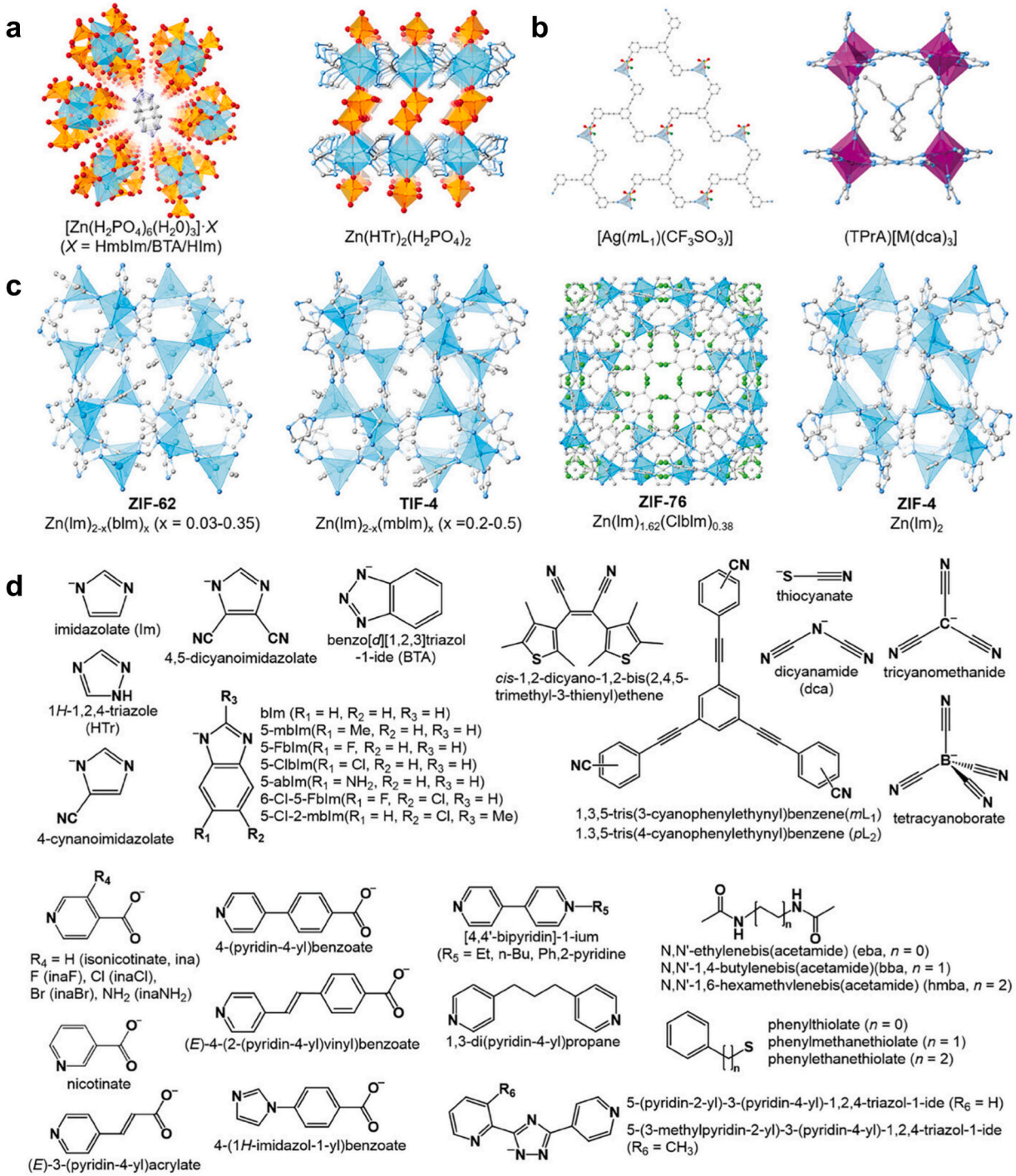

Fig. 1. Key structural components and ligands for constructing MOFs/CPs. Crystal structures of a) 2D $[Zn(H_2PO_4)_6(H_2O)_3]\cdot X$ and $[Zn(1,2,4\text{-triazole})_2(H_2PO_4)_2]$, b) 2D $[Ag(mL_1)(CF_3SO_3)]$ and 3D $[Co(bba)_3](CoCl_4)$, c) 3D $[Zn(imidazolate)_{1.75}(benzimidazolate)_{0.25}]$ (ZIF-62), $[Zn(imidazolate)_{1.5}(methylbenzimidazolate)_{0.5}]$ (TIF-4), $[Zn(imidazolate)_{1.62}$ $(chlorobenzimidazolate)_{0.38}]$ (ZIF-76), $[Zn(imidazolate)_2]$ (ZIF-4). d) Several organic/inorganic ligands used to produce MOF/CP glasses. Reproduced with permission [34]. Copyright 2022, The Authors. Published by American Chemical Society.

(e.g., Zn^{2+}, Zr^{4+}) with organic ligands (e.g., carboxylates, imidazolates) via coordination bonds, resulting in periodic three-dimensional frameworks with precisely tunable pore sizes at the nanoscale and specific surface areas exceeding 3000 m^2/g [37]. This structural tunability allows for the precise incorporation of luminescent centers via ligand functionalization or metal-node substitution, thereby overcoming issues such as heavy-metal toxicity and the limited tunability of energy levels inherent to traditional materials [38]. For instance, MOFs can facilitate efficient energy transfer through mechanisms such as ligand-to-metal charge transfer (LMCT) and metal-to-ligand charge transfer (MLCT), thereby enhancing PLQY, while the inherent flexibility of organic ligands provides superior environmental adaptability [39]. However, the brittleness and processing challenges of crystalline MOFs (such as difficulties in fabricating thin films or fibers) greatly limit their practical applications [40]. To overcome these limitations, MOF glasses were developed through melt-quenching techniques [41]. In 2015, Bennett et al. first reported the preparation of ZIF-4 glass, demonstrating that certain zeolitic imidazolate framework (e.g., ZIF-4, ZIF-62) can melt at relatively low temperatures (~400 °C) and be quenched to form transparent amorphous glasses [42]. These glasses retain the short-range coordination order characteristic of MOFs while introducing long-range structural disorder, thereby markedly improving mechanical flexibility and optical transparency (visible-light transmittance >80%). The number of MOFs and CPs capable of melting remains unclear, as thermal characterization using differential scanning calorimetry (DSC) is not yet a standard practice in this field [43]. Despite this knowledge gap, several families of MOFs and CPs have been reported to undergo vitrification, yielding glasses based on azolate, phosphonate, butyronitrile, thiocyanate, amide, pyridyl, and carboxylate ligands (Fig. 1) [33,34,44–48]. The relatively low melting points of MOF glasses (far below the ~1100 °C required for conventional glasses) reduce energy consumption and allow low-temperature doping, thereby preventing the degradation of luminescent centers [47]. More importantly, the amorphous host structure of MOF glasses suppresses lattice-defect localization, thereby reducing nonradiative losses, while their residual porosity on the angstrom scale facilitates guest encapsulation and further enhances luminescent performance [49]. These characteristics position MOF glasses as a promising platform to overcome the limitations of traditional luminescent materials and to advance the development of efficient, stable, and sustainable luminescent systems [50,51].

In this context, MOF glasses, as novel amorphous host materials, demonstrate unique advantages owing to their diverse coordination environments and tunable chemical reactivity [52–57], enabling the effective integration of various luminescent guests to produce multifunctional composite materials [58–60]. This strategy not only inherits the structural tunability of MOFs but also harnesses the flexibility and stability of the glassy state to overcome interfacial compatibility and thermal stability issues inherent to traditional composites [61]. For example, the porous structure of MOF glasses can act as nanoscale “containers” for encapsulating QDs, enabling stable loading and protection [62,63]. QDs, as highly efficient emitters, exhibit size-dependent emission and high PLQYs, but suffer from surface oxidation and aggregation-induced degradation in performance [64]. By employing MOF glasses as matrices, $CsPbI_3$ QDs can be embedded within the glass network via in situ synthesis, forming QDs@MOF-glass composites. This strategy effectively isolates QDs from the external environment, mitigates surface defects, and enhances overall luminescence efficiency via interfacial interactions such as trap passivation and phase stabilization. Consequently, this approach demonstrates significant potential for applications in white-light LEDs [62,63]. Recent studies have reported QD-based composites derived from ZIF glasses. For example, Hou et al. stabilized γ-$CsPbI_3$ QDs within agZIF-62 glass via liquid-phase sintering, achieving a PLQY above 50% and markedly improved stability against water, heat, and light [62]. Further elucidating the underlying mechanism, Li et al. identified an interfacial alloying effect between $CsPbI_3$ QDs and agZIF-62, where nanoscale interdiffusion layers effectively passivated defect traps, resulting in a record-high PLQY of 81.3% [63]. However, despite remarkable progress in QDs@MOF glass composites, there have been no successful demonstrations of direct RE ions (e.g., Eu^{3+}, Tb^{3+}) incorporation into MOF glasses to date. This challenge likely arises from the competitive coordination preferences between RE ions and intrinsic metal nodes (e.g., Zn^{2+}) within MOFs, which complicate the doping process. Moreover, the luminescence of RE ions depends strongly on well-defined coordination environments, which can be disrupted by the intrinsic amorphous nature of MOF glasses. Nevertheless, this field holds considerable potential for further exploration. To achieve stable incorporation of RE activators into MOF glasses, two strategies can be adopted: (i) constructing MOF precursors with RE-compatible coordination sites followed by melt-induced vitrification, or (ii) performing post-synthetic ion exchange on pre-formed MOF glasses.

MOF glasses, a class of glassy materials derived from metal–organic frameworks, exhibit exceptional performance in luminescent composite systems [65]. However, they are essentially a subset of coordination polymer CP glasses [66]. CPs encompass all coordination-driven network structures formed between metal ions and organic ligands, whereas MOFs refer specifically to three-dimensional CPs with permanent porosity [35]. This hierarchical relationship enables the synthesis and design principles of MOF glasses to be extended to the broader family of CP glasses, providing enhanced flexibility for optimizing diverse functionalities in luminescent composites. Research on luminescent CP glass composites is currently undergoing rapid development, with emphasis on employing amorphous CP glass matrices as hosts for diverse luminescent guests (including organic dyes and QDs) to construct hybrid systems with enhanced optical performance [67,68]. In practical applications, luminescent CP glass composites demonstrate substantial potential in photonic technologies, including multimodal optical information storage, dynamic anti-counterfeiting, and high-resolution X-ray imaging. In summary, the synergistic interactions between MOF/CP glasses and RE ions or QDs provide a promising avenue to overcome their common challenges in stability, dispersibility, and functional integration. A systematic and comprehensive review from a macroscopic perspective is urgently required to elucidate the correlations among composite design strategies, structural characteristics, and optical properties, thereby accelerating progress in optoelectronic and photonic applications.

Building on existing research, this review systematically summarizes recent advances in luminescent MOF glasses composites. It first elucidates the structural characteristics, glass-forming mechanisms, and optical advantages of MOF glasses, followed by an in-depth discussion of strategies for incorporating luminescent centers such as QDs and RE ions, as well as their energy transfer mechanisms. To address the challenges of structural integration and emission efficiency in RE@MOF glasses systems, insights from RE-based hybrid glasses are introduced, highlighting the importance of tailoring coordination environments and interfacial chemistry to enhance luminescence. Representative applications in optical fibers, LEDs, X-ray imaging, and optical sensing are summarized, and future directions in interface engineering and scalable fabrication are outlined. This review aims to provide systematic guidance and inspiration for the design and application of multifunctional luminescent materials based on MOF glasses.

2. Fundamentals and preparation of MOF glasses

2.1. Structural basis and properties of MOFs

The fundamental building units of MOFs comprise metal nodes (metal ions or metal clusters) and organic ligands, which assemble into frameworks through coordination bonds and often encapsulate guest molecules (Fig. 2). The metal nodes not only define the geometric architecture and coordination environment of the framework but also critically govern the electronic energy-level distribution and optical

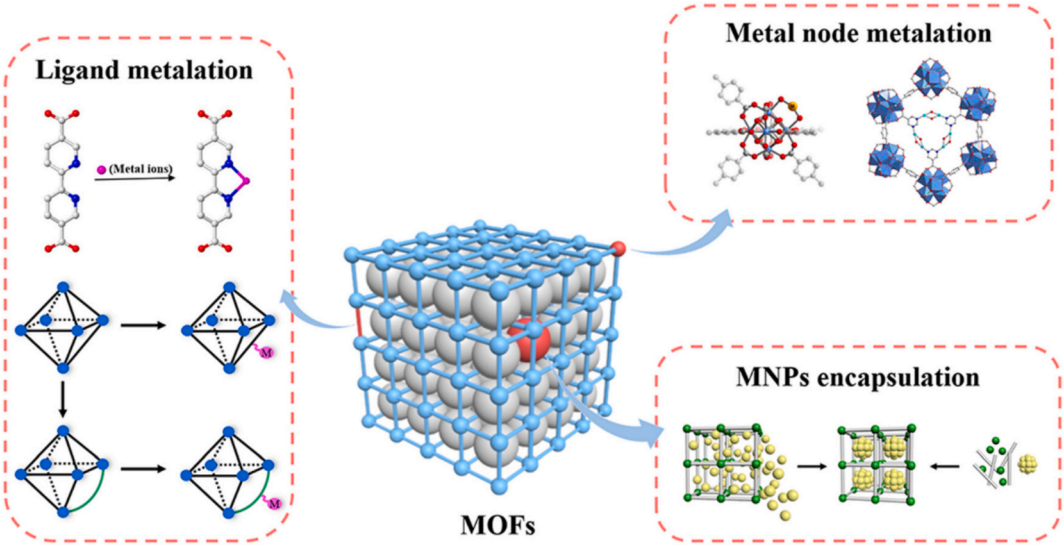

Fig. 2. Strategies developed for the metalation of MOFs (MNPs: Metallic Nanoparticles). Reproduced with permission [69]. Copyright 2024, Royal Society of Chemistry.

transitions [70–73]. For instance, transition metal nodes such as Zn^{2+}, Cu^{2+}, and Ti^{4+} can induce d–d transitions or MLCT, while RE ion nodes enable narrow-band emission through 4f–4f transitions [74]. Metal clusters (e.g., $Zr_6O_4(OH)_4$) typically exhibit higher coordination numbers, which enhance both framework stability and the density of luminescent centers [75]. Organic ligands function not only as structural linkers but also as active participants in light harvesting and energy transfer [76]. Representative ligands such as imidazoles, pyridines, and aromatic carboxylates absorb photons through π–π* or n–π* transitions and subsequently transfer energy to RE ions or transition-metal centers via the antenna effect [77–81]. The degree of energy-level alignment between the ligand and the excited state of the RE ion directly dictates the energy-transfer efficiency and luminescence intensity [82]. Guest molecules (such as solvents, small gas molecules, or dyes) can further modulate the luminescent properties [83]. Vibrational species such as water molecules or hydroxyl groups can induce nonradiative relaxation and quench luminescence, whereas the incorporation of fluorescent molecules or QDs into the pores can enhance emission through energy coupling or quantum confinement effects [84–88]. These features render MOFs a highly tunable and multifunctional luminescent platform [89].

The intrinsic characteristics of MOFs (such as high porosity and structural stability) stem from their modular design, providing distinct advantages over conventional materials [90–92]. MOFs exhibit exceptionally high specific surface areas (typically ranging from several hundred to several thousand m^2/g, with some, such as MOF-210 [93], reaching a BET surface area of 6240 m^2/g) and feature tunable porosity that facilitates guest-molecule diffusion throughout the framework [94]. This inherent porosity enables defect engineering; for instance, missing-linker defects can further increase the overall porosity [95]. Porosity plays a crucial role in luminescence, as it enables guest-induced fluorescence modulation for sensing applications [96]. For instance, HKUST-1 exhibits high porosity and structural tunability [97,98]. However, under high pressure, porosity may lead to framework compression, affecting mechanical properties [99]. The stability of MOFs encompasses thermal, chemical, and aqueous robustness [100]. Thermal stability is influenced by metal-ligand interactions and the types of functional groups [101]. Aqueous stability is a critical challenge, many MOFs are sensitive to water, but this can be improved by enhancing ligand basicity or employing functional group shielding [102–104]. For instance, introducing hydrophobic functional groups or establishing strong coordination bonds (e.g., Zr—O or Al—O) can markedly enhance hydrothermal stability, as exemplified by the UiO-66 [105] and MIL-101 [106] families. Stability ensures that MOFs maintain structural integrity in practical environments, thereby preserving their luminescent properties [107]. Recent advances include designing robust frameworks (e.g., MOFs constructed from metal clusters with high coordination numbers) to support diverse applications [108–114]. These properties establish MOFs as versatile materials, particularly in scenarios requiring persistent luminescence.

MOFs show significant potential in optics and photonics, primarily due to their tunable luminescence and structural diversity [115–118]. They can be used in fluorescence sensing (e.g., detecting biomarkers [119–122]), optoelectronic devices (e.g., LEDs [123–125]), and photonic crystals [126]. The anisotropy and size effects of crystalline MOF single crystals support their applications in areas such as photoelectric conversion and X-ray scintillators [127,128]. Glassy MOFs (prepared via methods like melt-quenching) overcome the brittleness and processing difficulties of crystalline materials, offering improved formability and light transmission properties [129]. They retain a degree of porosity and short-range order, and can exhibit enhanced nonlinear optical properties suitable for optical modulation and sensing. For example, studies show that MOF glasses (e.g., agZIF-62) possess good transparency from UV to NIR, high refractive index, and low dispersion, enabling the fabrication of micro-optical components such as microlens arrays [130]. The vitrification process also allows for compositional variation, increasing the flexibility of material design. In summary, the structural designability and functional tunability of MOFs (spanning both their crystalline and glassy states) establish them as a pivotal platform for advancing innovation in optics and photonics [131,132].

2.2. Formation mechanism of MOF glasses

The structural evolution accompanying glass formation represents a central topic in glass science, as it is intimately associated with the structural origins of the vitreous state [135]. Therefore, elucidating the structural differences between MOFs before and after vitrification necessitates a comparative approach employing multiple complementary characterization techniques. Using the zeolitic imidazolate framework ZIF-62 as an example [136], its fundamental building unit is the Zn(Im/bIm)$_4$ tetrahedron (Im: imidazolate, $C_3H_3N_2^-$; bIm: benzimidazolate, $C_7H_5N_2^-$) [137], in which Zn atoms coordinate with N atoms from the ligands via Zn—N bonds (Fig. 3a, b). Studies have confirmed that both Im and bIm ligands are preserved in the glassy state of ZIF-62. However, the Zn—N coordination bonds become increasingly disordered,

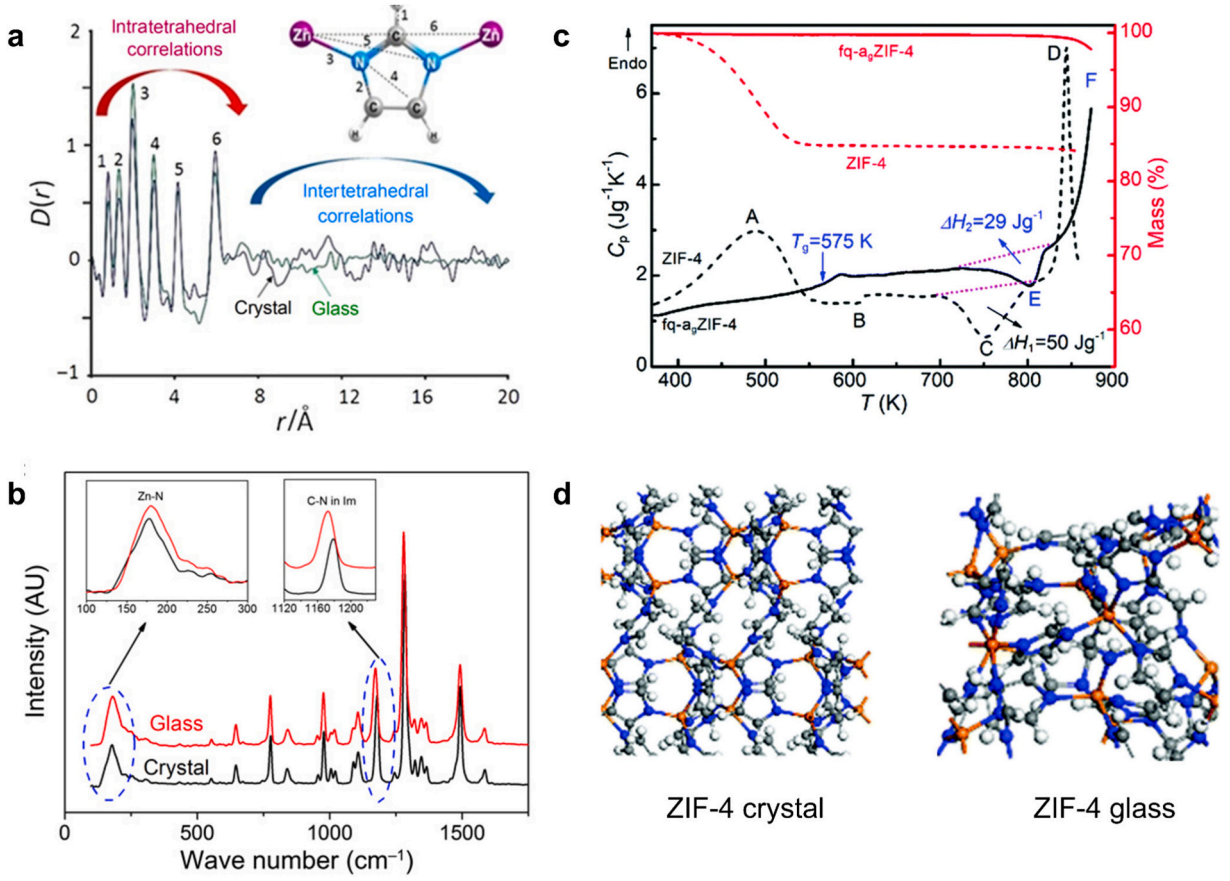

Fig. 3. Structural and thermal behaviors of glassy ZIF-4. a) Crystalline and glass pair distribution functions *D*(r) with Im geometry identifying peaks 1 to 6. b) Raman spectra of crystal and glass. Insets: Changes in nodes (Zn—N) and linkers (C—N). Reproduced with permission [133]. Copyright 2018. The American Association for the Advancement of Science. c) Thermal analysis of ZIF-4 and fq-agZIF-4 (fq-ag: fast quenched amorphous glass; C_p: black; TGA: red); Key events: A (desolvation), B (amorphization), C (crystallization), D (melting), F (decomposition). d) ZIF-4 crystal structure and agZIF-4 amorphous configuration (Zn: orange, N: blue, C: gray, H: white). Reproduced with permission [134]. Copyright 2019. Royal Society of Chemistry. (For interpretation of the references to color in this figure legend, the reader is referred to the web version of this article.)

accompanied by a shortened average bond length, indicating overall network densification [138]. Although the Zn–Im/bIm tetrahedra persist in the glass, confirming the chemical integrity of the organic ligands (Im, bIm) during vitrification, the disordering of the Zn—N bonds is identified as the key factor leading to structural disorder [139]. Further structural analyses reveal that vitrification causes no substantial alteration to the fundamental framework, with the Zn—N coordination environment and bonding configuration remaining largely preserved. Consequently, distortion of the Zn–Im/bIm tetrahedra—induced by the disordering of Zn—N coordination bonds—is regarded as the primary structural origin of the vitreous state in ZIF-62 [140,141].

From a chemical-mechanistic perspective, the nucleation of supercooled liquids is governed by two essential factors: (i) overcoming the thermodynamic barrier to form structurally ordered regions with specific interfacial energy [43,142,143], and (ii) overcoming the kinetic barrier (involving the breaking and reformation of chemical bonds) to enable atomic migration across interfaces [144]. In general, successful glass formation requires a sufficiently high cooling rate to suppress both nucleation and crystallization [145]. Using ZIF-4 as an example, Yue Yuanzheng's research group proposed a mechanism for its structural evolution during vitrification [146,147]. They suggested that the larger structural fragments of Zn(Im)$_x$ (x = 1–4) exhibit low mobility, creating a significant kinetic barrier during heat treatment that hinders the establishment of long-range order in the supercooled liquid. Furthermore, the melting process of ZIF-4 involves the breaking of metal-ligand coordination bonds and the formation of uncoordinated zinc centers [148]. Consequently, the melt-quenching-induced transformation of crystalline ZIF-4 into glass can be described as follows: the ZIF-4 crystal first undergoes a structural transition to form the ZIF-zni crystalline phase. Subsequently, during the melt-quenching process, the short-range ordered structure of ZIF-zni is largely preserved, while some Zn—N bonds break, the intact imidazolate rings undergo deformation, and the Zn(Im) tetrahedral structures are partially disrupted [149]. In 2019, Zhang Jiayan et al. reported that ZIF-4 glass exhibited no signs of recrystallization even after prolonged high-temperature annealing or repeated thermal cycling [134]. Accordingly, the exothermic peak observed in its DSC curve (Fig. 3c) can be attributed to two possible origins: (i) densification of the glass structure and collapse of pore channels (Fig. 3d), (ii) a short-range order-disorder transition occurring during dynamic heating or isothermal treatment. This phenomenon may be related to the significantly larger Zn—Zn distance (5.9 Å) compared to the Si—Si distance (3.1 Å) in silicate glasses. This results in the substantially larger size of Zn(Im) tetrahedra relative to SiO_4 tetrahedra, along with the notably lower bond strength of Zn—N coordination bonds compared to Si—O bonds in oxide glasses. For MOF materials in general, the rupture of coordination bonds between metal ions and ligands represents the critical step that enables melting [150]. Coordination bonds dominate the glass-forming behavior of MOF glasses, while the steric hindrance effect introduced by large ligands also significantly influences their melting and vitrification processes. Owing to the large size of the structural units and their strong mutual interference during movement, the viscosity of MOF glasses is typically higher than that of traditional silicate glasses.

Therefore, the melting and vitrification of MOF materials can be

generalized as follows: initially, thermal vibration induces the breaking of Zn—N bonds, triggering Lindemann melting and generating a large number of mobile structural units; subsequently, the substantial size of these mobile units creates pronounced steric hindrance, inhibiting the viscous flow of the structural units; concurrently, the continuous breaking and reformation of Zn—N bonds collectively influence the melting process. Consequently, the physical behavior of MOF melts is dominated by the continuous rupture and reformation of Zn—N coordination bonds. Upon rapid cooling, this results in a structure characterized by a disordered state of Zn—N bonds, ultimately leading to the formation of a MOF glass. In conclusion, as an emerging class of glass-forming systems, the melting and vitrification mechanisms of MOF materials hold significant importance for understanding the fundamental nature of glasses. The discovery of MOF glasses has greatly expanded the compositional diversity of glassy materials and opened new avenues for designing advanced functional glasses.

2.3. Regulation of MOF glass-forming ability (GFA) by ligand chemistry

In the early stages of MOF glass research, major breakthroughs were predominantly centered on ZIF systems, particularly the discovery of ZIF-4 and ZIF-62, which laid the foundation for understanding the regulatory role of ligands on GFA. Around 2015, the research groups led by Dr. Thomas D. Bennett and Professor Yuanzheng Yue first reported that ZIF-4 could form a glass through melt-quenching [42]. ZIF-4 has the chemical composition $Zn(Im)_2$, with $[ZnIm_4]$ tetrahedra as its fundamental building units. Its crystalline structure belongs to the orthorhombic system (space group Pbca) and adopts a cag-type topology. Upon heating, ZIF-4 undergoes a sequence of transformations, including solvent removal, structural collapse and amorphization, polyamorphic transition, recrystallization, melting, and eventual decomposition. The resulting melt exhibits poor thermal stability, decomposing within a narrow temperature window of merely 8–10 K after melting completes. However, quenching the melt at a rate exceeding 10 K·min^{-1} under an inert atmosphere effectively suppresses crystallization, thereby enabling the glass transition. ZIF-4 exhibits a high GFA, with a glass transition temperature to melting point ratio (T_g/T_m) of approximately 0.64 (Fig. 4a), identifying it as a typical easy-glass-forming system [151–153].

Subsequently, researchers developed ZIF-62 via a mixed-ligand

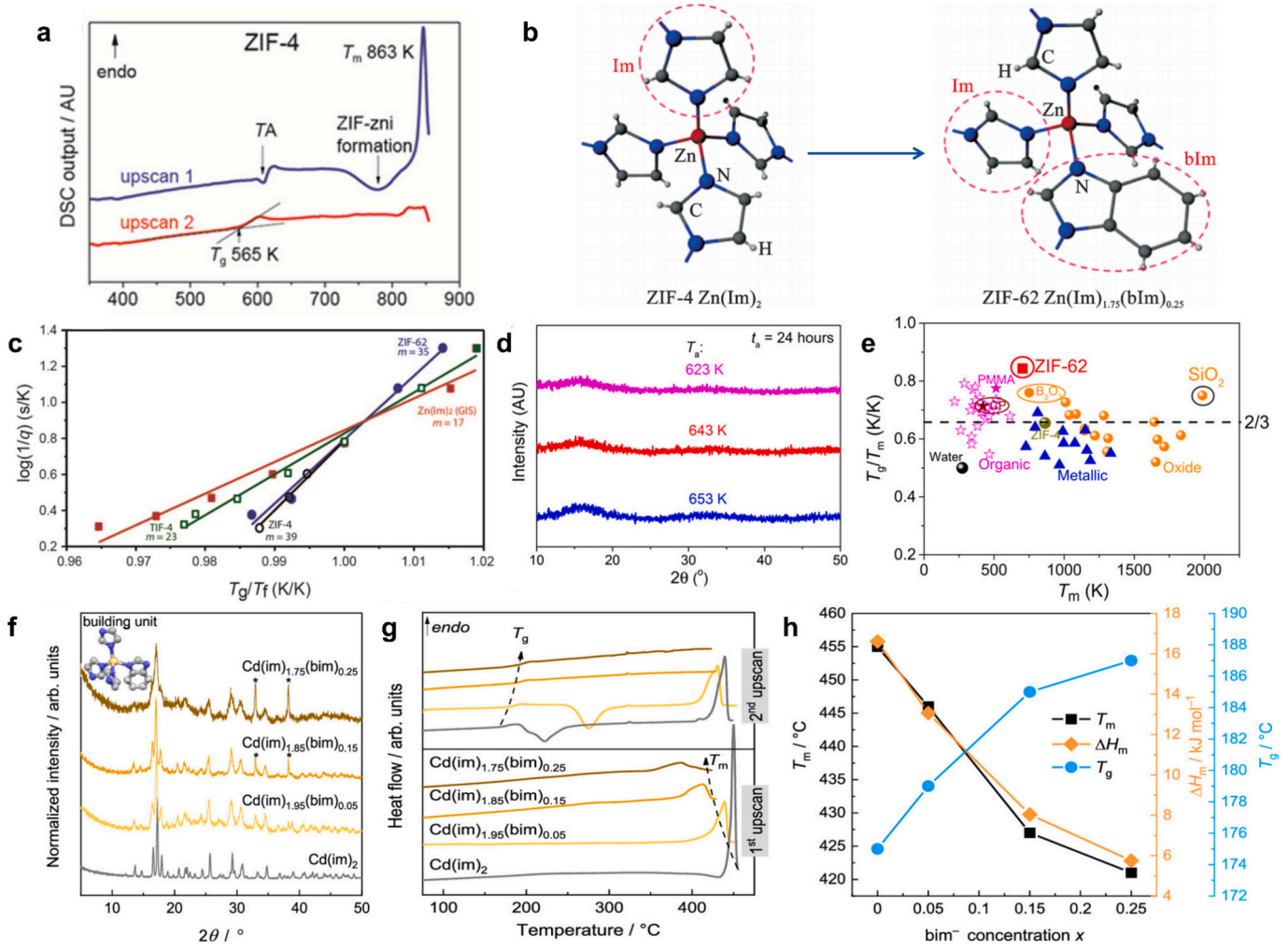

Fig. 4. Glass-forming properties of ZIFs and ligand-tuned Cd-based MOFs. a) The first (blue line) and second (red line) DSC scanning curves of ZIF-4 sample. Reproduced with permission [151]. Copyright 2016, American Chemical Society. b) Structural units of ZIF-4 and ZIF-62. Reproduced with permission [133]. Copyright 2018. The American Association for the Advancement of Science. c) Fragility indices (m) of representative ZIF glasses (fictive temperature T_f). Reproduced with permission [151]. Copyright 2016, American Chemical Society. d) Thermal stability of ZIF-62 glass near T_m. e) T_g/T_m ratios of various glass-formers. Reproduced with permission [133]. Copyright 2018. The American Association for the Advancement of Science. f) XRD patterns of Cd(Im)$_{2-x}$bIm$_x$ series. g) DSC profiles showing thermal transitions. h) Correlation between ligand composition (x) and thermal parameters (T_m, ΔH_m, T_g). Reproduced with permission [154]. Copyright 2025, American Chemical Society. (For interpretation of the references to color in this figure legend, the reader is referred to the web version of this article.)

strategy, which further improved its GFA. ZIF-62 has the chemical composition $Zn(Im)_{1.75}(bIm)_{0.25}$. It shares the same crystal structure and topology as ZIF-4 [155], differing only in the partial substitution of Im by bIm in its chemical composition (Fig. 4b). The incorporation of bIm increases steric hindrance, requiring greater energy to overcome the melting barrier and consequently elevating the T_m. Meanwhile, the enhanced degree of structural polymerization results in an elevated T_g [156]. The enthalpy of fusion (ΔH_m) increases owing to hindered molecular motion, whereas the entropy of fusion (ΔS_m) rises due to the increased configurational freedom. These chemical modifications render the ZIF-62 framework more rigid and thermally stable. Upon heating, ZIF-62 experiences only solvent removal and melting, without structural collapse or amorphization, and exhibits a wide temperature window of approximately 150 K between melting and decomposition. The T_g of ZIF-62 is 595 K, and transparent bulk glass can be obtained, marking the first successful preparation of a bulk metal-organic framework glass. ZIF-62 demonstrates exceptionally high viscosity at its melting point. Its fragility index ($m = 23.3$, Fig. 4c) categorizes it as a "strong" glass. The material retains its glassy state even after isothermal heat treatment at various temperatures between T_g and T_m for up to 24 h, or when cooled at a slow rate of 1 $K{\cdot}min^{-1}$ (Fig. 4d). This behavior reflects a crystallization resistance comparable to that of quartz or B_2O_3 glass [157]. This originates from the combination of high viscosity, which inhibits atomic migration, and the large size of the structural units (organic ligands) [158]. According to the Stokes–Einstein relation ($D \propto 1/(\eta\lambda)$), the high viscosity ($\eta$) and large characteristic size (λ) markedly reduce the diffusion coefficient (D), thus suppressing nucleation and crystal growth [159]. The T_g/T_m ratio of ZIF-62 reaches 0.84, far exceeding the empirical "two-thirds rule" (Fig. 4e), thereby confirming its outstanding GFA [160]. Based on topological constraint theory, ZIF-62 is composed of rigid $[ZnN_4]$ tetrahedra linked by flexible Zn–N–Zn bonds, analogous to the $[SiO_4]$ tetrahedra in SiO_2. However, the $[ZnN_4]$ units are larger and less constrained, and the Zn—N coordination bonds possess much lower bond energy than the covalent Si—O bonds. Consequently, ZIF-62 exhibits exceptionally strong GFA, although both T_g and T_m are substantially lower than those of SiO_2. If Im is completely replaced by bIm, ZIF-7 is formed, which cannot be melted, indicating that bIm provides stability while Im provides flexibility, and the two complement each other to enhance GFA [161].

Building upon the foundational research described above, the universality of the ligand modulation strategy has been progressively validated as the field deepens its exploration. This strategy applies not only to zinc-based systems but has also been successfully extended to MOF materials based on other transition metals, including Cd, Fe, and Co. [151,162–165] Recent investigations on cadmium-based imidazolate frameworks have systematically confirmed the critical role of ligand modulation on GFA, elucidating the decisive influence of ligand type, size, and electronic effects on vitrification behavior. The formation of MOF glasses essentially results from the interplay between thermodynamics and kinetics: a crystalline MOF must melt prior to decomposition, and crystallization must be suppressed during melt cooling to yield a stable glassy state [166]. Therefore, any structural factor that lowers crystal cohesive energy, weakens long-range order, or increases local conformational flexibility contributes to enhanced GFA. A recent study on a Cd-based imidazolate framework, involving the incorporation of a larger [154], more rigid co-ligand (bIm), systematically elucidated the regulatory mechanism of ligand chemistry on vitrification, providing clear thermodynamic evidence via X-ray diffraction (XRD) and DSC (Fig. 4f–4h). From a structural evolution perspective, XRD results (Fig. 4f) indicate that as the bIm content increases from 0 to 0.25 mol, the diffraction peaks of $Cd(Im)_2$ gradually weaken, broaden, and partially vanish, reflecting a marked reduction in long-range order [167]. In contrast, Pair Distribution Function (PDF) analysis and infrared spectroscopy confirm that short-range ordered units are retained [168]. This structural motif of "long-range disorder and short-range order" constitutes the fundamental basis for MOF glass formation [169]. The incorporation of the bulky bIm ligand introduces significant steric hindrance, disrupting the close packing of the original imidazolate network, rendering the framework more susceptible to relaxation and collapse, thereby weakening overall crystal stability and providing a prerequisite for subsequent melting and vitrification. DSC thermal analysis (Fig. 4g) further elucidates the regulatory mechanism of ligand mixing on thermodynamic behavior. For pure $Cd(Im)_2$ ($x = 0$), a distinct melting endotherm ($T_m \approx 455$ °C) and a glass transition ($T_g \approx 175$ °C) upon reheating after quenching are observed. As the bIm content increases, the melting peak gradually weakens, and the ΔH_m decreases from 16.6 to 5.7 $kJ{\cdot}mol^{-1}$ ($x = 0.25$), indicating a reduction in crystal cohesive energy and a lower energy barrier for the melting process. Concurrently, T_m decreases to approximately 421 °C, widening the temperature window between melting and decomposition and thereby mitigating the challenge of "decomposition before melting". Moreover, the incorporation of bIm markedly suppresses cold crystallization, hindering melt recrystallization, thereby enhancing the thermal stability of the glassy state and preventing its transformation into a glass-ceramic. A systematic summary of the thermodynamic parameters in Fig. 4h further elucidates the mechanism of ligand-modulated GFA. As the bIm content increases, T_m and ΔH_m decrease significantly, while T_g increases slightly (from 175 °C to 187 °C). This synergistic effect of "$T_m\downarrow$, $\Delta H_m\downarrow$, and $T_g\uparrow$" raises the T_g/T_m ratio from 0.385 to 0.444, indicating a significant enhancement of GFA. A higher T_g/T_m ratio facilitates bypassing nucleation and crystallization zones during melt cooling, thereby promoting glass formation; the reduction in ΔH_m indicates weakened crystal cohesive energy, aligning with ligand-induced structural perturbations [170]. Consequently, the incorporation of bIm significantly enhances the GFA of Cd-based MOFs by concurrently modulating crystal stability and melt-glass transition kinetics. This study clearly establishes the pivotal role of ligand chemistry in MOF vitrification: smaller, highly symmetric ligands typically form densely packed, highly crystalline frameworks that hinder vitrification, while larger, more rigid, or irregularly shaped ligands disrupt long-range order through steric hindrance and electronic effects, reducing melting enthalpy and melting point, increasing the T_g/T_m ratio, and thus markedly enhancing GFA. This approach exhibits broad applicability and can be extended to various metal-based MOF systems (e.g., Zn, Fe, Co), enabling precise control over material vitrification through tailored ligand design and composition.

2.4. Preparation of MOF glasses

2.4.1. Melt-quenching

Amorphous materials, encompassing glasses and other non-crystalline solids, exhibit long-range structural disorder, evidenced by the absence of Bragg diffraction peaks in XRD patterns and the lack of electron diffraction spots in transmission electron microscopy (TEM) [175]. However, only glassy materials exhibit a distinct glass transition, which serves as the primary criterion for differentiating glasses from other amorphous solids [176]. Melt-quenching is the predominant method for preparing various glass-forming systems, including MOF glasses [177,178]. Most MOF crystals undergo irreversible thermal decomposition and framework collapse upon heating without transitioning to a molten state, primarily because the coordination bonds between metal nodes and organic ligands are stronger than the covalent bonds within the ligands [179]. However, certain MOF systems, including ZIFs, phosphazene-based frameworks, thiocyanate/butyronitrile-based frameworks, and metal bis(acetamide) frameworks, can form a molten amorphous phase when the T_m is below the thermal decomposition temperature (T_d) [67,180] (Fig. 5a). The solid-liquid transition in MOFs originates from the dynamic breaking and reformation of metal-ligand coordination bonds, while their inorganic and organic structural units are retained in the liquid state [181]. Taking ZIF-4 as an example, its melting process involves the rapid dissociation and re-coordination of zinc centers and imidazolate ligands, a

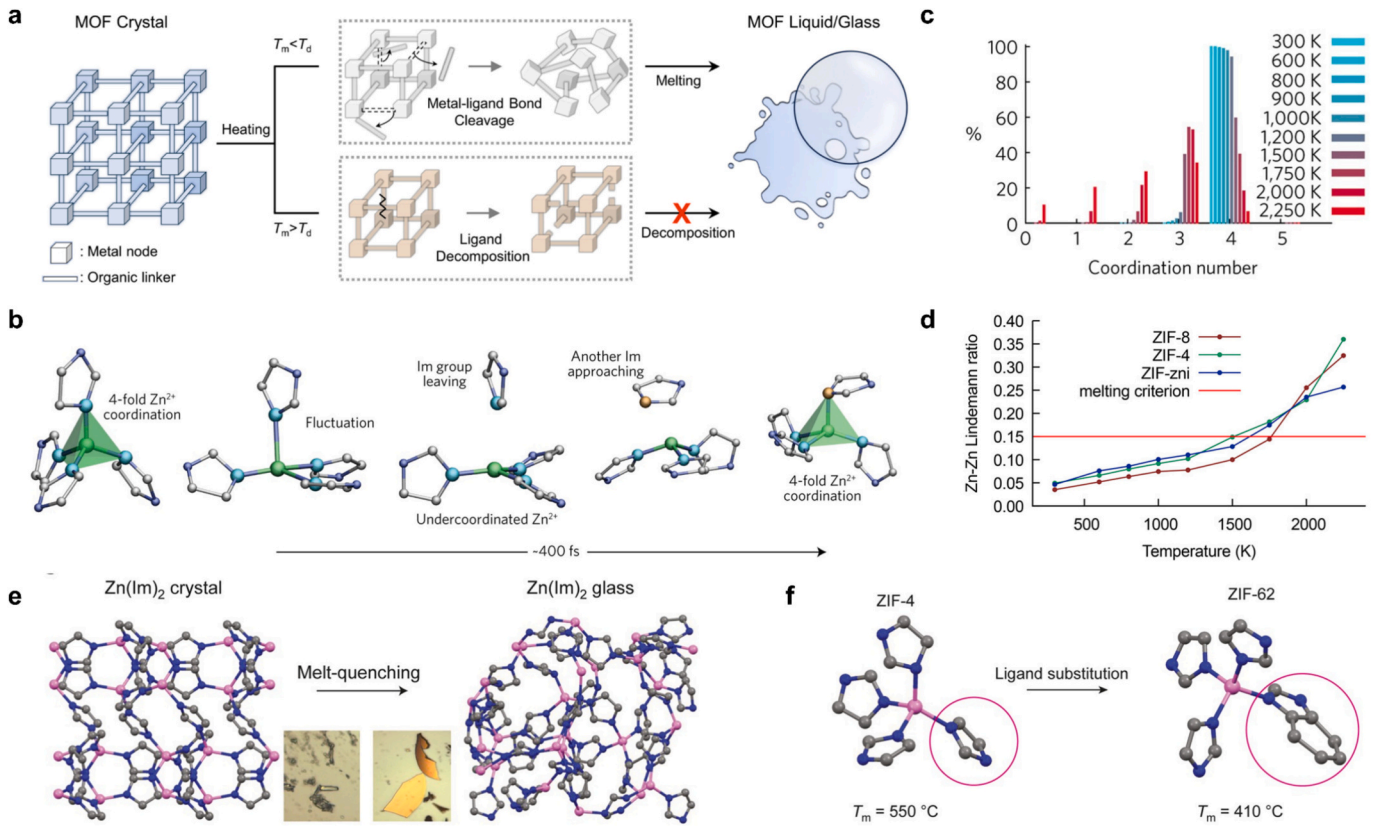

Fig. 5. Formation mechanism and thermal properties of MOF glasses. a) Schematic illustrating the competition between ligand decomposition and metal-ligand bond cleavage in determining MOF glass formation. Reproduced with permission [171]. Copyright 2014, International License. b) MD simulation showing imidazolate ligand exchange events during ZIF-4 melting. c) Temperature-dependent evolution of zinc coordination numbers in ZIF-4. Reproduced with permission [172]. Copyright 2017, Springer Nature. d) Correlation between atomic vibration amplitude and melting initiation in ZIFs. Reproduced with permission [173]. Copyright 2018, American Chemical Society. e, f) Defect engineering for melting point depression through partial substitution of imidazolate with benzimidazolate linkers, enabling glass formation at a lower temperature. Reproduced with permission [174]. Copyright 2016, Springer Nature.

mechanism that has been studied via first-principles molecular dynamics (MD) simulations (Fig. 5b, 6c) [172]. Melting takes place when the amplitude of atomic thermal vibrations surpasses a critical fraction of the nearest-neighbor bond length (Fig. 5d) [173,182]. Although the metal–ligand bond strength is a key factor governing the GFA of MOFs, additional factors such as porosity and intermolecular interactions also play crucial roles in determining their meltability [183]. Compared with ZIF-8, the ZIF-4 framework is relatively dense, allowing non-coordinated ligands to remain in contact and maintain stability through dispersion forces. In contrast, in the highly porous ZIF-8, non-coordinated ligands in intermediate states are more spatially isolated, resulting in a higher energy barrier that elevates the T_m above the T_d, thereby preventing glass formation [184,185]. Because the T_m of most MOFs exceeds their T_d, conventional melt-quenching methods are often unsuitable for achieving vitrification. Consequently, research efforts have shifted toward lowering the T_m of MOFs below their T_d by tailoring the metal nodes or optimizing ligand chemistry. Reported MOF systems capable of glass formation include: ZIF-4 [$Zn(Im)_2$; Im: imidazolate, $C_3H_3N_2^-$] [186], ZIF-62 [$Zn(Im)_{1.75}(bIM)_{0.25}$; bIm: benzimidazolate, $C_7H_5N_2^-$] [133], ZIF-76 [$Zn(Im)_{1.5}(ClbIm)_{0.5}$; ClbIm: 5-

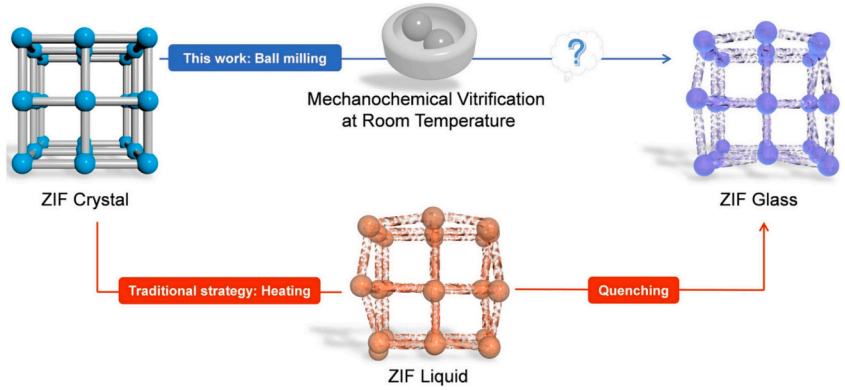

Fig. 6. Schematic representation of the traditional route to ZIF glass formation (red line) and the mechanochemical vitrification approach (blue line). Reproduced with permission [187]. Copyright 2024, Copyright 2024, Wiley-VCH GmbH. (For interpretation of the references to color in this figure legend, the reader is referred to the web version of this article.)

chlorobenzimidazolate, $C_7H_4ClN_2^-$], ZIF-76-Im [$Zn(Im)_{1.33}(Im)_{0.67}$; Mbm: 5-methylbenzimidazolate, $C_8H_7N_2^-$] [41], as well as structures like UiO-67, UiO-68, and DUT-5 (UiO: University of Oslo; DUT: Dresden University of Technology) [171]. Taking ZIF-4 as an example, heating to 550 °C produces a macroscopic liquid that, upon cooling, solidifies into a glass with the same composition as the parent crystal, composed of imidazolate-linked tetrahedral units (Fig. 5e, f). Introducing a small fraction of a secondary ligand (e.g., bIm) during synthesis yields the mixed-linker ZIF-62[$(Im)_{1.75}(bIm)_{0.25}$], which melts at a lower temperature (410 °C) while retaining the same topology. The discovery of these meltable MOFs opens new avenues for expanding the family of vitrifiable systems by leveraging host–guest interactions.

2.4.2. *Mechanical milling*

The conventional preparation of MOF glasses primarily relies on the melt-quenching technique, in which MOF crystals are heated to a molten state under an inert atmosphere and subsequently cooled rapidly [188]. Although this method has proven effective, its applicability is largely confined to systems in which the metal–ligand bonds exhibit high thermal stability, thereby limiting the diversity of material compositions and functional design possibilities. In recent years, mechanical ball milling has emerged as both a synthesis and post-synthetic modification technique that operates at room temperature and has been widely employed in the preparation of microcrystalline and amorphous MOF materials (for a comparison of experimental routes, see Fig. 6) [187]. Studies have demonstrated that solvent-free post-synthetic ball milling (PSBM) can induce rapid amorphization in ZIF materials. However, it has long remained unclear whether the resulting amorphous phases exhibit characteristic glassy behavior, such as a discernible glass transition.

In 2024, Xue et al. conducted a systematic investigation that effectively clarified this crucial issue [187]. The study aimed to explore the universality of the mechanical ball-milling approach and to elucidate the nature of the resulting products. Twelve distinct ZIFs were selected, exhibiting substantial variations in metal centers (Zn^{2+}, Co^{2+}, Cu^{2+}), topology (e.g., cag (Cagliotiite), zni (Zinc Iminodiphosphate), sod (Sodalite)) [189–192], as well as porosity, with theoretical void fractions (tVF) ranging from 6.8% to 66.8% (Fig. 7a). The XRD patterns of representative ZIFs (e.g., ZIF-4, ZIF-8, and ZIF-zni) before and after ball milling are shown in Fig. 7b. It is clearly observed that the sharp Bragg diffraction peaks of all crystalline ZIFs completely disappear after ball milling, being replaced by broad amorphous diffuse halos, which

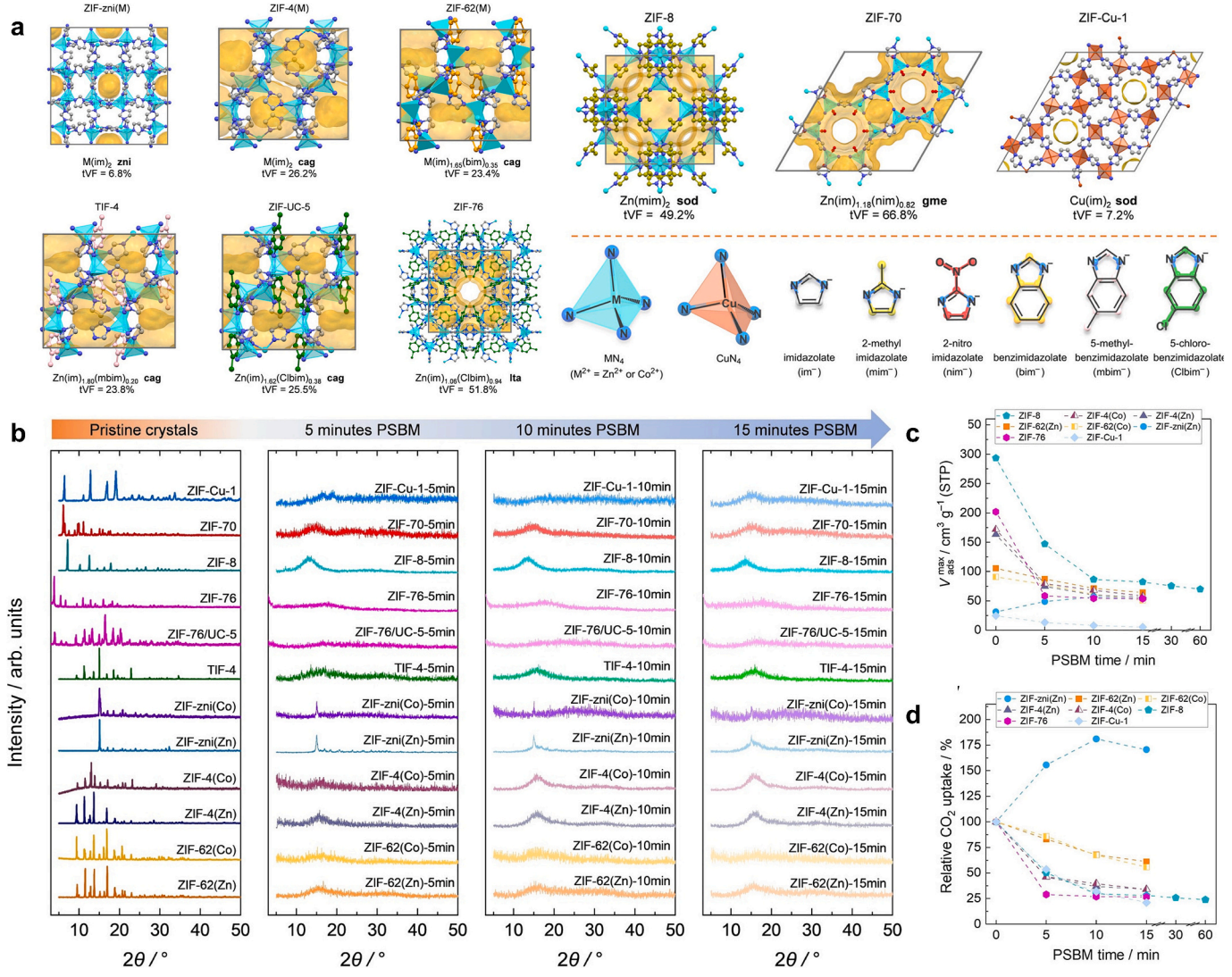

Fig. 7. Structural and porosity evolution during ball milling. a) Crystal structures (top) and building units (bottom) of representative ZIFs with tVFs indicated in pale yellow. Hydrogen atoms are omitted for clarity. ZIF compositions were verified by ^{1}H NMR spectroscopy after acid digestion. b) XRD patterns showing amorphization of ZIFs after PSBM. c) Absolute and d) relative CO_2 uptaken as a function of milling time. Reproduced with permission [187]. Copyright 2024, Copyright 2024, Wiley-VCH GmbH. (For interpretation of the references to color in this figure legend, the reader is referred to the web version of this article.)

provide direct evidence of the loss of long-range order [193,194]. Fig. 7c and d illustrate the evolution of material porosity during ball milling, as determined by CO_2 adsorption measurements. For most ZIFs, ball milling results in a pronounced reduction in porosity, indicating structural densification [195]. However, ZIF-zni (Zn) exhibits anomalous behavior, as its porosity increases markedly after ball milling. This phenomenon is attributed to the fact that ZIF-zni possesses one of the densest known ZIF topologies, in which mechanical perturbation instead introduces additional disorder and free volume [196–198]. In stark contrast, ZIF-Cu-1, despite its similar chemical composition, transforms into an almost non-porous amorphous solid after ball milling. This contrast arises from the fundamentally different coordination geometries of their metal centers, with the latter favoring denser packing under mechanical stress.

The most compelling evidence is provided by DSC analysis. Previous studies have demonstrated that ZIF materials known to be meltable and capable of forming glasses (such as ZIF-4, ZIF-62, and ZIF-zni) exhibit this behavior after short-duration (5–15 min) ball milling treatment, as evidenced by a distinct glass transition in their DSC curves (Fig. 8) [199,200]. This observation confirms that the resulting amorphous phases exhibit the characteristic thermal behavior of glasses. A major breakthrough lies in the first successful vitrification of several ZIF systems traditionally regarded as non-meltable (achieved through mechanical ball milling) such as ZIF-76 (evidence of vitrification shown in Fig. 9a) and ZIF-Cu-I (TG/DSC data in Fig. 9b-9d). Particularly noteworthy is the successful vitrification of the Cu(II)-based ZIF-Cu-I, which overcomes the previous limitation of ZIF glasses to primarily Zn(II)- and Co(II)-based systems, thereby significantly broadening the chemical diversity of MOF glasses. Furthermore, the T_g of ball-milled glasses is generally lower than that of their melt-quenched counterparts and decreases progressively with longer milling durations. This phenomenon is primarily attributed to the structural defects (such as uncoordinated metal sites and dangling bonds) introduced by mechanical treatment, which enhance network flexibility and mobility. The reduced T_g provides opportunities for low-temperature processing and facile shaping of these materials. The study further revealed that the evolution of porosity during ball milling is closely correlated with the coordination geometry of the metal centers. For example, the porosity of the high-density ZIF-zni increases after ball milling, while ZIF-Cu-I—owing to the flattened tetrahedral coordination geometry of Cu(II)—undergoes pronounced densification, ultimately forming an almost non-porous amorphous solid [201–203]. The diverse structural responses of different ZIFs to mechanical stress offer new insights into their glass-forming abilities. This work not only demonstrates that mechanical ball milling serves as an energy-efficient and highly effective route for the preparation of MOF glasses, but also underscores its unique advantage in broadening the compositional scope of vitrifiable MOFs. Specifically, this method circumvents high-temperature decomposition issues, rendering it suitable for ligands bearing thermally sensitive functional groups (e.g., halogens, nitro groups) or redox-active metal centers (e.g., Cu(II)) [204]. Consequently, mechanical ball milling offers a promising platform for the rational design and fabrication of multifunctional MOF glass composites (such as those incorporating organic molecules or functional complexes) thereby paving the way for their broader applications in catalysis, electronic devices, and separation membranes.

2.4.3. Desolvation

In the field of MOF crystal engineering, carboxylate ligands are considered highly promising building blocks owing to their strong coordination capabilities and highly tunable structural characteristics

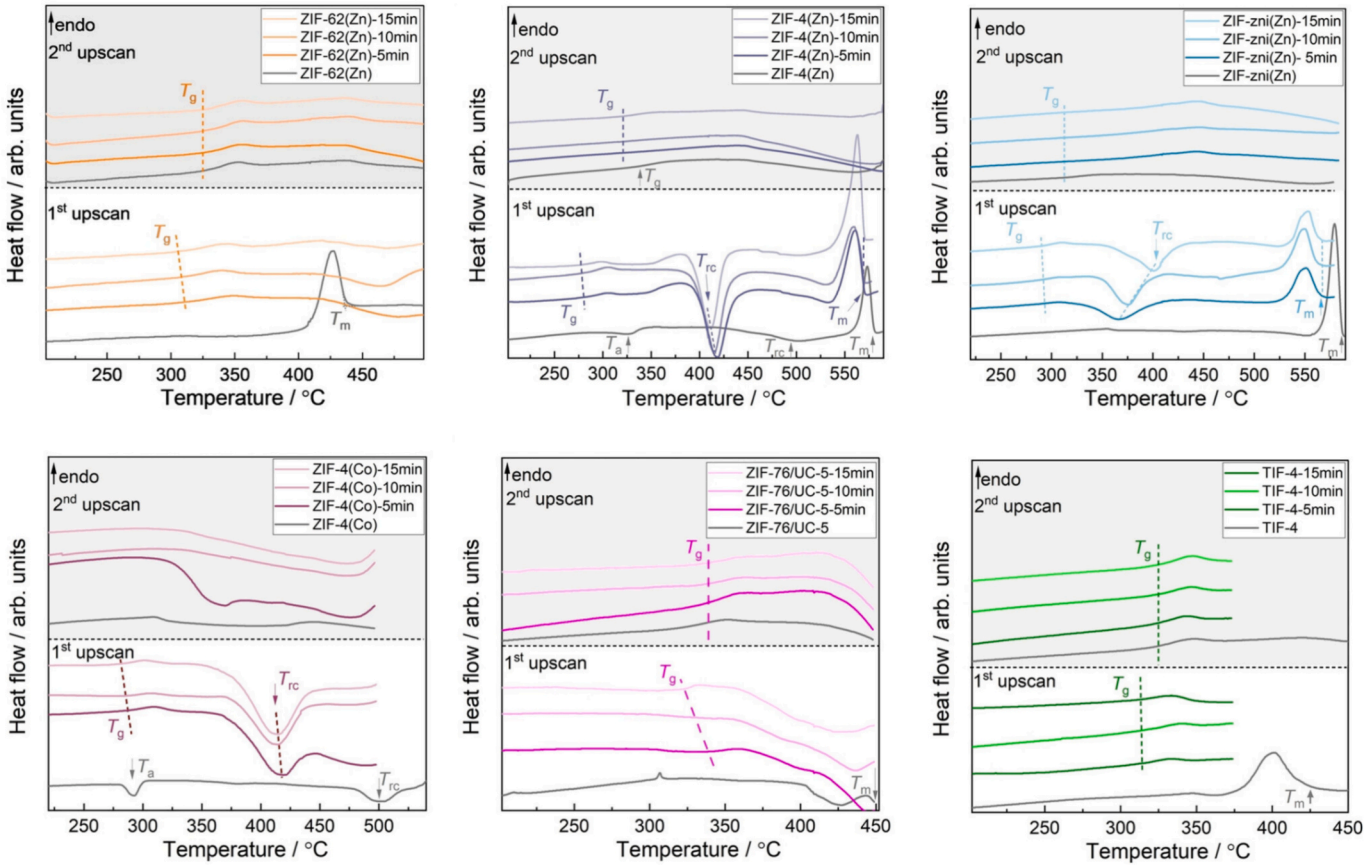

Fig. 8. DSC analysis of ZIFs before and after ball milling. First and second heating scans show thermal transitions various ZIF systems after different PSBM durations. The colored arrows and dotted lines indicate the amorphization temperature (T_a), T_g, recrystallization temperature (T_{rc}), and T_m of the ZIFs. Heating rate: +10 °C min^{-1}. Reproduced with permission [187]. Copyright 2024, Copyright 2024, Wiley-VCH GmbH.

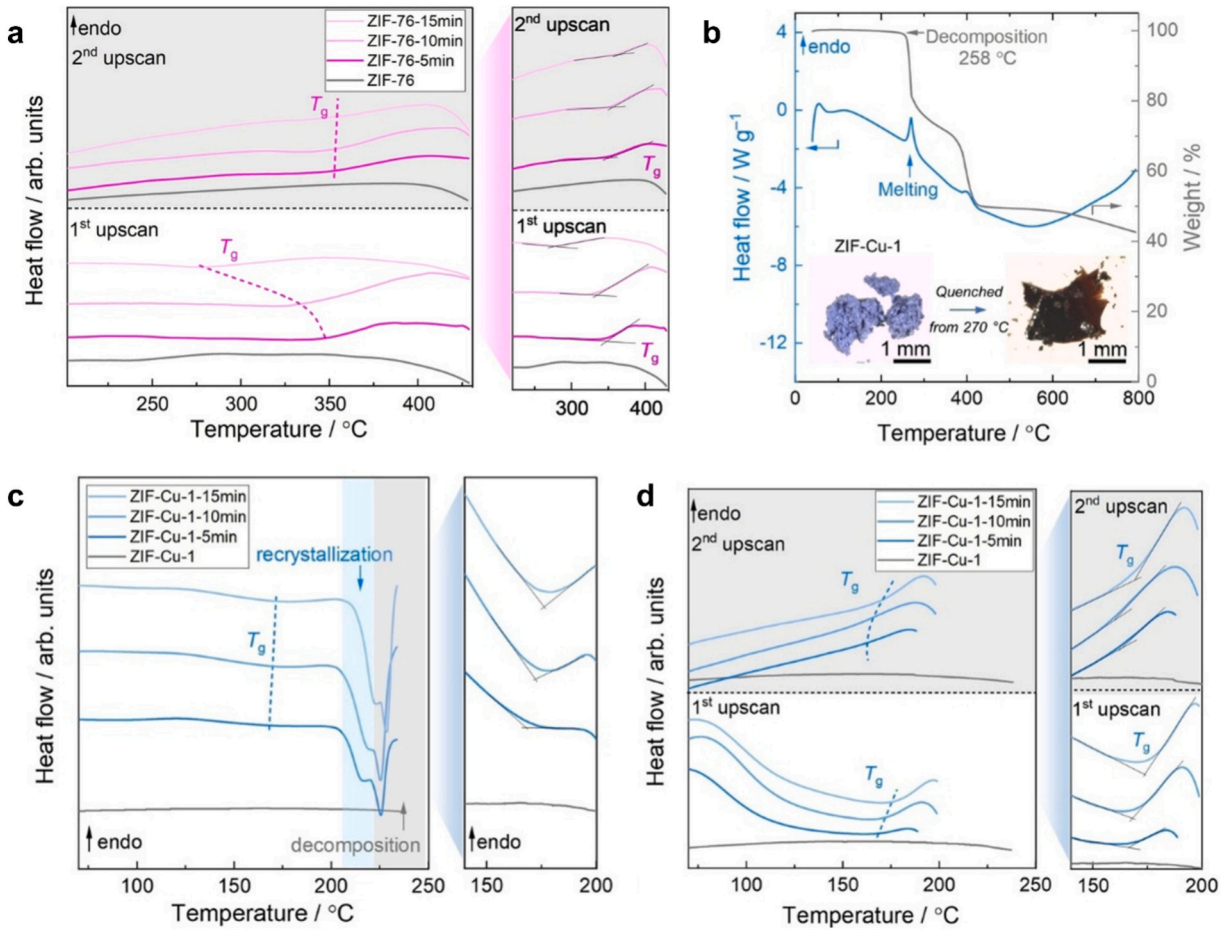

Fig. 9. Thermal analysis of ball-milled ZIF glasses. a) DSC scans of ZIF-76 showing glass transitions after PSBM. b) TG/DTA of ZIF-Cu-1 with optical images of crystalline and glassy phases. c, d) Cyclic DSC measurements of ZIF-Cu-1 and PSBM derivatives, highlighting glass transition behavior. All heating rates: +10 °C min^{-1}. Reproduced with permission [187]. Copyright 2024, Wiley-VCH GmbH.

[206]. However, conventional approaches such as thermal melt-quenching and mechanical ball milling encounter substantial limitations when applied to carboxylate-based MOFs, as the relatively strong metal–carboxylate coordination bonds often cause material decomposition under elevated temperatures or mechanical stress, thereby hindering the formation of a molten glassy state. To address this limitation, the desolvation approach has been proposed as an innovative route for MOF vitrification. This method begins with solvated metal–organic precursors (such as discrete species $[M(L)_n(Solv)_m]$) and induces the partial cleavage and reorganization of metal–ligand bonds through the controlled removal of coordinated solvent molecules, thereby directly constructing a continuous amorphous network. This process circumvents the dependence on the thermal stability of MOF crystals and instead exploits pre-existing hydrogen-bonded networks to direct vitrification [207].

Taking the cobalt-based [Co(4-(4-pyridyl)benzoate)$_2$] and manganese-based [Mn(bis[2-(4-pyridyl)vinyl]benzoate)$_2$] systems as representative examples, the removal of solvent molecules (e.g., H_2O) induces distortions in the coordination geometry and rearrangements of the framework conformation, ultimately yielding a glassy MOF characterized by short-range order [208]. Fig. 10 illustrates the evolution of the coordination environment and the amorphization pathway of a cobalt carboxylate–based MOF during hydration and dehydration. In the hydrated state, water molecules insert between cobalt ions and

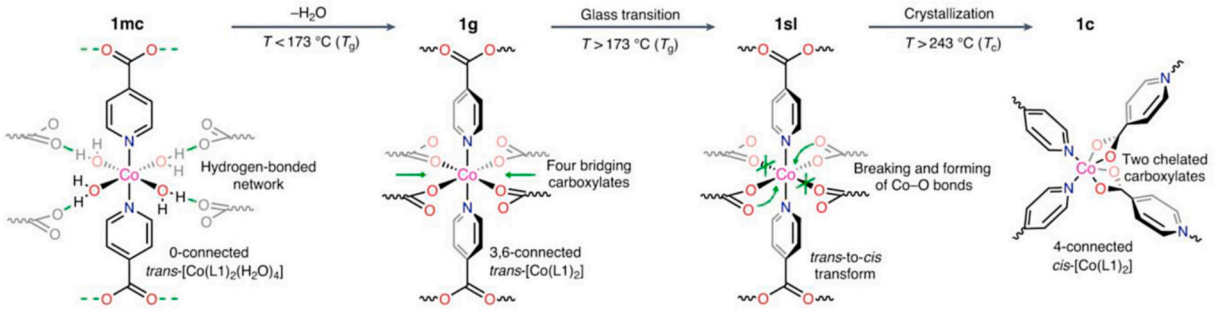

Fig. 10. Evolution of the Co coordination environment during desolvation and crystallization of $Co(L_1)_2$. Structural states include hydrogen-bonded framework (1mc), glass (1 g), supercooled liquid (1sl) and crystal (1c). Reproduced with permission [205]. Copyright 2023, Springer Nature Limited.

carboxylate ligands, modifying the original coordination mode [207,209]. Subsequent thermal dehydration further distorts the coordination geometry, ultimately yielding an amorphous phase [205]. Continued heating induces a glass transition followed by recrystallization, a process analogous to that observed in melt-quenched glasses. This method has been successfully extended to twelve ligands containing carboxylate, azole, and pyridyl groups, systematically demonstrating its universality across systems with different chain lengths, configurations, and functional substituents (e.g., —F, -NH_2) [205]. Mechanistic investigations reveal that the hydrogen-bond network within the metal complex functions as a "structural template" during desolvation, directing the disordered reorganization of the metal–organic framework. In situ techniques (including infrared spectroscopy (IR), X-ray absorption fine structure (XAFS), and PDF analysis) confirm both the reorganization of coordination bonds and the preservation of local coordination environments (e.g., octahedral Co^{2+} centers), alongside the formation of a long-range disordered glassy structure. MOF glasses prepared via this method exhibit highly tunable physicochemical properties: their T_g can be precisely adjusted within 120–280 °C, and the supercooled liquid region (T_g to the crystallization temperature T_c) can extend up to 124 °C, offering a broad processing window for low-temperature fabrication. Furthermore, this method enables the fabrication of boundary-free, transparent monolithic bulk materials without applying external pressure, thereby greatly simplifying the forming process. Gas adsorption measurements confirm the presence of permanent porosity, with pore sizes tunable by ligand length (e.g., longer ligands produce larger pores) [210]. This tunable control over both structure and properties endows MOF glasses obtained via the desolvation method with broad application potential in gas separation, solid-state electrolytes, and catalytic support systems [211].

2.5. Classification and development of MOF glasses

Compared with the extensive family of crystalline MOFs, research on MOF glasses began relatively late but has advanced rapidly over the past decade. Initially centered on ZIF-4 and its derivatives, the field has gradually expanded to encompass nitrile-, amide-, bisphenol-, and carboxylate-based MOF glasses. Following the successive reports of Fe- and Cd-based MOF glasses between 2023 and 2025, researchers have steadily elucidated the fundamental principles and critical factors governing the crystalline-to-amorphous transition in MOF materials.

Research on MOF glasses dates back to 2010, when ZIF-4 was observed to transform into a high-density amorphous phase upon heating, owing to its metastable structure [149]. Although not a "melt-quenched glass" in the strictest sense, this material first demonstrated that MOFs can adopt an amorphous state, marking the inception of research into their vitrification. In 2015, ZIF-4 glass was successfully fabricated via melt-quenching for the first time, and a low-density amorphous phase was identified within the material [186]. This work not only confirmed that MOFs can form a stable glassy state via melting but also revealed that their kinetic behavior exhibits features of "strong" or "fragile" liquids, akin to inorganic glasses, thus providing a theoretical foundation for subsequent studies. In 2016, melt-quenched ZIF-62 glass was successfully fabricated [151]. Owing to its low glass transition temperature and excellent GFA, it rapidly became a model system in the field. In the same year, derivative systems such as $Zn(Im)_2$ (GIS) and TIF-4 were also reported [151], further broadening the chemical diversity of MOF glasses. Concurrently, Angell, Yaghi, and colleagues proposed a Ti-based MOF glass [$Ti_{16}O_{16}(BPA)_x(OR)_{32-x}$] employing a bisphenol-A ligand, constructing a novel glassy framework via bulky ligands and polynuclear metal nodes, thus achieving the first vitrification of a non-imidazolate MOF [212]. In 2018, significant progress was achieved in the preparation of melt-quenched ZIF-76 glass. This material was found to retain permanent porosity (4–8 Å) even in its amorphous state [213], challenging the long-standing assumption that vitrification inevitably causes pore collapse. Notably, pure ZIF-76, owing to its larger ligands (mbIm and ClbIm), typically decomposes before melting. However, introducing a flux (such as TIF-4) or tuning the proportion of the smaller Im ligand can effectively promote its melting and subsequent glass formation. This discovery underscored the crucial role of ligand size, flexibility, and compositional ratio in governing the GFA of MOFs [185,214]. Since 2021, the research focus has gradually expanded toward non-imidazolate systems. The successful fabrication of nitrile-based MOF glass [$Ag(pL_2)(CF_3SO_3)]_2C_6H_6$ (pL_2 = 1,3,5-tris(4-cyanophenyl)benzene) [215] and amide-based MOF glass [$Co(bba)_3CoCl_4$] (bba = N,N′-1,4-butylene bis(benzamide)) [53] demonstrated the ability of diverse functional-group-containing ligands to form glassy frameworks, opening new avenues for the chemical design and functional development of MOF glasses. Between 2022 and 2023, carboxylate-based MOF glasses emerged as a major research focus. Through melt-quenching or thermal dehydration, researchers synthesized a variety of carboxylate-based glasses with distinct structures, including [$Co(L_1)_2]_{4n}$ (L_1 = 4-(pyridin-4-yl)benzoic acid) [207], [$Mn_3(peb)_6$]·2DMF (Hpeb = 4,4′-(ethene-1,2-diyl)dibenzoic acid) [216], and Mg- and Mn-based fatty acid salt glasses (C-Mg-adp, C-Mn-adp) [204]. These achievements not only expanded the diversity of MOF glass systems but also highlighted the unique advantages of carboxylate ligands in facilitating vitrification. After 2023, research entered a new stage characterized by "metal node modulation." The emergence of Fe-based ZIF glass [$Fe_3(Im)_6(HIm)_2$] demonstrated that altering the metal center can broaden the chemical space of MOF glasses and impart new functionalities such as magnetism and catalysis. In 2024, an optimized Mn-based carboxylate glass demonstrated a new strategy for tuning structural stability through the incorporation of bridging carboxylic acids. The most recent studies in 2025 successfully fabricated a Cd-based MOF glass, opening new opportunities for exploring heavy-metal-based glasses in optical and electronic applications.

Overall, the development of MOF glasses can be categorized into three distinct stages: the initial phase (2010–2015), exemplified by ZIF-4 and characterized by studies on crystal collapse and melt-quenching behavior; the expansion phase (2016–2020), centered on ZIF-62, marked by the continuous diversification of derivative systems and the extension to bisphenol-based MOFs; and the diversification phase (2021–present), encompassing nitrile-, amide-, and carboxylate-based systems, as well as functional exploration through metal-node modulation (e.g., Fe, Mn, Cd). Currently, ZIF-based glasses remain dominant owing to their low melting points and excellent GFA. Research on nitrile-, amide-, and bisphenol-based MOF glasses remains relatively limited but holds considerable potential for future advancement (Fig. 11). The emergence of carboxylate- and transition-metal-based MOF glasses signifies a new and promising trend in the field.

In summary, the development of MOF glasses has progressed from single-component systems to structurally diverse architectures, and further toward functional exploration. With the introduction of advanced strategies such as RE ion and quantum dot doping, future research is expected to focus not only on the mechanisms of structural evolution but also on application-oriented areas including optoelectronics, sensing, and energy storage, thereby driving MOF glasses toward practical and industrial implementation.

3. Luminescent metal coordination compound glasses

Metal–coordination compound (MCC) glasses (including MOF glasses, CP glasses, and their derivative systems) have recently emerged as a cutting-edge research frontier in luminescent materials, owing to their distinctive amorphous coordination networks and highly tunable optical properties [217].

3.1. Luminescent MOF glasses

MOF glasses exhibit remarkable potential as optical materials owing to their high transparency and outstanding processability. These

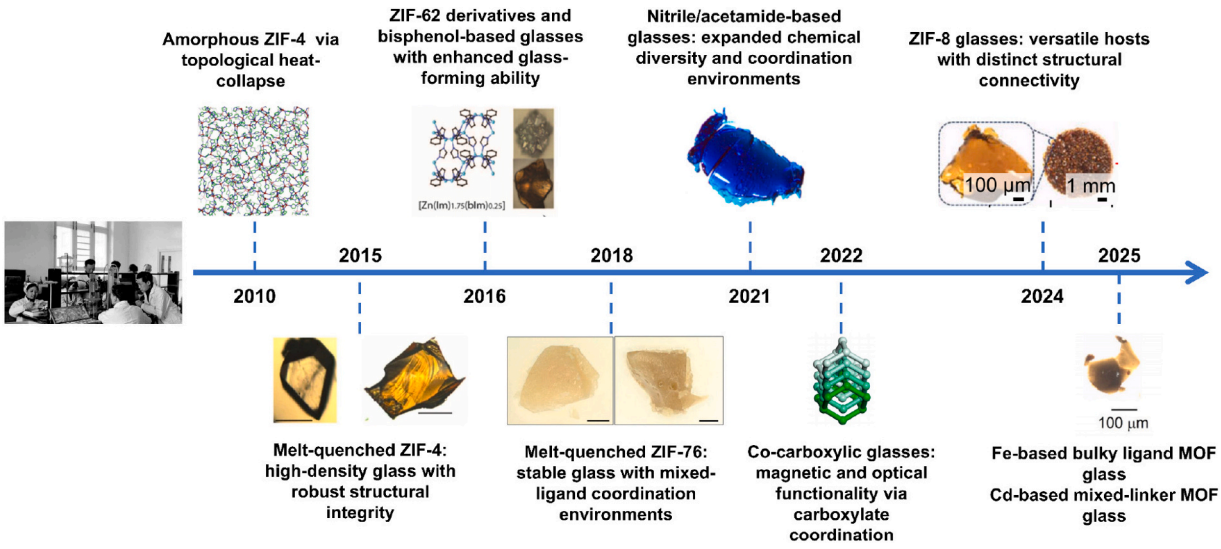

Fig. 11. Development history of MOF glasses in the past decades.

materials feature desirable optical properties, including high transmittance [217], optical isotropy, facile processability, fluorescence [218,219], nonlinear optical (NLO) responses [65,220–222], and excellent compatibility with molecular dopants. Among these properties, room-temperature phosphorescence (RTP) has attracted particular attention due to its promising applications in imaging, sensing, and catalysis [223–230]. Conventional molecular RTP systems typically suffer from excited-state lifetime competition, resulting in PLQY below 50%, where RTP appears merely as a delayed emission following the cessation of excitation [231]. In contrast, MOF glasses, owing to their rigid molecular environments and higher density and hardness compared with their crystalline counterparts, can effectively suppress nonradiative relaxation and minimize energy dissipation (Fig. 12a) [35]. Zn(4,5-dicyanoimidazole)$_2$ (denoted Zn-DCI) and Cd(4,5-dicyanoimidazole)$_2$ (denoted Cd-DCI) glasses are synthesized via slow evaporation of aqueous solutions containing zinc or cadmium nitrates and 4,5-dicyanoimidazole (Fig. 12b). The resulting glasses exhibit high Young's moduli of 9.73 GPa and 1.95 GPa, respectively. These rigid and densely packed amorphous coordination networks facilitate intersystem crossing (ISC) while suppressing the nonradiative decay of triplet excitons [232]. Delayed-emission spectroscopy and density-functional-theory (DFT) calculations reveal two distinct triplet emission peaks in the blue and green regions for these materials. The Cd–DCI glass exhibits emission maxima at 441 nm and 530 nm, featuring a long RTP lifetime of 0.63 s and a high PLQY of 75% (Fig. 12c). Under UV excitation, the Zn–DCI glass retains its luminescence when fabricated into one-dimensional (1D) fibers (with negligible photon transmission loss) or into two-dimensional (2D) thin films exhibiting anisotropic optical waveguiding behavior (Fig. 12d) [233].

Leveraging the dynamic phase-transition behavior of MOF glasses allows for the fabrication of nanocomposites in which these materials serve as precursors. Kulachenkov et al. employed femtosecond laser pulses to induce rapid melting of a MOF, yielding a novel MOF-derived material with a core–shell architecture, consisting of metal oxide dendrites at the core and an amorphous organic layer as the shell (Fig. 12e) [234]. The resonant interaction between these microspheres and light markedly enhances second-harmonic generation and three-photon luminescence, rendering them highly suitable for nonlinear nanophotonic applications. Vaidya et al. fabricated the first transparent and luminescent thioaurate MOF glass through simple mechanical pressing, exhibiting a transmittance of 26% and red emission at 93 K [221]. Other types of MOF glasses are also capable of exhibiting multicolor luminescence. Recent studies have revealed that MOF glasses composed of d^{10} metal cyanides and triphenylphosphine, exhibiting over 80% transmittance in the visible to NIR region, display intense green emission attributed to metal-to-ligand charge transfer (Fig. 12f) [221].

Li et al. demonstrated that the successful synthesis of high-quality ZIF-62 MOF glass established the material foundation for the development of core–cladding hybrid optical fibers [235]. The researchers selected commercial fluorophosphate glass HFK95N as the cladding material, whose softening temperature (758 K) closely matches the melting point of ZIF-62 (694 K), thereby satisfying the co-drawing temperature window requirements. The refractive indices of the cladding and core at 589 nm are 1.44 and 1.56, respectively, producing a notable refractive index contrast ($\Delta n \approx 0.12$) that ensures total internal reflection for effective optical waveguiding. The Zn25 fiber (representing 25% Zn in the standard formulation, Zn^{2+}:Im:bIm = 0.25:13.5:1.5) (Fig. 12g) was fabricated via a melt-drawing process, yielding a fiber diameter of 680 μm and a core diameter of 150 μm. Energy-dispersive X-ray spectroscopy (EDS) confirmed that the core region is enriched in Zn, whereas the cladding primarily contains Al, Si, F, Mg, and P (Fig. 12h). Near-field imaging (Fig. 12i) demonstrates that blue, green, and red light can be independently emitted through optical filter modulation. The fiber exhibits outstanding optical performance (Fig. 12j), with a transmission loss as low as 0.72 dB·cm^{-1}. Under 365 nm UV excitation, the fiber displays its strongest emission peak at 440 nm on the end face (Fig. 12k). By adjusting the Zn25, Zn50 (Zn^{2+}:Im:bIm = 0.5:13.5:1.5), and Zn100 (Zn^{2+}:Im:bIm = 1:13.5:1.5) glasses through optical filtering, blue, green, and red emissions can be obtained (Fig. 12l-12n). Further investigations revealed that ZIF-62 glass exhibits pronounced phosphorescence under a nitrogen atmosphere (Fig. 12o): it emits a green afterglow lasting several seconds after cessation of UV excitation, whereas the emission is completely quenched in the presence of oxygen. Based on this finding, a highly sensitive optical oxygen-sensing platform was developed (Fig. 12p). The phosphorescence intensity decreases monotonically with increasing oxygen partial pressure, exhibiting a detection limit of 3.5% and excellent reversibility—the original performance can be fully restored within 10 min of nitrogen exposure. After five testing cycles (Fig. 12q, r), no signal attenuation was observed, confirming the excellent chemical stability and structural robustness of the ZIF-62 glass host. This study integrates the gas responsiveness of MOF glass with long-lived phosphorescence for the first time, offering new design insights for the development of reusable optical sensors.

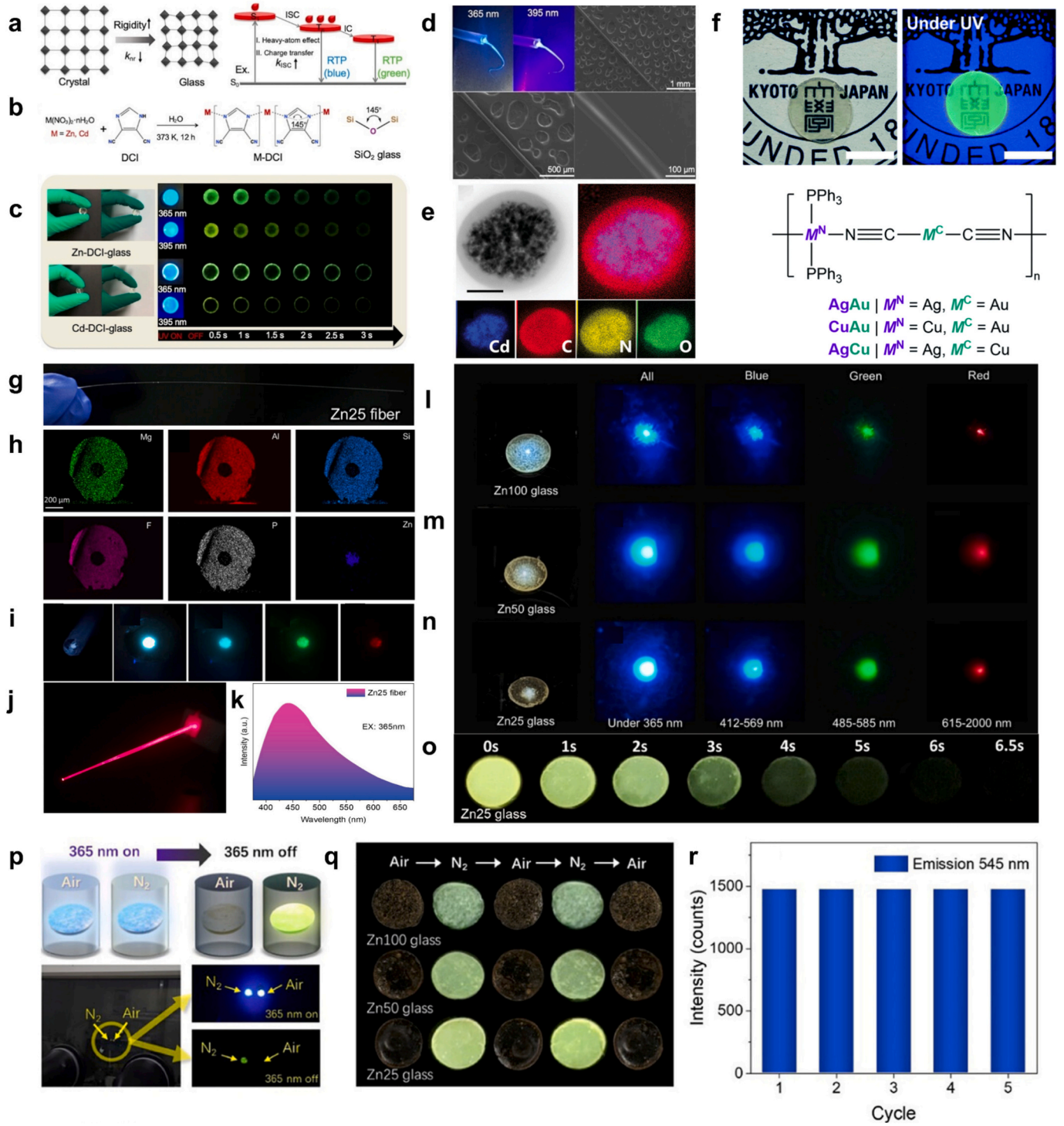

Fig. 12. Synthesis, characterization, and applications of luminescent MOF glasses. a) Mechanism of efficient RTP in MOF glasses via rigid molecular environments and enhanced ISC processes. b) Comparison of synthetic approaches between MOF glasses and conventional silicate glasses. c) Photographs of MOF glasses under UV excitation (365 nm, 395 nm) and after cessation. d) SEM image of Zn-DCI glass fiber. Reproduced with permission [233]. Copyright 2022 Wiley-VCH GmbH. e) Core-shell morphology from femtosecond laser melting of MOF with nonlinear optical enhancement. Reproduced with permission [234]. Copyright 2019 Wiley-VCH GmbH. f) Transparent $([Cu(PPh_3)_2][Au(CN)_2]_n$ glass exhibiting green emission. Reproduced with permission [221]. Copyright 2022, Royal Society of Chemistry. g) Cross-section of Zn25 fiber under 365 nm excitation. h) Elemental mapping (Mg, Al, Si, F, P, Zn) in fiber cross-section. i) Near-field output pattern from Zn25 fiber. j) Red laser transmission through Zn25 fiber. k) PL spectrum about the cross section of Zn25. l-n) Photoluminescence of Zn100, Zn50, and Zn25 glasses under 365 nm light excitation. o) Phosphorescence decay of Zn25 glass in N_2 atmosphere. p) Atmospheric oxygen sensing demonstration. q, r) Cyclic phosphorescence response and intensity stability at 545 nm. Reproduced with permission [235]. Copyright 2025 Wiley-VCH GmbH. (For interpretation of the references to color in this figure legend, the reader is referred to the web version of this article.)

3.2. Luminescent PeQDs@MOF glasses

In the field of MOF glass research, ZIF-series glasses remain dominant owing to their relatively low melting points and exceptional glass-forming ability. However, the synthesis of ZIF glasses generally depends on melt-quenching their crystalline precursors, while the intrinsic lattice constraints of ZIF structures severely restrict the incorporation of diverse metal ions, which are currently limited to non-luminescent species such as Zn^{2+} and Co^{2+}. This limitation substantially hinders the direct incorporation of functional luminescent centers, such as RE ions. Consequently, embedding luminescent centers as guest species within the MOF glass matrix has emerged as a highly promising alternative strategy. Among various luminescent guests, perovskite quantum dots (PeQDs) have attracted considerable attention owing to their exceptional optoelectronic properties, including high PLQY [236], narrow emission peaks [237], and tunable emission spectra [238]. Corresponding composite strategies have been shown to markedly enhance both the stability and luminescent efficiency of these materials.

In 2021, Hou et al. reported a groundbreaking contribution to this field in Science [62]. They developed a liquid-phase sintering strategy to successfully fabricate a series of composites composed of $CsPbX_3$ lead halide perovskites embedded in ZIF glass. Specifically, the method involves mixing $CsPbI_3$ powder with agZIF-62 glass powder in a defined ratio, sintering the mixture under an inert argon atmosphere at temperatures typically ranging from 175 to 350 °C (above the T_g of the ZIF glass but below its melting point) followed by rapid quenching (e.g., in liquid nitrogen) (Fig. 13a). This process produces scalable monolithic composites, in which the MOF glass host stabilizes the metastable black phase (γ-$CsPbI_3$) through interfacial interactions, preventing its transition to the non-perovskite yellow phase. Moreover, the composite exhibits remarkable stability against water, organic solvents, heat, light, air, and humidity. For example, its luminescence remains stable even after 10,000 h of immersion in water (Fig. 13b). In addition, the composite demonstrates self-confinement of lead, effectively preventing lead ion leakage. Transmission electron microscopy (TEM) characterization provides direct evidence for the material's high performance. Annular Dark Field Scanning TEM (ADF-STEM) images (Fig. 13c) clearly reveal $CsPbI_3$ nanocrystals (bright contrast) measuring 20–50 nm, uniformly embedded in the ZIF glass host (dark contrast), with a well-bonded interface between the two phases. Electron diffraction analysis confirms that these nanocrystals adopt the γ-$CsPbI_3$ phase. Furthermore, Cathodoluminescence STEM (CL-STEM) mapping (Fig. 13d) shows that the luminescence originates from individual perovskite nanocrystals encapsulated within the glass, exhibiting uniform emission wavelengths, indicating a pronounced interfacial passivation effect. By adjusting the halogen composition, the emission wavelength can be tuned across the entire visible spectrum, laying the groundwork for the development of white LEDs with a wide color gamut (Fig. 13e, f).

In 2023, Li et al. reported the interfacial alloying mechanism in $CsPbI_3$–ZIF glass composites [63]. During sintering, an atomically thin alloyed interfacial layer formed between $CsPbI_3$ and amorphous ZIF-62 glass, predominantly consisting of disordered Pb—I frameworks (Fig. 14a). Extended X-ray Absorption Fine Structure (EXAFS) analysis (Fig. 14b) revealed the formation of Zn—I bonds at the interface, indicating effective chemical passivation and stabilization of the γ-$CsPbI_3$ phase. Furthermore, ADF-STEM combined with electron energy loss spectroscopy (EELS) (Fig. 14c, d) confirmed iodine diffusion of approximately 10 nm into the glass matrix, providing direct evidence that the enhanced luminescent stability arises from chemical alloying rather than simple physical encapsulation. Ghasemi et al. demonstrated that agZIF-62 suppresses phase separation in $CsPb(Br_{1-x}I_x)_3$ [239]. Upon liquid-phase sintering, the $CsPbBr_{1.5}I_{1.5}$@agZIF-62 composite exhibited two distinct coordination environments in the agZIF-62 framework, associated with zinc-terminated and imidazole-terminated sites. Consequently, the Zn and Im moieties are exposed on the surface of the mixed-halide perovskites, allowing direct interactions (Fig. 14e). The interaction energies between agZIF-62 and various surface defects of the mixed-halide perovskites are high in magnitude, indicating stable interactions (Fig. 14f) that effectively suppress defect migration. CL-STEM combined with EDS confirmed a linear correlation between the Br/I

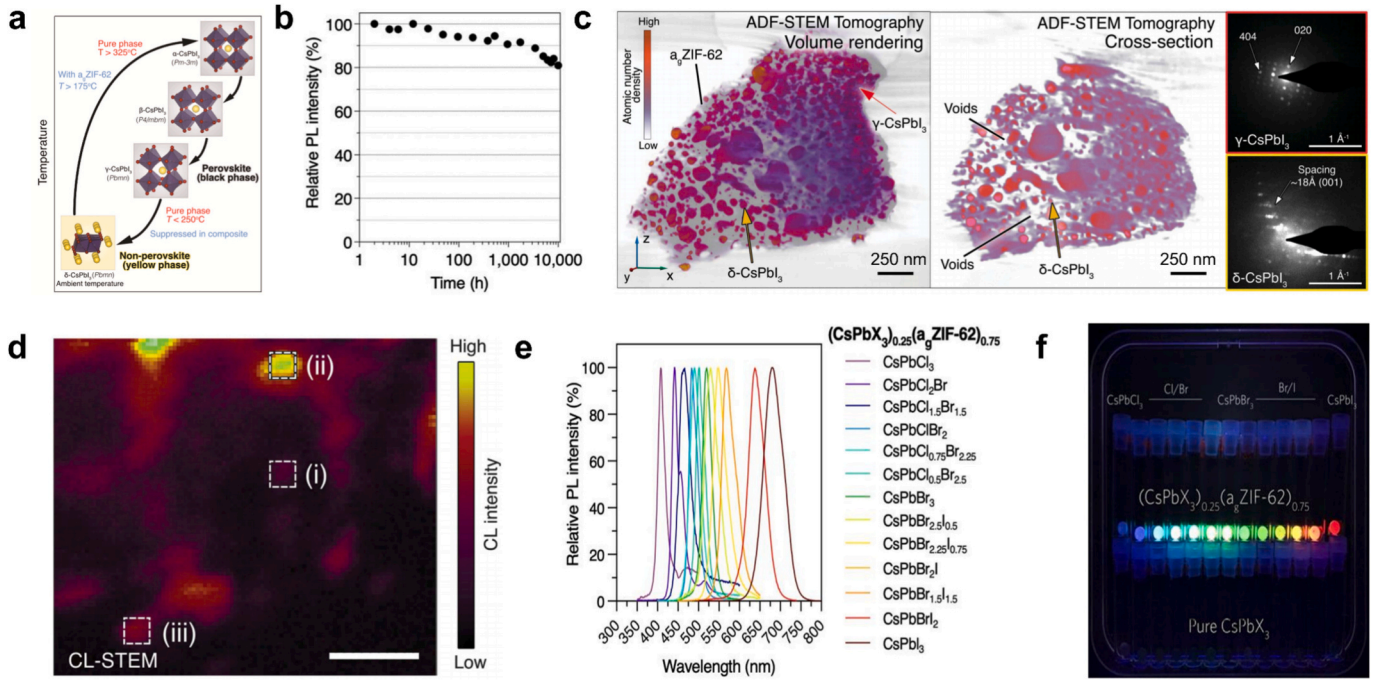

Fig. 13. Characterization and applications of PeQDs@MOF Glasses. a) Phase transition of $CsPbI_3$ in its pure phase and within the composites. b) Alteration of relative PL intensity for $(CsPbI_3)_{0.25}(agZIF\text{-}62)_{0.75}$ immersed in the water. c) Volume rendering of a tomographic reconstruction of $(CsPbI_3)_{0.25}(agZIF\text{-}62)_{0.75}$ and a single cross-sectional plane extracted from the volume. Color-coded arrows indicate the regions where electron diffraction data were collected. d) CL-STEM mapping of the sample. Scale bar, 70 nm. e) PL spectra of the $(CsPbX_3)_{0.25}(agZIF\text{-}62)_{0.75}$ composites (X = Cl, Br, I, and mixed halide ions). f) Optical photos of the composites and pure $CsPbX_3$ under 365 nm UV light. Reproduced with permission [62]. Copyright 2021, AAAS Publishing.

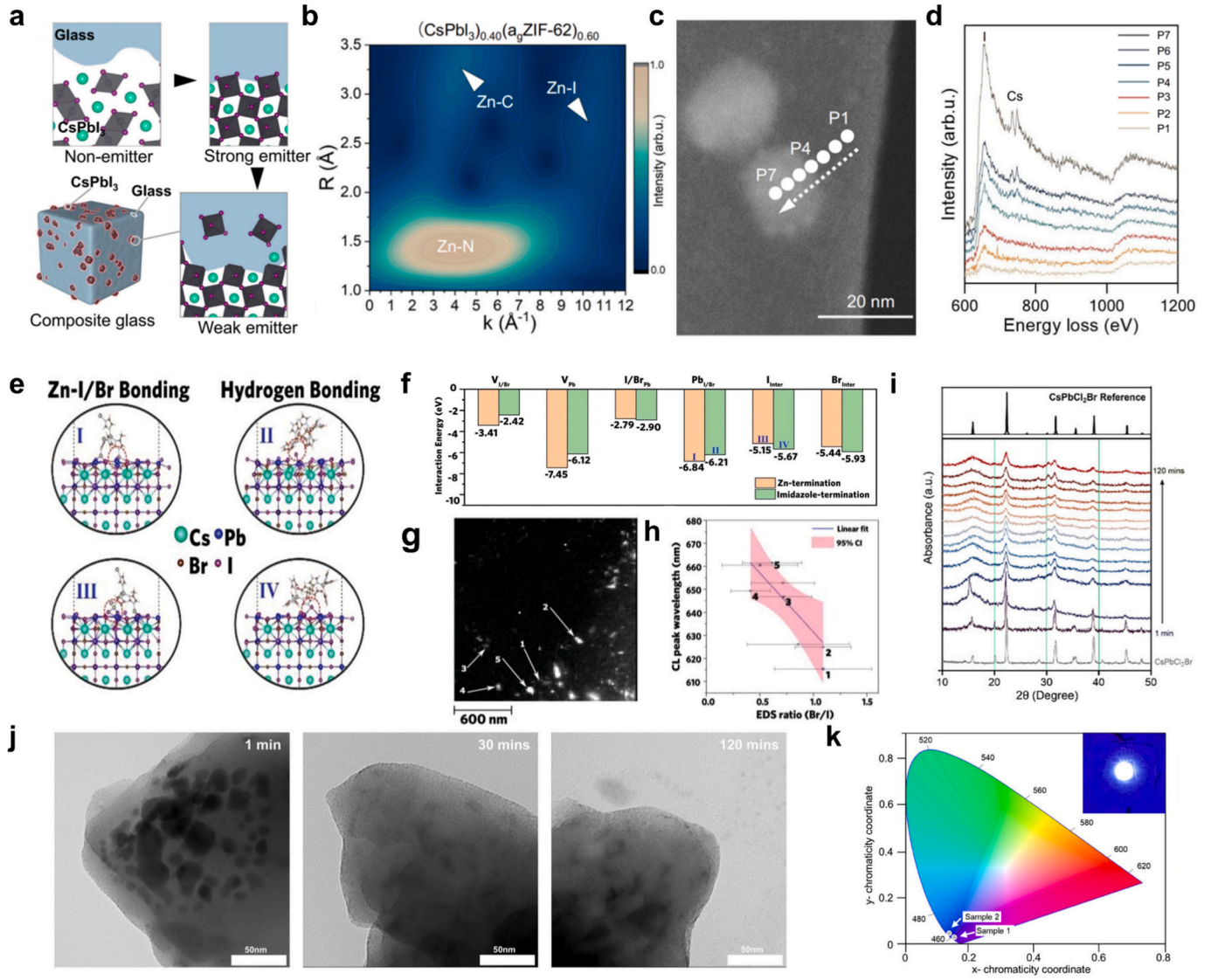

Fig. 14. Characterization and applications of PeQDs@MOF Glasses. a) Schematic diagram of the $CsPbI_3$ phase transition and evolution of the interfacial atomic structures during sintering. Arrows indicate the progress of sintering. b) EXAFS analysis of the $CsPbI_3$–ZIF glass composite. c) ADF-STEM image of $(CsPbI_3)_{0.1}(agZIF\text{-}62)_{0.9}$ composites. d) EELS core loss spectra acquired from the marked points shown in TEM image with background subtracted. Reproduced with permission [63]. Copyright 2023, AAAS Publishing. e) Adsorption behavior of imidazole- and Zn-terminated groups on defective $CsPb(Br_{1-x}I_x)_3$. (I–II) denote antisite defects (PbI/Br), (III–IV) interstitial defects (I/Br_{Inter}). Zn-termination strongly binds surface I/Br atoms, whereas imidazole-termination forms hydrogen bonds. f) Adsorption energies for imidazole- and Zn-terminated groups on various defects, including I/Br vacancies, Pb vacancies, interstitials, and antisite defects. g) Panchromatic STEM-CL image; arrows indicate grains used for CL-EDS registration. h) Correlation between emission wavelength and Br/I ratio for eight grains in the overlapping region of two independent scans. Reproduced with permission [239]. Copyright 2025 Wiley-VCH GmbH. i) Ex situ X-ray diffraction of $(CsPbCl_2Br)_{0.25}(agZIF\text{-}62)_{0.75}$ from 1 min to 120 min milling, with perovskite reference pattern. j) TEM of $(CsPbCl_2Br)_{0.25}(a_gZIF\text{-}62)_{0.75}$. k) CIE color coordination of fabricated blue and violet LEDs; inset is photo of the fabricated LED. Reproduced with permission [240]. Copyright 2025 Wiley-VCH GmbH. (For interpretation of the references to color in this figure legend, the reader is referred to the web version of this article.)

ratio and the emission wavelength (610–690 nm) at the nanoscale (Fig. 14j, h).

Subsequently, in 2025, Wang et al. employed a solvent-free mechanochemical approach to synthesize $CsPb(Br_xCl_{1-x})_3$@MOF glass composites [240]. As shown in Fig. 14i, after prolonged grinding, the XRD peaks gradually broadened. The peak broadening is attributed to interfacial interactions between the perovskite phase and the MOF glass phase during the mechanochemical process. The particle size distribution within the composite confirms the presence of a quantum confinement effect (Fig. 14j), which significantly enhances phase stability, PLQY, and solvent resistance. Structural analysis reveals that the mechanochemical process facilitates interfacial bonding between the perovskite and the MOF glass, including Zn-halogen and Pb-imidazolate bonds, effectively passivating surface defects and suppressing phase separation. This enables deep blue and violet emissions with CIE chromaticity coordinates of (0.134, 0.045) and (0.152, 0.031), respectively, rendering the composites suitable for next-generation LED devices (Fig. 14k). Collectively, these studies elucidate the critical role of MOF glasses in perovskite luminescent composites. Through physical confinement and chemical interface engineering, the MOF host significantly enhances quantum yield and stability. This approach offers a scalable route for developing high-performance white and blue LEDs, while simultaneously mitigating lead toxicity concerns, thereby advancing sustainable optoelectronic applications.

3.3. Luminescent RE@MOF glasses

Despite the considerable potential of MOF glasses in luminescent materials, the effective incorporation of RE ions (e.g., Eu^{3+}, Tb^{3+}, Nd^{3+}) remains challenging, keeping research on RE-doped MOF luminescent glasses at an early stage. First, the large ionic radius and complex coordination preferences of RE ions are often incompatible with the metal nodes (e.g., Zn^{2+}, Co^{2+}) in conventional MOF frameworks, hindering stable incorporation [241]. Furthermore, melt-quenching of MOF glasses generally requires high temperatures (300–500 °C), which can cause RE ions to be lost via thermal decomposition, coordination bond cleavage, or side reactions with organic ligands (e.g., imidazolates),

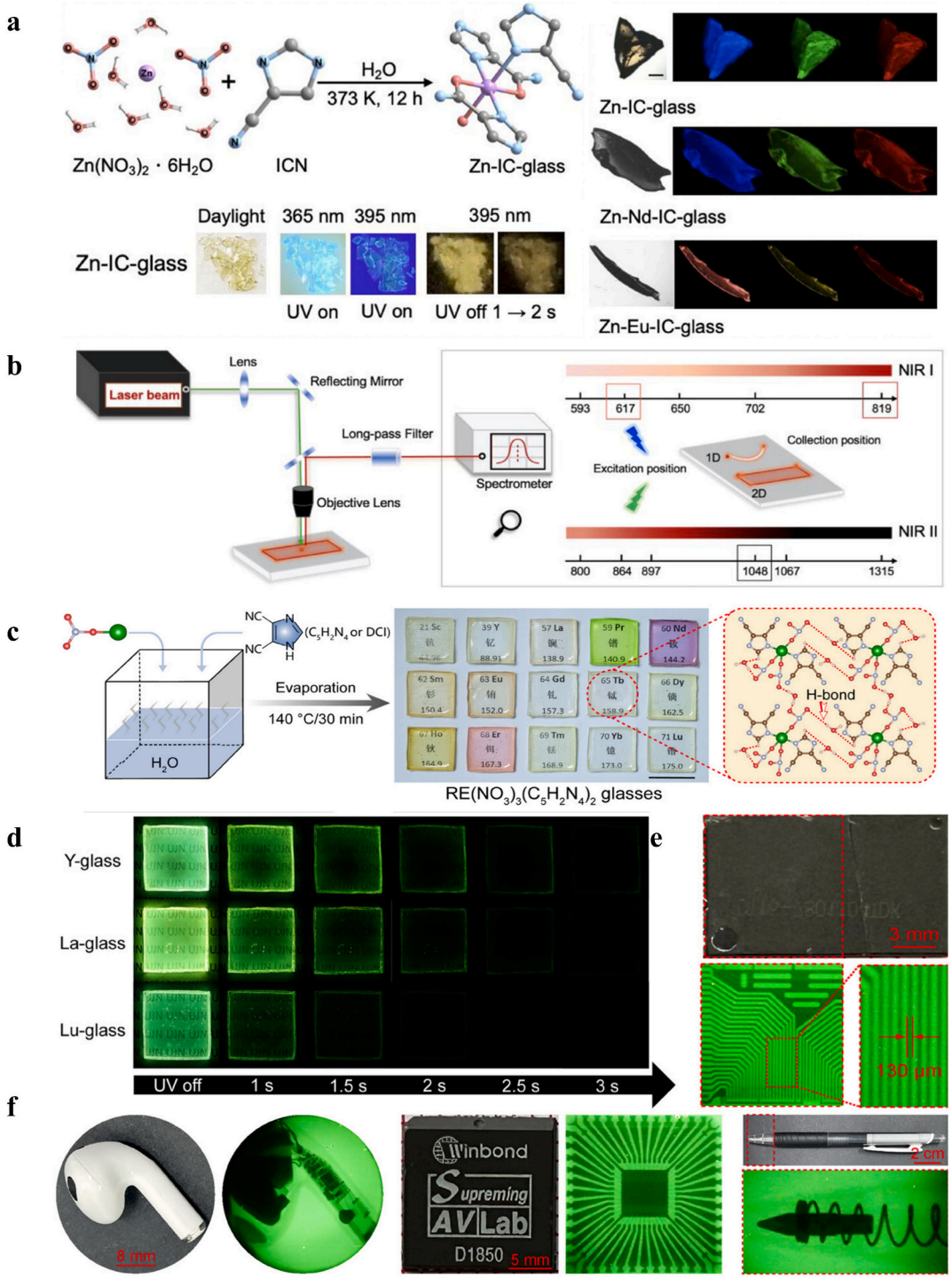

Fig. 15. Preparation and applications of RE Hybrid Glasses. a) Synthesis process of Zn–IC–glass and the photographs under daylight and UV light (365/395 nm), Fluorescence microscopy images of the undoped, Nd^{3+}-doped, and Eu^{3+}-doped glasses (scale bar: 500 μm). b) Experimental setup for optical waveguide measurements. Reproduced with permission [247]. Copyright 2025, Wiley-VCH GmbH. c) Desolvation synthesis of RE hybrid glasses (scale bar: 2 cm). Inset: Proposed hydrogen-bonding network (Color codes: Tb-green, O-red, N-silver, C-brown, H-pink). d) Afterglow photographs of Y-, La-, and Lu-based hybrid glass under 365 nm excitation. X-ray imaging of e) a cellphone chip, f) an earphone, a microchip, and a pen. Reproduced with permission [248]. Copyright 2025, SCUT, AIEI, and John Wiley & Sons Australia, Ltd. (For interpretation of the references to color in this figure legend, the reader is referred to the web version of this article.)

producing non-luminescent byproducts. This consequently decreases luminescence efficiency and impairs the glass-forming ability. Second, while the disordered structure of MOF glasses helps mitigate concentration quenching, the low absorption cross-section of RE ions makes them highly reliant on the "antenna effect" provided by organic ligands [242–245]. Vitrification is often accompanied by pore collapse and ligand degradation, which diminishes energy transfer efficiency and generally results in low PLQY, often below 10% [246]. This incompatibility stems from the fact that traditional high-temperature melt-quenching can induce decomposition of organic ligands or disrupt the coordination environment around RE ions, resulting in luminescence quenching. Coupled with the difficulties of low-temperature alternative methods (e.g., sol–gel) in maintaining the integrity of MOF frameworks, these factors often lead to failed vitrification or aggregation of luminescent centers. These challenges arise from the intrinsic mismatch between the organic-inorganic hybrid nature of MOF systems and the chemical characteristics of RE elements, leading to a significant delay in the development of RE@MOF glasses compared to QDs@MOF systems.

Notably, the RE single-atom hybrid glass [e.g., Zn–Nd–IC glasses (Zinc–Neodymium–4-cyanoimidazolate hybrid glasses)] developed by Dai et al. [247] in 2025 and the transparent RE-based hybrid glass [e.g., $RE(NO_3)_3(C_5H_2N_4)_2$ glasses ($C_5H_2N_4$ = 4,5-dicyanoiazole or DCI)] reported by Zhang's group [248], although not strictly classified as RE@MOF glasses, provide important guidance for future research through their successful strategies in RE ion incorporation and performance optimization. These metal-organic composite glasses effectively resolve critical challenges (including RE ion dispersion, stability, and luminescence efficiency in amorphous hosts) through innovative synthetic approaches and structural design, providing feasible technical strategies for the future development of RE@MOF glasses.

Dai et al. prepared an RE single-atom hybrid glass using a bottom-up self-assembly strategy (Fig. 15a). Using an Nd^{3+}-doped metal-organic complex as the host, they realized ultra-long room-temperature phosphorescence and efficiently activated Nd^{3+} emission in the second NIR window (NIR-II, up to 1.32 μm) via highly efficient energy transfer (93.55%), achieving a PLQY of 5.7%, setting a record for this class of materials in the NIR-II region. The significance of this approach for RE MOF glasses lies in its employment of a triplet-to-RE resonance energy transfer mechanism within the complex glass, analogous to the ligand antenna effect in MOFs, while circumventing high-temperature processing. The glass exhibits both flexibility and high transparency, enabling low-loss optical waveguiding in Eu^{3+}/Nd^{3+}-doped microstructures (loss of 0.978 $dB{\cdot}mm^{-1}$ at 819 nm and 5.1 $dB{\cdot}mm^{-1}$ at 1048 nm), demonstrating potential for optical communication and tumor diagnostics (Fig. 15b). This self-assembly strategy serves as a reference for future studies on RE@MOF luminescent glasses, particularly regarding low-temperature synthesis and energy transfer optimization. Similarly, Wei et al. developed a mild desolvation method, rapidly synthesizing a complete RE family-based hybrid glass (including Y, Sc, and lanthanides), $RE(NO_3)_3(C_5H_2N_4)_2$, within 1 h at 140 °C (Fig. 15c). This glass demonstrates a transmittance exceeding 88% and a high PLQY of 70%. It preserves the structural integrity of the organometallic framework via hydrogen bonding, promoting singlet/triplet radiative recombination in the organic moiety (DCI) and facilitating efficient energy transfer (antenna effect) to RE ions. Doping with non-luminescent RE elements (e.g., La, Y, Lu) further enhanced room-temperature phosphorescence and expanded the range of multicolor luminescence (Fig. 15d). In X-ray imaging, this material exhibited excellent radiation hardness as a high-spatial-resolution scintillation screen, making it suitable for medical diagnostics (Fig. 15e, f). The relevance of this research to RE@MOF glasses lies in its use of hydrogen bonding to enhance framework stability and the antenna effect. Its low-temperature desolvation strategy offers a reference for the stable integration of RE ions into MOF frameworks and the achievement of efficient NIR emission.

Although the two aforementioned studies focused on complex glasses rather than MOF systems, their low-temperature and self-assembly strategies can be directly applied to the development of RE-based MOF glasses. For example, adopting desolvation or self-assembly routes can effectively lower the melting temperature, while optimizing ligand frameworks (e.g., imidazole- or cyano-based ligands) can enhance the antenna effect and hydrogen-bond stability, thus enabling uniform RE-ion dispersion and efficient NIR-II emission in MOF glasses [249]. In future studies, optimizing the RE–MOF coordination environment through interface engineering and DFT simulations holds great potential for addressing the current research gap in RE@MOF glasses. Such efforts are expected to enable breakthrough applications in NIR communication, optical waveguides, and X-ray imaging. The implementation of these strategies is expected to substantially reduce fabrication challenges and enhance energy-transfer efficiency, paving the way toward RE-based MOF glasses with high PLQY and versatile luminescent properties.

3.4. Luminescent diversity of CP glasses

While MOF glasses, especially ZIF systems, show significant potential in luminescent applications, their development is constrained by a severe trade-off between GFA and the intrinsic luminescent efficiency of the precursors. Conceptually, MOFs typically refer to 3D coordination networks with potential porosity and highly ordered crystalline structures. In contrast, CPs represent a more inclusive category, encompassing all infinite repeating hybrid networks constructed from metal centers and organic ligands via coordination bonds. From a taxonomic perspective, MOFs constitute a subset of the CP family with specific topological features. However, due to the milestone progress in the melting behavior of classical systems such as ZIF-4 and ZIF-62, early literature predominantly focused on "MOF glass" as the core terminology. While this terminological bias defined initial research boundaries, it obscured the lack of material diversity: most 3D MOFs undergo thermal decomposition before reaching the glass transition temperature. Consequently, "dual-functional" candidates combining melt-processability with high-efficiency luminescence are extremely scarce. This scarcity of candidate matrices has become a major bottleneck limiting performance breakthroughs in luminescent composite glasses. Therefore, expanding the research perspective from restricted MOFs to the broader field of CPs is a logical evolution and a return to the essence of coordination chemistry. Although "CP glass" appeared less frequently in early literature, its structural flexibility far exceeds that of traditional MOFs. By breaking the rigid constraints of 3D frameworks, CPs offer a complete dimensional spectrum ranging from 1D chains and 2D layers to complex 3D networks [211,213,250]. This dimensional expansion greatly enriches the tunability of coordination environments, allowing a wider range of luminescent centers—such as rare-earth ions, transition metal complexes, and functional ligands—to achieve optimal anchoring within the amorphous matrix. This shift in perspective provides a solid theoretical and material foundation for overcoming the intrinsic defects of MOF glasses and achieving the on-demand design of high-performance hybrid luminescent glasses [220].

Notably, after amorphization, the traditional distinction between MOF glasses and CP glasses becomes increasingly blurred. Collectively, they can be classified under the broader category of MCC glasses. Regardless of whether they originate from MOFs or CPs, their amorphous states exhibit three-dimensional coordination networks composed of metal nodes and organic ligands linked through coordination bonds, characterized by long-range disorder yet short-range order, and displaying comparable glass-transition behaviors and structural stability mechanisms. Therefore, when examining their luminescent properties, it is advantageous to integrate them within the unified framework of "luminescent coordination compound glasses". This approach not only compensates for the limitations of studies focusing solely on individual MOF systems but also, from a more fundamental perspective of metal–ligand coordination chemistry, elucidates their structure–property

relationships and luminescence mechanisms, thereby advancing the field toward more diverse and sophisticated optical functional applications.

The potential of CP glasses for achieving diverse luminescent behaviors is further exemplified by their ability to precisely regulate RTP. In a 2024 study, Gong et al. synthesized transparent $ZnX_2(bIm)_2$ glasses via a melt-quenching process (Fig. 16a), successfully realizing dynamic modulation of both temporal and spectral phosphorescence characteristics [67]. By exploiting the intrinsic molecular rigidity of $ZnX_2(bIm)_2$ glasses and the tunable spin–orbit coupling effect, the authors developed a glass system featuring customizable ultra-long phosphorescence lifetimes. Notably, introducing heavy halogen atoms (e.g., Br or I) markedly enhanced spin–orbit coupling, accelerating the singlet-to-triplet intersystem crossing and consequently prolonging phosphorescence lifetimes while improving overall luminescence efficiency. This exploitation of the heavy-atom effect offers a novel pathway for finely

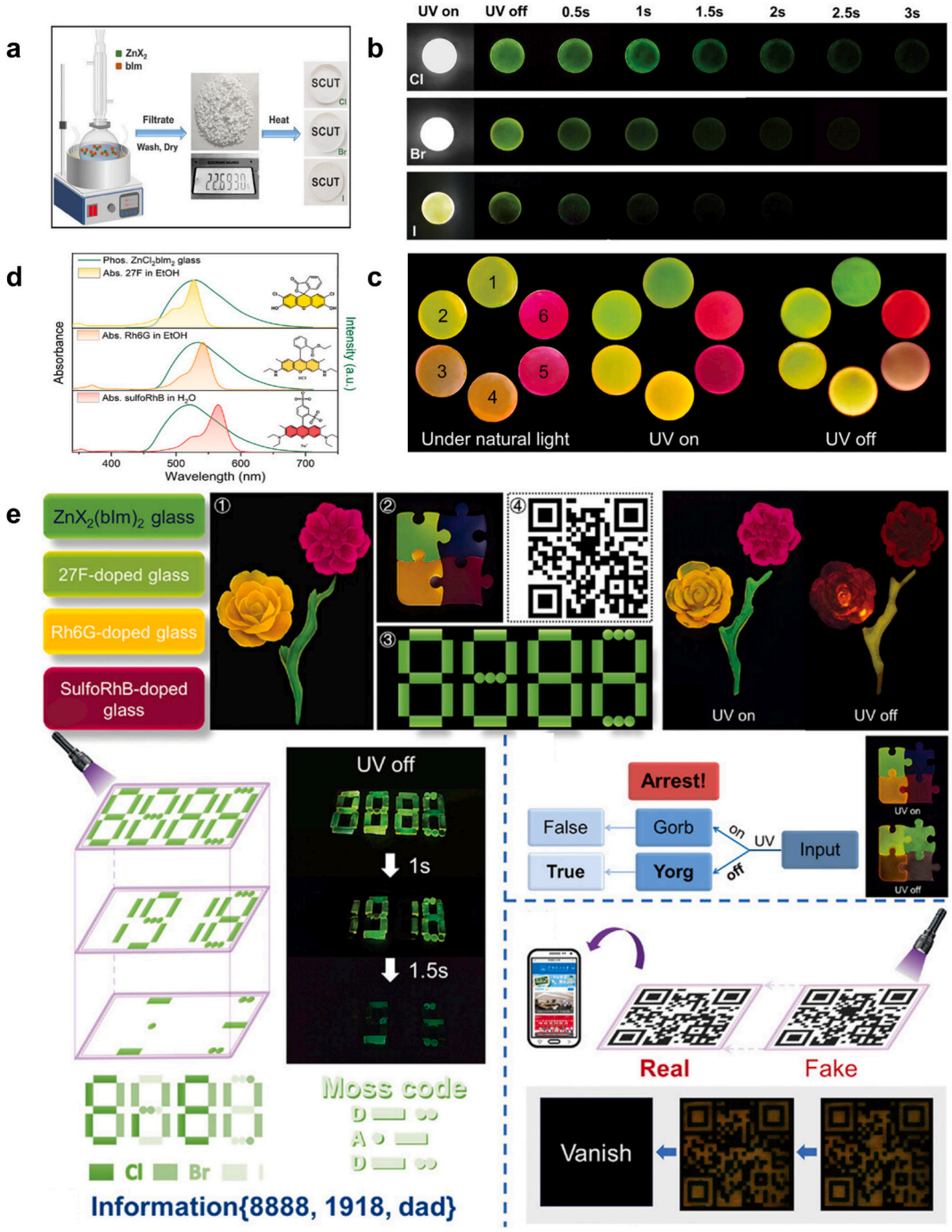

Fig. 16. Preparation and applications of $ZnX_2(bIm)_2$ (X = Cl, Br, and I) Glasses. a) Preparation procedures for the $ZnX_2(bIm)_2$ glass, the photos are taken under natural room light illumination. b) Luminescence photographs of $ZnX_2(bIm)_2$ glass taken under illumination with a UV lamp and the series of photographs taken after switching off UV light for different durations. c) Luminescence photographs of dye-codoped $ZnCl_2(bIm)_2$ glass under illumination with natural light (left), UV on (middle), and UV off (right). 1–2: 27F-codoped, 3–4: Rh6G-codoped and 5–6: sulfoRhB-codoped glass with different doping concentrations. d) Overlapped phosphorescence spectrum of $ZnCl_2(bIm)_2$ glass (energy donor: green line) and the absorption spectrum of dye (energy acceptor: yellow, orange and red line). e) Schematic illustration of various applications in the dye-encapsulated glass system. Reproduced with permission [67]. Copyright 2024, Wiley-VCH GmbH. (For interpretation of the references to color in this figure legend, the reader is referred to the web version of this article.)

tuning phosphorescence lifetimes, allowing controllable modulation over a wide temporal range from milliseconds to several seconds (Fig. 16b). Furthermore, doping dye molecules into the $ZnCl_2(bIm)_2$ glass host enabled tunable photoluminescence, with the emission color shifting from green to yellow, orange, and finally red under UV irradiation (Fig. 16c, middle). In contrast, the delayed luminescence of the doped glass shifts from yellowish-green to red after cessation of UV excitation (Fig. 16c, right). Optimization of the dye composition and concentration further enabled wavelength-tunable and long-lived delayed fluorescence. Through an efficient delayed sensitization mechanism, the emission spectrum was broadened to cover a wide range from 520 to 630 nm (Fig. 16d). This strategy not only expanded the accessible luminescent color range but also enabled multimodal optical information storage and dynamic anti-counterfeiting functionalities through multi-channel spectral modulation (Fig. 16e). For example, in dynamic anti-counterfeiting applications, differences in phosphorescence lifetime and emission wavelength were exploited to design time-resolved information display systems, offering enhanced security and authentication capabilities. The hybrid material platform and design methodology established in this work open new avenues for realizing long-persistent luminescence with tunable lifetimes and precisely controllable emission wavelengths. Compared with conventional inorganic glasses, CP glasses offer distinctive advantages arising from their intrinsic molecular rigidity and flexible coordination bonding, rendering them ideal candidates for time-resolved displays, high-density optical data storage, and dynamic anti-counterfeiting applications. This advancement not only deepens the understanding of luminescence mechanisms in CP glasses but also introduces innovative design paradigms for photofunctional coordination materials, particularly highlighting their significant potential in halogen-controlled modulation and phosphorescence tuning.

Furthermore, composites integrating CP glasses with PeQDs have recently emerged as a major breakthrough in the field of luminescent materials. By integrating $CsPbX_3$ (X = Cl, Br, I) QDs with low-melting-point CP glasses (e.g., $ZnBr_2(bIm)_2$), these composites achieve a synergistic combination of high optical transparency, excellent environmental stability, and tunable luminescent performance. In 2025, Peng et al. reported an in situ crystallization strategy to embed $CsPbBr_3$ QDs within a $ZnBr_2(bIm + DMSO)_2$ (DMSO stands for dimethyl sulfoxide.) glass host, thereby realizing a high-resolution X-ray scintillation screen (Fig. 17a) [68]. The $CsPbBr_3$@$ZnBr_2(bIm + DMSO)_2$ (CPB@$ZnBr_2(bIm + DMSO)_2$) glass was fabricated via melt-quenching of a homogeneous mixture of $ZnBr_2(bIm)_2$, CsBr, $PbBr_2$, and DMSO at 280 °C, followed by a mild post-annealing treatment (50 °C, 0–15 min). Optical photographs of CPB@$ZnBr_2(bIm + DMSO)_2$ glasses subjected to different annealing durations are shown in Fig. 17b. The untreated glass exhibits blue emission under UV excitation, originating from the $ZnBr_2(bIm + DMSO)_2$ glass host. With increasing annealing time, the glasses exhibit uniform and intense green emission, indicating the formation and growth of emissive $CsPbBr_3$ nanocrystals (NCs). The in situ thermally induced crystallization process is schematically illustrated in Fig. 17c. For practical demonstration, Fig. 17d presents the indirect X-ray imaging setup, where the CPB@$ZnBr_2(bIm + DMSO)_2$ glass functions as a scintillating screen. The material achieves a spatial resolution of 25 $lp{\cdot}mm^{-1}$ (Fig. 17e), surpassing most previously reported perovskite and inorganic glass scintillators. As shown in Fig. 17f, the fine internal circuitry of an integrated chip is clearly visualized, while Fig. 17g reveals distinct imaging of a copper grid with 25 μm features, underscoring the material's exceptional spatial resolution and imaging precision. In summary, CP glass/PeQDs composites fabricated via the in situ crystallization strategy exhibit highly efficient, stable, and tunable luminescent properties. These materials show broad application potential in X-ray imaging, LEDs, and photodetectors. Future research should focus on precise interface engineering and optimization of scalable fabrication processes.

4. Summary and outlook

As an emerging class of amorphous functional materials, MOF glasses have rapidly evolved into a frontier research field at the intersection of materials science and photonics, owing to their exceptional structural tunability, outstanding processability, and versatile optical functionalities [197,251]. This review systematically summarizes recent advances in MOF glasses, encompassing their structural fundamentals, formation mechanisms, synthesis strategies, luminescent behaviors, and emerging applications. It further incorporates CP glasses to present a comprehensive perspective on the broader class of coordination compound glasses. Nevertheless, a significant research gap remains: the effective integration of MOF glasses with RE activators is still in its infancy, representing not only a present limitation but also a crucial direction for future breakthroughs.

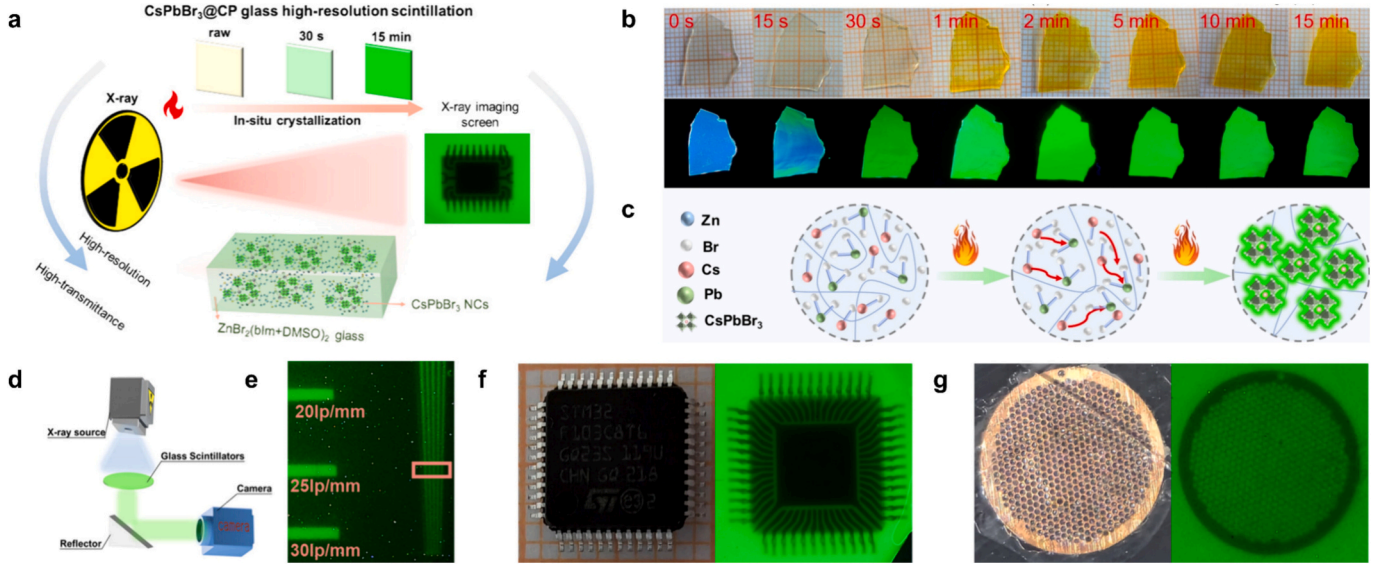

Fig. 17. In Situ crystallization and applications of CPB@$ZnBr_2(bIm + DMSO)_2$ Glass. a) Composite material of CP glass and PeQDs. b) Photographs of the CPB@$ZnBr_2(bIm + DMSO)_2$ glasses prepared with different thermal treatment times. c) Schematic diagram of in situ crystallization process of CPB@$ZnBr_2(bIm + DMSO)_2$ glass. d) Schematic illustration of the as-designed indirect X-ray imaging system. e) X-ray imaging of a lead-made line pair card. f, g) Photographs and X-ray images of differently sized chips and the copper wire mesh. Reproduced with permission [68]. Copyright 2025, American Chemical Society.

Research on MOF glasses began with the melt-quenching amorphization of ZIF-4 crystals, with foundational work on systems like ZIF-62 establishing their formation basis. The core mechanism lies in the thermally induced breaking and reformation of coordination bonds (e.g., Zn—N), combined with the steric hindrance effects of large-sized ligands, which collectively inhibit crystallization and result in a glassy state characterized by long-range disorder and short-range order. Ligand chemistry is decisive for the GFA. For instance, introducing large-volume ligands like bIm into Cd-based or Zn-based systems can lower the T_m and ΔH_m, while raising the T_g, thereby enhancing GFA. Preparation methods include melt-quenching (limited by high temperatures), mechanical ball milling (enabling room-temperature amorphization and expanding the diversity of metal nodes and ligands), and desolvation (directly inducing a glassy state by solvent removal, suitable for carboxylate systems). These methods have collectively driven the diversification of MOF glasses beyond ZIF systems to include nitrile-, amide-, and carboxylate-based frameworks, with recent Fe-based and Cd-based systems further enriching their chemical diversity.

Regarding luminescent properties, the amorphous host of MOF glasses offers high transparency, isotropy, and formability, which effectively disperses luminescent centers, suppresses concentration quenching, and enhances luminescence efficiency through a rigid environment. For example, ZIF-62 glass can be drawn into low-loss optical fibers (~0.72 dB·cm^{-1}), enabling multicolor luminescence and dynamic phosphorescence-based oxygen sensing. When composited with PeQDs, interfacial coordination (e.g., Pb—N, Zn—I) passivates surface defects, achieving PLQY >65%, maintaining stability even after 10,000 h in water, and leading to successful applications in wide-color-gamut white LEDs and X-ray imaging. It is noteworthy that due to the limited number of MOF precursors suitable for vitrification and the difficulty of directly incorporating RE ions into classic frameworks like ZIFs, research on RE luminescence in MOF glasses is currently almost non-existent. This, however, is precisely a key direction for future breakthroughs. Achieving this integration requires innovative synthesis strategies, such as, designing novel RE-based MOF precursors capable of low-temperature melting or mechanochemical vitrification, developing post-synthetic doping techniques to introduce RE ions into pre-formed MOF glass networks, or exploring the encapsulation of RE complexes as guest molecules within the pores of MOF glasses. Concurrently, the broader family of CP glasses offers greater flexibility for luminescent material design. For instance, $ZnX_2(bIm)_2$ glasses utilize the halogen heavy-atom effect to tune phosphorescence for anti-counterfeiting and imaging applications. This highlights the importance of exploring new luminescent materials from the fundamental perspective of "metal-ligand" coordination chemistry.

Notably, MOF and CP glasses present a range of promising opportunities alongside significant challenges. The foremost challenge lies in addressing the research gap in integrating MOF glasses with RE centers. Achieving this goal necessitates close collaboration among chemists, materials scientists, and photonics experts to design innovative coordination systems that simultaneously exhibit high GFA and efficient RE ions luminescence. Concurrently, for QDs and MOF glasses composite systems, critical challenges (such as uniform QDs dispersion within the MOF host, interfacial stability, and energy transfer efficiency) must be tackled. For instance, current challenges like QDs agglomeration and surface oxidation necessitate optimization through ligand engineering or interfacial bonding (e.g., Zn—I, Pb—N bonds) to passivate defects, thereby enhancing PLQY and environmental tolerance. Secondly, it is essential to advance the understanding of structure–property relationships during vitrification, particularly regarding the local coordination environment of luminescent centers, energy transfer pathways, and interfacial interactions. This necessitates the employment of advanced in-situ characterization techniques combined with theoretical simulations. Thirdly, efforts should be directed toward expanding the diversity of CP glass systems by exploring a broader array of metal nodes (e.g., lanthanides, actinides) and functional ligands, with the goal of developing luminescent glasses exhibiting advanced functionalities such as magnetism, chirality, and stimuli-responsiveness. Fourthly, it is imperative to advance the translation of these materials from laboratory research to practical applications. This entails the development of scalable fabrication techniques (e.g., 3D printing, thin-film deposition, fiber drawing) and the exploration of their integration into devices such as micro-lasers, flexible sensors, radiation detection screens, and quantum information storage systems. Finally, achieving the synergistic integration of RE ions and QDs within MOF/CP glasses represents a highly promising avenue. In such systems, QDs could serve as broadband absorption "antennas," efficiently transferring energy to RE ions to enable broad-spectrum modulation from UV to NIR and achieve multimodal luminescence. Such an approach would establish a foundational material platform for next-generation lighting, display, communication, and bioimaging technologies.

Declaration of competing interest

The authors declare that they have no known competing financial interests or personal relationships that could have appeared to influence the work reported in this paper.

Acknowledgements

This research was supported by National Natural Science Foundation of China (52572155, 52272141), and Natural Science Foundation of Fujian Province (2024J02014).

Data availability

Data will be made available on request.

References

[1] J. Sun, H. Fu, H. Jing, X. Hu, D. Chen, F. Li, Y. Liu, X. Qin, W. Huang, Synergistic integration of halide perovskite and rare-earth ions toward photonics, Adv. Mater. 37 (2025) 2417397, https://doi.org/10.1002/adma.202417397.
[2] J.-B. Luo, J.-H. Wei, Z.-L. He, J.-H. Chen, Q.-P. Peng, Z.-Z. Zhang, D.-B. Kuang, Bisphosphonium cation based metal halide glass scintillators with tunable melting points, Chem. Sci. 15 (2024) 16338–16346, https://doi.org/10.1039/D4SC04229H.
[3] J. Wei, J. Luo, Z. He, Q. Peng, J. Chen, Z. Zhang, X. Guo, D. Kuang, Phosphonium iodide featuring blue thermally activated delayed fluorescence for highly efficient X-ray scintillator, Angew. Chem. Int. Ed. 63 (2024) e202410514, https://doi.org/10.1002/anie.202410514.
[4] J. Luo, J. Wei, Z. Zhang, Z. He, D. Kuang, A melt-quenched luminescent glass of an organic–inorganic manganese halide as a large-area scintillator for radiation detection, Angew. Chem. Int. Ed. 62 (2023) e202216504, https://doi.org/10.1002/anie.202216504.
[5] X. Pei, Y. Cai, Z. Mi, L. Fan, T. Jiang, L. Liu, C. Li, H. Lin, S. Li, W. Yang, F. Zeng, Dual-site cooperative regulation strategy enables high-performance near-infrared luminescence and wireless communication applications of Cr^{3+} activated garnet phosphors, Laser Photonics Rev. (2025) e01792, https://doi.org/10.1002/lpor.202501792.
[6] H. Guo, Y. Lin, S. Gu, G. Hu, Q. Wang, C. Bai, Y. Sun, C. Yang, T. Fang, X. Chen, D. Li, D. Kong, Stretchable and breathable electroluminescent displays based on ultrathin nanocomposite designs, Nano Lett. 24 (2024) 5904–5912, https://doi.org/10.1021/acs.nanolett.4c01332.
[7] G. Xi, S. Lin, T. Shen, T. Pang, Z. Yu, Y. Peng, L. Zeng, Y. Ke, Z. Zhou, R. Chen, F. Huang, D. Chen, Transparent ceramic@sapphire composites for high-power laser-driven lighting, Adv. Sci. 12 (2025) 2505232, https://doi.org/10.1002/advs.202505232.
[8] B. Xu, C. Jin, J. Park, H. Liu, X. Lin, J. Cui, D. Chen, J. Qiu, Emerging near-infrared luminescent materials for next-generation broadband optical communications, InfoMat 6 (2024) e12550, https://doi.org/10.1002/inf2.12550.
[9] Y. Wang, X.-B. Yin, Persistent luminescence materials for imaging and therapeutic applications, Coord. Chem. Rev. 522 (2025) 216192, https://doi.org/10.1016/j.ccr.2024.216192.
[10] B. Wang, H. Wang, B. Zhang, Y. Hu, S. Lu, Hot exciton carbon dots-based deep blue electroluminescent light-emitting diodes exceeding 7% external quantum efficiency, Adv. Funct. Mater. 34 (2024) 2404437, https://doi.org/10.1002/adfm.202404437.
[11] Y. Li, W. Gao, H. Ruan, L. Wang, S. Liao, Y. Huang, Li^{+} co-doping and hydrophobic surface modification enhance the luminescence and moisture resistance of Mn^{4+}-doped fluoride phosphors, Mater. Today Chem. 48 (2025) 102909, https://doi.org/10.1016/j.mtchem.2025.102909.

[12] J. Liu, Z. Yang, B. Ye, Z. Zhao, Y. Ruan, T. Guo, X. Yu, G. Chen, S. Xu, A review of stability-enhanced luminescent materials: fabrication and optoelectronic applications, J. Mater. Chem. C 7 (2019) 4934–4955, https://doi.org/10.1039/C8TC06292G.

[13] Y. Wang, K. Wang, Z. Han, Z. Yin, C. Zhou, F. Du, S. Zhou, P. Chen, Z. Xie, High color rendering index trichromatic white and red LEDs prepared from silane-functionalized carbon dots, J. Mater. Chem. C 5 (2017) 9629–9637, https://doi.org/10.1039/C7TC02297B.

[14] X.-Q. Pei, L.-N. Liu, C. Li, H. Lin, S.-S. Li, W.-L. Yang, F.-M. Zeng, The synergy of structural constraints and lattice engineering endows $Ba_{2.80}Sr_{0.20}Sc(BO_2)_9$: Eu^{3+} phosphor with a concentration-free quenching effect and far-red emission, Rare Metals (2025), https://doi.org/10.1007/s12598-025-03513-6.

[15] D.P. Strandell, D. Zenatti, P. Nagpal, A. Ghosh, D.N. Dirin, M.V. Kovalenko, P. Kambhampati, Hot excitons cool in metal halide perovskite nanocrystals as fast as CdSe nanocrystals, ACS Nano 18 (2024) 1054–1062, https://doi.org/10.1021/acsnano.3c10301.

[16] M.S. Zaini, J. Ying Chyi Liew, S.A. Alang Ahmad, A.R. Mohmad, M.A. Kamarudin, Quantum confinement effect and photoenhancement of photoluminescence of PbS and PbS/MnS quantum dots, Appl. Sci. 10 (2020) 6282, https://doi.org/10.3390/app10186282.

[17] L. Protesescu, S. Yakunin, M.I. Bodnarchuk, F. Krieg, R. Caputo, C.H. Hendon, R. X. Yang, A. Walsh, M.V. Kovalenko, Nanocrystals of cesium Lead halide perovskites ($CsPbX_3$, X = cl, Br, and I): novel optoelectronic materials showing bright emission with wide color gamut, Nano Lett. 15 (2015) 3692–3696, https://doi.org/10.1021/nl5048779.

[18] Q.A. Akkerman, G. Rainò, M.V. Kovalenko, L. Manna, Genesis, challenges and opportunities for colloidal lead halide perovskite nanocrystals, Nat. Mater. 17 (2018) 394–405, https://doi.org/10.1038/s41563-018-0018-4.

[19] F. Zhang, H. Zhong, C. Chen, X. Wu, X. Hu, H. Huang, J. Han, B. Zou, Y. Dong, Brightly luminescent and color-tunable colloidal $CH_3NH_3PbX_3$ (X = Br, I, cl) quantum dots: potential alternatives for display technology, ACS Nano 9 (2015) 4533–4542, https://doi.org/10.1021/acsnano.5b01154.

[20] Y. Wei, Z. Cheng, J. Lin, Correction: An overview on enhancing the stability of lead halide perovskite quantum dots and their applications in phosphor-converted LEDs, Chem. Soc. Rev. 48 (2019) 405, https://doi.org/10.1039/C8CS90134A.

[21] X. Li, Y. Wu, S. Zhang, B. Cai, Y. Gu, J. Song, H. Zeng, $CsPbX_3$ quantum dots for lighting and displays: room-temperature synthesis, photoluminescence superiorities, underlying origins and white light-emitting diodes, Adv. Funct. Mater. 26 (2016) 2435–2445, https://doi.org/10.1002/adfm.201600109.

[22] J.A. Steele, H. Jin, I. Dovgaliuk, R.F. Berger, T. Braeckevelt, H. Yuan, C. Martin, E. Solano, K. Lejaeghere, S.M.J. Rogge, C. Notebaert, W. Vandezande, K.P. F. Janssen, B. Goderis, E. Debroye, Y.-K. Wang, Y. Dong, D. Ma, M. Saidaminov, H. Tan, Z. Lu, V. Dyadkin, D. Chernyshov, V. Van Speybroeck, E.H. Sargent, J. Hofkens, M.B.J. Roeffaers, Thermal unequilibrium of strained black $CsPbI_3$ thin films, Science 365 (2019) 679–684, https://doi.org/10.1126/science.aax3878.

[23] A. Swarnkar, W.J. Mir, A. Nag, Can B-site doping or alloying improve thermal- and phase-stability of all-inorganic $CsPbX_3$ (X = cl, Br, I) perovskites? ACS Energy Lett. 3 (2018) 286–289, https://doi.org/10.1021/acsenergylett.7b01197.

[24] A. Swarnkar, V.K. Ravi, A. Nag, Beyond colloidal cesium Lead halide perovskite nanocrystals: analogous metal halides and doping, ACS Energy Lett. 2 (2017) 1089–1098, https://doi.org/10.1021/acsenergylett.7b00191.

[25] M. Zhang, Z. Lin, Efficient interconnecting layers in monolithic all-perovskite tandem solar cells, Energy Environ. Sci. 15 (2022) 3152–3170, https://doi.org/10.1039/D2EE00731B.

[26] Z. Zeng, B. Huang, X. Wang, L. Lu, Q. Lu, M. Sun, T. Wu, T. Ma, J. Xu, Y. Xu, S. Wang, Y. Du, C. Yan, Multimodal luminescent Yb^{3+} /Er^{3+} /Bi^{3+} -doped perovskite single crystals for X-ray detection and anti-counterfeiting, Adv. Mater. 32 (2020) 2004506, https://doi.org/10.1002/adma.202004506.

[27] L. Lu, M. Sun, T. Wu, Q. Lu, B. Chen, B. Huang, All-inorganic perovskite nanocrystals: next-generation scintillation materials for high-resolution X-ray imaging, Nanoscale Adv. 4 (2022) 680–696, https://doi.org/10.1039/D1NA00815C.

[28] B. Chen, R. Chen, B. Huang, Strong electron–phonon coupling induced self-trapped excitons in double halide perovskites, Adv. Energy Sustainability Res. 4 (2023) 2300018, https://doi.org/10.1002/aesr.202300018.

[29] Y. Jiang, X. Wang, A. Pan, Properties of excitons and Photogenerated charge carriers in metal halide perovskites, Adv. Mater. 31 (2019) 1806671, https://doi.org/10.1002/adma.201806671.

[30] M.V. Kovalenko, L. Protesescu, M.I. Bodnarchuk, Properties and potential optoelectronic applications of lead halide perovskite nanocrystals, Science 358 (2017) 745–750, https://doi.org/10.1126/science.aam7093.

[31] M. Gandini, I. Villa, M. Beretta, C. Gotti, M. Imran, F. Carulli, E. Fantuzzi, M. Sassi, M. Zaffalon, C. Brofferio, L. Manna, L. Beverina, A. Vedda, M. Fasoli, L. Gironi, S. Brovelli, Efficient, fast and reabsorption-free perovskite nanocrystal-based sensitized plastic scintillators, Nat. Nanotechnol. 15 (2020) 462–468, https://doi.org/10.1038/s41565-020-0683-8.

[32] X.-K. Liu, W. Xu, S. Bai, Y. Jin, J. Wang, R.H. Friend, F. Gao, Metal halide perovskites for light-emitting diodes, Nat. Mater. 20 (2021) 10–21, https://doi.org/10.1038/s41563-020-0784-7.

[33] J.M. Tuffnell, C.W. Ashling, J. Hou, S. Li, L. Longley, M.L. Ríos Gómez, T. D. Bennett, Novel metal–organic framework materials: blends, liquids, glasses and crystal–glass composites, Chem. Commun. 55 (2019) 8705–8715, https://doi.org/10.1039/C9CC01468C.

[34] N. Ma, S. Horike, Metal–organic network-forming glasses, Chem. Rev. 122 (2022) 4163–4203, https://doi.org/10.1021/acs.chemrev.1c00826.

[35] Y. Wei, C.W. Ashling, T. Watcharatpong, Z. Fan, S. Horike, Hierarchical metal-organic network-forming glasses toward applications, Adv. Funct. Mater. 34 (2024) 2307226, https://doi.org/10.1002/adfm.202307226.

[36] S.S. Kaye, A. Dailly, O.M. Yaghi, J.R. Long, Impact of preparation and handling on the hydrogen storage properties of Zn_4 O(1,4-benzenedicarboxylate)$_3$ (MOF-5), J. Am. Chem. Soc. 129 (2007) 14176–14177, https://doi.org/10.1021/ja076877g.

[37] H. Furukawa, K.E. Cordova, M. O'Keeffe, O.M. Yaghi, The chemistry and applications of metal-organic frameworks, Science 341 (2013) 1230444, https://doi.org/10.1126/science.1230444.

[38] S.R. Batten, N.R. Champness, X.-M. Chen, J. Garcia-Martinez, S. Kitagawa, L. Öhrström, M. O'Keeffe, M. Paik Suh, J. Reedijk, Terminology of metal–organic frameworks and coordination polymers (IUPAC recommendations 2013), Pure Appl. Chem. 85 (2013) 1715–1724, https://doi.org/10.1351/PAC-REC-12-11-20.

[39] C. Zhu, J. Hou, X. Wang, S. Wang, H. Xu, J. Hu, L. Jing, S. Wang, Optimizing ligand-to-metal charge transfer in metal–organic frameworks to enhance photocatalytic performance, Chem. Eng. J. 499 (2024) 156527, https://doi.org/10.1016/j.cej.2024.156527.

[40] S. Horike, D. Umeyama, M. Inukai, T. Itakura, S. Kitagawa, Coordination-network-based ionic plastic crystal for anhydrous proton conductivity, J. Am. Chem. Soc. 134 (2012) 7612–7615, https://doi.org/10.1021/ja301875x.

[41] S. Li, R. Limbach, L. Longley, A.A. Shirzadi, J.C. Walmsley, D.N. Johnstone, P. A. Midgley, L. Wondraczek, T.D. Bennett, Mechanical properties and processing techniques of bulk metal–organic framework glasses, J. Am. Chem. Soc. 141 (2019) 1027–1034, https://doi.org/10.1021/jacs.8b11357.

[42] T.D. Bennett, J.-C. Tan, Y. Yue, E. Baxter, C. Ducati, N.J. Terrill, H.H.-M. Yeung, Z. Zhou, W. Chen, S. Henke, A.K. Cheetham, G.N. Greaves, Hybrid glasses from strong and fragile metal-organic framework liquids, Nat. Commun. 6 (2015) 8079, https://doi.org/10.1038/ncomms9079.

[43] Q. Zheng, Y. Zhang, M. Montazerian, O. Gulbiten, J.C. Mauro, E.D. Zanotto, Y. Yue, Understanding glass through differential scanning calorimetry, Chem. Rev. 119 (2019) 7848–7939, https://doi.org/10.1021/acs.chemrev.8b00510.

[44] T.D. Bennett, S. Horike, Liquid, glass and amorphous solid states of coordination polymers and metal–organic frameworks, Nat. Rev. Mater. 3 (2018) 431–440, https://doi.org/10.1038/s41578-018-0054-3.

[45] S. Horike, N. Ma, Z. Fan, S. Kosasang, M.M. Smedskjaer, Mechanics, ionics, and optics of metal–organic framework and coordination polymer glasses, Nano Lett. 21 (2021) 6382–6390, https://doi.org/10.1021/acs.nanolett.1c01594.

[46] T.D. Bennett, F.-X. Coudert, S.L. James, A.I. Cooper, The changing state of porous materials, Nat. Mater. 20 (2021) 1179–1187, https://doi.org/10.1038/s41563-021-00957-w.

[47] D. Liu, H. Zhu, W. Zhang, X. Chen, Nonlinear optical glass-ceramic from a new polar phase-transition organic-inorganic hybrid crystal, Angew. Chem. Int. Ed. 62 (2023) e202218902, https://doi.org/10.1002/anie.202218902.

[48] R. Lin, M. Chai, Y. Zhou, V. Chen, T.D. Bennett, J. Hou, Metal–organic framework glass composites, Chem. Soc. Rev. 52 (2023) 4149–4172, https://doi.org/10.1039/D2CS00315E.

[49] L. Ruan, Y. Zhang, NIR-excitable heterostructured upconversion perovskite nanodots with improved stability, Nat. Commun. 12 (2021) 219, https://doi.org/10.1038/s41467-020-20551-z.

[50] F. Nie, K.-Z. Wang, D. Yan, Supramolecular glasses with color-tunable circularly polarized afterglow through evaporation-induced self-assembly of chiral metal–organic complexes, Nat. Commun. 14 (2023) 1654, https://doi.org/10.1038/s41467-023-37331-0.

[51] W. Xu, N. Hanikel, K.A. Lomachenko, C. Atzori, A. Lund, H. Lyu, Z. Zhou, C. A. Angell, O.M. Yaghi, High-porosity metal-organic framework glasses, Angew. Chem. Int. Ed. 62 (2023) e202300003, https://doi.org/10.1002/anie.202300003.

[52] D. Möncke, E.I. Kamitsos, D. Palles, R. Limbach, A. Winterstein-Beckmann, T. Honma, Z. Yao, T. Rouxel, L. Wondraczek, Transition and post-transition metal ions in borate glasses: borate ligand speciation, cluster formation, and their effect on glass transition and mechanical properties, J. Chem. Phys. 145 (2016) 124501, https://doi.org/10.1063/1.4962323.

[53] M. Liu, R.D. McGillicuddy, H. Vuong, S. Tao, A.H. Slavney, M.I. Gonzalez, S.J. L. Billinge, J.A. Mason, Network-forming liquids from metal–Bis(acetamide) frameworks with low melting temperatures, J. Am. Chem. Soc. 143 (2021) 2801–2811, https://doi.org/10.1021/jacs.0c11718.

[54] C. Ye, L.N. McHugh, C. Chen, S.E. Dutton, T.D. Bennett, Glass formation in hybrid organic-inorganic perovskites, Angew. Chem. Int. Ed. 62 (2023) e202302406, https://doi.org/10.1002/anie.202302406.

[55] A.E. Khudozhitkov, N. Ogiwara, M. Donoshita, H. Kobayashi, A.G. Stepanov, D. I. Kolokolov, H. Kitagawa, Dynamics of linkers in metal–organic framework glasses, J. Am. Chem. Soc. 146 (2024) 12950–12957, https://doi.org/10.1021/jacs.3c13156.

[56] B. Li, Y. Wang, Y. Xu, Z. Xia, Emerging 0D Hybrid Metal Halide Luminescent Glasses, Adv. Mater. 37 (2025) 2415483, https://doi.org/10.1002/adma.202415483.

[57] X. He, Y. Zheng, Z. Luo, Y. Wei, Y. Liu, C. Xie, C. Li, D. Peng, Z. Quan, Bright circularly polarized Mechanoluminescence from 0D hybrid manganese halides, Adv. Mater. 36 (2024) 2309906, https://doi.org/10.1002/adma.202309906.

[58] C.W. Ashling, D.N. Johnstone, R.N. Widmer, J. Hou, S.M. Collins, A.F. Sapnik, A. M. Bumstead, P.A. Midgley, P.A. Chater, D.A. Keen, T.D. Bennett, Synthesis and properties of a compositional series of MIL-53(Al) metal–organic framework crystal-glass composites, J. Am. Chem. Soc. 141 (2019) 15641–15648, https://doi.org/10.1021/jacs.9b07557.

[59] P.G. Debenedetti, F.H. Stillinger, Supercooled liquids and the glass transition, Nature 410 (2001) 259–267, https://doi.org/10.1038/35065704.

[60] L.L. Beecroft, C.K. Ober, Nanocomposite materials for optical applications, Chem. Mater. 9 (1997) 1302–1317, https://doi.org/10.1021/cm960441a.

[61] C. Wang, L. Yan, J. Si, N. Wang, T. Li, X. Hou, Exceptional stability against water, UV light, and heat for CsPbBr3 @Pb-MOF composites, Small Methods 8 (2024) 2400241, https://doi.org/10.1002/smtd.202400241.

[62] J. Hou, P. Chen, A. Shukla, A. Krajnc, T. Wang, X. Li, R. Doasa, L.H.G. Tizei, B. Chan, D.N. Johnstone, R. Lin, T.U. Schülli, I. Martens, D. Appadoo, M.S. Ari, Z. Wang, T. Wei, S.-C. Lo, M. Lu, S. Li, E.B. Namdas, G. Mali, A.K. Cheetham, S. M. Collins, V. Chen, L. Wang, T.D. Bennett, Liquid-phase sintering of lead halide perovskites and metal-organic framework glasses, Science 374 (2021) 621–625, https://doi.org/10.1126/science.abf4460.

[63] X. Li, W. Huang, A. Krajnc, Y. Yang, A. Shukla, J. Lee, M. Ghasemi, I. Martens, B. Chan, D. Appadoo, P. Chen, X. Wen, J.A. Steele, H.G. Hackbarth, Q. Sun, G. Mali, R. Lin, N.M. Bedford, V. Chen, A.K. Cheetham, L.H.G. Tizei, S.M. Collins, L. Wang, J. Hou, Interfacial alloying between lead halide perovskite crystals and hybrid glasses, Nat. Commun. 14 (2023) 7612, https://doi.org/10.1038/s41467-023-43247-6.

[64] B.-C. Liu, Q. Lin, S.-Q. Sun, Q. Sun, X. Peng, X. Chen, Y. Li, Y.-M. Xie, S.-T. Lee, M.-K. Fung, Tailored large-particle quantum dots with high color purity and excellent electroluminescent efficiency, Sci. Bull. 70 (2025) 905–913, https://doi.org/10.1016/j.scib.2025.01.017.

[65] Mohamed.A. Ali, J. Ren, T. Zhao, X. Liu, Y. Hua, Y. Yue, J. Qiu, Broad mid-infrared luminescence in a metal–organic framework glass, ACS Omega 4 (2019) 12081–12087, https://doi.org/10.1021/acsomega.9b01559.

[66] M. Kim, Y. Lee, H.R. Moon, Carboxylate-based metal–organic framework and coordination polymer glasses: progress and perspectives, Acc. Chem. Res. 57 (2024) 2347–2357, https://doi.org/10.1021/acs.accounts.4c00290.

[67] Y. Gong, H. Zhang, P. Li, Y. Bai, B. Yin, M. Ouyang, N. Zheng, X. Liu, Z. Zhao, J. Qiu, Z. Yang, G. Dong, Spectral and temporal manipulation of ultralong phosphorescence based on melt-quenched glassy metal–organic complexes for multi-mode photonic functions, Adv. Funct. Mater. 34 (2024) 2312491, https://doi.org/10.1002/adfm.202312491.

[68] Q.-P. Peng, J.-H. Wei, Z.-L. He, J.-B. Luo, J.-H. Chen, Z.-Z. Zhang, X.-X. Guo, D.-B. Kuang, *In situ crystallization of CsPbBr3 nanocrystals within a melt-quenched glassy coordination polymer*, ACS Nano 19 (2025) 5295–5304, https://doi.org/10.1021/acsnano.4c12049.

[69] H.-Y. Li, X.-J. Kong, S.-D. Han, J. Pang, T. He, G.-M. Wang, X.-H. Bu, Metalation of metal–organic frameworks: fundamentals and applications, Chem. Soc. Rev. 53 (2024) 5626–5676, https://doi.org/10.1039/D3CS00873H.

[70] J.-R. Li, J. Sculley, H.-C. Zhou, Metal–organic frameworks for separations, Chem. Rev. 112 (2012) 869–932, https://doi.org/10.1021/cr200190s.

[71] R. Jin, R. Li, M. Ma, D. Chen, J. Zhang, Z. Xie, L. Ding, Y. Xie, J. Li, Beyond tradition: a MOF-on-MOF cascade Z-scheme heterostructure for augmented CO2 photoreduction, Small (2025) 2409759, https://doi.org/10.1002/smll.202409759.

[72] I. Senkovska, V. Bon, A. Mosberger, Y. Wang, S. Kaskel, Adsorption and separation by flexible MOFs, Adv. Mater. (2025) 2414724, https://doi.org/10.1002/adma.202414724.

[73] X. Zheng, X. Ma, Z. Yuan, X. Zhang, R. Zhai, R. Duan, X. Song, C. Teng, Y. Zhou, L. Jiang, Large-area fabrication of robust, foldable MOF/ANF membrane, Adv. Funct. Mater. 35 (2025) 2504519, https://doi.org/10.1002/adfm.202504519.

[74] C. Liu, S.V. Eliseeva, T.-Y. Luo, P.F. Muldoon, S. Petoud, N.L. Rosi, Near infrared excitation and emission in rare earth MOFs *via* encapsulation of organic dyes, Chem. Sci. 9 (2018) 8099–8102, https://doi.org/10.1039/C8SC03168A.

[75] C. Dong, J. Bai, X.-L. Lv, W. Wu, J. Lv, J.-R. Li, Fixing flexible arms of Core-shared ligands to enhance the stability of metal-organic frameworks, Inorg. Chem. 58 (2019) 15909–15916, https://doi.org/10.1021/acs.inorgchem.9b02397.

[76] L. Cao, Z. Lin, W. Shi, Z. Wang, C. Zhang, X. Hu, C. Wang, W. Lin, Exciton migration and amplified quenching on two-dimensional metal–organic layers, J. Am. Chem. Soc. 139 (2017) 7020–7029, https://doi.org/10.1021/jacs.7b02470.

[77] J. Guo, Q. Wang, Q. Wu, X. Yang, M. Fang, Y. Li, L. Zhang, L. Wang, Synergistic enhancement of white luminescence in WLEDs via g-C_3N_4-integrated ln-MOF composites with suppressed antenna effect, Electron. Mater. Lett. 21 (2025) 599–612, https://doi.org/10.1007/s13391-025-00578-4.

[78] F. Castro, F. Igoa Saldaña, M. Pistón, J. González-Platas, C. Kremer, L. Suescun, J. Torres, Tunable dual-emission of mixed-lanthanide MOFs with no antenna effect, Chem. Asian J. 20 (2025) e202401496, https://doi.org/10.1002/asia.202401496.

[79] S.Sh. Mohammed Ameen, K.M. Omer, Merging dual antenna effect with target-insensitive behavior in bimetal Biligand MOFs to form efficient internal reference signal: color tonality-Ratiometric designs, ACS Materials Lett. 6 (2024) 2339–2349, https://doi.org/10.1021/acsmaterialslett.4c00845.

[80] L. Zhao, B. Wang, C. Wang, D. Fan, X. Liu, Q. Wei, H. Ju, D. Wu, Dual-strategy ECL biosensor based on rare Eu(II,III)-MOF as probe with antenna effect and sensitization for CYFRA 21-1 trace analysis, Sensors Actuators B Chem. 377 (2023) 133101, https://doi.org/10.1016/j.snb.2022.133101.

[81] H. Xu, W. Yu, K. Pan, G. Wang, P. Zhu, Confinement and antenna effect for ultrasmall Y2O3:Eu3+ nanocrystals supported by MOF with enhanced near-UV light absorption thereby enhanced luminescence and excellently multifunctional applications, Nano Res. 14 (2021) 720–729, https://doi.org/10.1007/s12274-020-3104-2.

[82] Z.-Z. Zhang, Y.-F. Ma, M.-L. Zhang, Y.-X. Ren, J.-J. Wang, Synthesis and structure study of coumarin 6 modified Zn-MOF and its application in artificial light capture system, Dyes Pigments 242 (2025) 112953, https://doi.org/10.1016/j.dyepig.2025.112953.

[83] X. Wu, P. Luo, Z. Wei, Y. Li, R. Huang, X. Dong, K. Li, S. Zang, B.Z. Tang, Guest-triggered aggregation-induced emission in silver chalcogenolate cluster metal–organic frameworks, Adv. Sci. 6 (2019) 1801304, https://doi.org/10.1002/advs.201801304.

[84] S.Sh. Mohammed Ameen, F.K. Algethami, K.M. Omer, Precisely engineered dual-antenna europium MOF with intrinsic dual-state luminescence for sensitive dexamethasone sensing, Spectrochim. Acta A 343 (2025) 126598, https://doi.org/10.1016/j.saa.2025.126598.

[85] S.Sh. Mohammed Ameen, F.K. Algethami, K.M. Omer, Improving ratiometric-based analysis via designing intense bi-ligand metal-organic frameworks: dual-mode for detection of amoxicillin in milk and pharmaceutical samples, Food Chem. 491 (2025) 145185, https://doi.org/10.1016/j.foodchem.2025.145185.

[86] X. Peng, Y. He, K. Tan, R. Yuan, S. Chen, Novel samarium-based metal-organic frameworks with antenna effect-induced electrochemiluminescence for acetamiprid assay, Sens. Actuators B 430 (2025) 137343, https://doi.org/10.1016/j.snb.2025.137343.

[87] G. Ji, J. Liu, X. Gao, W. Sun, J. Wang, S. Zhao, Z. Liu, A luminescent lanthanide MOF for selectively and ultra-high sensitively detecting Pb^{2+} ions in aqueous solution, J. Mater. Chem. A 5 (2017) 10200–10205, https://doi.org/10.1039/C7TA02439H.

[88] Y. Deng, S. Jiang, Z. Yan, Y. Chu, W. Wu, H. Xiao, Fluorescent Eu-MOF@nanocellulose-based nanopaper for rapid and sensitive detection of uranium (VI), Anal. Chim. Acta 1292 (2024) 342211, https://doi.org/10.1016/j.aca.2024.342211.

[89] Y. Liu, X.-Y. Xie, C. Cheng, Z.-S. Shao, H.-S. Wang, Strategies to fabricate metal–organic framework (MOF)-based luminescent sensing platforms, J. Mater. Chem. C 7 (2019) 10743–10763, https://doi.org/10.1039/C9TC03208H.

[90] V.J. Pastore, T.R. Cook, J. Rzayev, Polymer–MOF hybrid composites with high porosity and stability through surface-selective ligand exchange, Chem. Mater. 30 (2018) 8639–8649, https://doi.org/10.1021/acs.chemmater.8b03881.

[91] H. Tang, D. Fan, Y. Chen, S. Han, Exploring enzyme–MOF (metal–organic framework) catalytic systems: trade-offs between enzyme activity and MOF stability, Green Chem. 27 (2025) 2605–2628, https://doi.org/10.1039/D4GC05154H.

[92] H. Ghasempour, K.-Y. Wang, J.A. Powell, F. ZareKarizi, X.-L. Lv, A. Morsali, H.-C. Zhou, Metal–organic frameworks based on multicarboxylate linkers, Coord. Chem. Rev. 426 (2021) 213542, https://doi.org/10.1016/j.ccr.2020.213542.

[93] K. Yang, Z. Zhang, X. Zhang, Q. Wang, X. Hao, G. Ye, J. Luo, H. Yang, Energy performance evaluation and life cycle assessment on a novel hydrogen storage system with cryo-adsorption approach using MOF, Chem. Eng. J. 520 (2025) 165656, https://doi.org/10.1016/j.cej.2025.165656.

[94] Y. Liu, Z. Lin, Y. Luo, R. Wu, R. Fang, A. Umar, Z. Zhang, Z. Zhao, J. Yao, S. Zhao, Superhydrophobic MOF based materials and their applications for oil-water separation, journal of cleaner production, J. Clean. Prod. 420 (2023) 138347, https://doi.org/10.1016/j.jclepro.2023.138347.

[95] X. Na, S. Xing, M. Tan, W. Su, Fine-tuning porous structure of zirconium-based metal–organic frameworks for efficient separation and purification of astaxanthin by defect engineering, Adv. Sci. 11 (2024) 2409451, https://doi.org/10.1002/advs.202409451.

[96] S. Furukawa, J. Ashburne, Greater porosity with redox reaction speeds up MOF color change, Chem 1 (2016) 186–188, https://doi.org/10.1016/j.chempr.2016.07.002.

[97] T. Zhao, S. Nie, M. Luo, P. Xiao, M. Zou, Y. Chen, Research progress in structural regulation and applications of HKUST-1 and HKUST-1 based materials, J. Alloys Compd. 974 (2024) 172897, https://doi.org/10.1016/j.jallcom.2023.172897.

[98] Q. Li, W. Zhu, Y. Lian, Y. Peng, Z. Deng, One-dimensional HKUST-1 nanobelts from cu nanowires, Chin. Chem. Lett. 31 (2020) 517–520, https://doi.org/10.1016/j.cclet.2019.05.005.

[99] T.C. Wang, A.M. Wright, W.J. Hoover, K.J. Stoffel, R.K. Richardson, S. Rodriguez, R.C. Flores, J.P. Siegfried, N.A. Vermeulen, P.E. Fuller, M.H. Weston, O.K. Farha, W. Morris, Surviving under pressure: the role of solvent, crystal size, and morphology during pelletization of metal–organic frameworks, ACS Appl. Mater. Interfaces 13 (2021) 52106–52112, https://doi.org/10.1021/acsami.1c09619.

[100] O. Zaremba, S. Dutta, J. Requies, J. Andreo, S. Wuttke, Zirconium *vs.* hafnium: a comparative study of mesoporous MOF stability, Chem. Commun. 61 (2025) 2794–2797, https://doi.org/10.1039/D4CC03103B.

[101] H.U. Escobar-Hernandez, L.M. Pérez, P. Hu, F.A. Soto, M.I. Papadaki, H.-C. Zhou, Q. Wang, Thermal stability of metal–organic frameworks (MOFs): concept, determination, and model prediction using computational chemistry and machine learning, Ind. Eng. Chem. Res. 61 (2022) 5853–5862, https://doi.org/10.1021/acs.iecr.2c00561.

[102] R.J. Marshall, C.T. Lennon, A. Tao, H.M. Senn, C. Wilson, D. Fairen-Jimenez, R. S. Forgan, Controlling interpenetration through linker conformation in the modulated synthesis of Sc metal–organic frameworks, J. Mater. Chem. A 6 (2018) 1181–1187, https://doi.org/10.1039/C7TA09699B.

[103] I. Goodenough, V.S.D. Devulapalli, W. Xu, M.C. Boyanich, T.-Y. Luo, M. De Souza, M. Richard, N.L. Rosi, E. Borguet, Interplay between intrinsic thermal stability and expansion properties of functionalized UiO-67 metal–organic frameworks, Chem. Mater. 33 (2021) 910–920, https://doi.org/10.1021/acs.chemmater.0c03889.

[104] J. Zhang, K. Wang, S. Xu, L. Chen, H. Gu, Y. Yang, Q. Zhao, Y. Huo, B. Li, Y. Wang, Y. Xie, N. Li, J. Zhang, J. Zhang, Q. Li, Silk fibroin-coated Nano-MOFs enhance the thermal stability and immunogenicity of HBsAg, ACS Appl. Mater. Interfaces 16 (2024) 8346–8364, https://doi.org/10.1021/acsami.3c16358.

[105] M. Wang, X. Chen, Z. Liu, J. Li, J. Yu, M. Han, Y. Li, J. Hou, J. Pei, X. Li, D. Qiu, Revisiting the thermal stability of MOFs employed for radioactive iodine vapor adsorption, Mater. Today Chem. 42 (2024) 102452, https://doi.org/10.1016/j.mtchem.2024.102452.
[106] S. Zhao, J. Mei, H. Xu, W. Liu, Z. Qu, Y. Cui, N. Yan, Research of mercury removal from sintering flue gas of iron and steel by the open metal site of mil-101(Cr), J. Hazard. Mater. 351 (2018) 301–307, https://doi.org/10.1016/j.jhazmat.2017.12.016.
[107] X. Wang, T. Qin, S.-S. Bao, Y.-C. Zhang, X. Shen, L.-M. Zheng, D. Zhu, Facile synthesis of a water stable 3D Eu-MOF showing high proton conductivity and its application as a sensitive luminescent sensor for Cu^{2+} ions, J. Mater. Chem. A 4 (2016) 16484–16489, https://doi.org/10.1039/C6TA06792A.
[108] S. Wang, X. Li, C. Yuan, Z. Sun, Y. Lu, S. Pei, Y. Wu, C.-C. Wang, B. Wang, Asymmetric electric field-induced modulation on MOFs for boosting heterogeneous photo-Fenton process: porous coordination structure and selective oxidation, Appl. Catal. B 379 (2025) 125717, https://doi.org/10.1016/j.apcatb.2025.125717.
[109] S. Yu, H. Kang, S. Jee, W. Moon, D. Jang, W. Huang, D. Kim, K. Chung, D. Won, J. Park, R. Liu, K. Choi, S. Kim, L.P. Lee, D.H. Kim, MOF-based single-atom and metal cluster catalysts by room-temperature synthesis for tumor therapy, Adv. Healthc. Mater. 14 (2025) 2501058, https://doi.org/10.1002/adhm.202501058.
[110] B.A. Habte, C.-C. Hu, G.-S. Liou, C.-F. Wang, W.-S. Hung, K.-R. Lee, J.-Y. Lai, Designing MOF-74/Pebax mixed matrix membranes for improved gas separation performance through metal cluster modification and aminosilane functionalization in MOF-74, J. Membr. Sci. 735 (2025) 124577, https://doi.org/10.1016/j.memsci.2025.124577.
[111] Y.-Y. Yang, F.-C. Pan, J.-L. Li, F. Gong, J. Hu, Q. Zheng, D. Lin, Y. Huo, Construction of Ni2P/WS2/CoWO4@C multi-heterojunction electrocatalysis derived from heterometallic clusters for superior overall water splitting, J. Colloid Interface Sci. 685 (2025) 196–204, https://doi.org/10.1016/j.jcis.2025.01.075.
[112] L. Yu, S. Li, X. Zhou, B. Zhang, K. Zhou, Q. Xia, S. Wang, J. Li, H. Wang, Building ultramicroporous zirconium metal–organic frameworks with ligands of high coordination density through a reticular approach, Nat. Chem. 17 (2025) 1207–1215, https://doi.org/10.1038/s41557-025-01836-6.
[113] M. Zhang, P. Huang, R. Li, Y. Huang, M. Qin, Y. Peng, S. Wang, Y. Yan, M. Lu, Y. Lan, Reticular synthesis of 3D metal cluster-based COFs with record high-connectivity for efficient photocatalytic H_2O_2 synthesis, Angew. Chem. Int. Ed. 64 (2025) e202507624, https://doi.org/10.1002/anie.202507624.
[114] M. Wang, Y.-R. Meng, W. Xu, T. Shen, Y. Wang, Q. Yu, C. Liu, Y. Gu, Z. Tie, Z. Fan, J.-L. Zuo, J. Su, Z. Jin, Square-planar tetranuclear cluster-based high-symmetry coordination metal–organic polymers for efficient electrochemical nitrate reduction to ammonia, J. Am. Chem. Soc. 147 (2025) 18327–18337, https://doi.org/10.1021/jacs.5c06650.
[115] R.A. Salinas Domínguez, J. Águila Rosas, S.E. Martínez Tolibia, E. Lima, A. Dutt, Opportunities in functionalized metal-organic frameworks (MOFs) with open metal sites for optical biosensor application, Adv. Colloid Interf. Sci. 344 (2025) 103598, https://doi.org/10.1016/j.cis.2025.103598.
[116] X. Wei, F. Chun, Y. Cao, X. Zhang, J. Chen, Z. Xing, Y. Fang, F. Wang, Reversible Thermo/hydrochromic luminescence in a ln-MOF film for Anticounterfeiting application, ACS Appl. Opt. Mater. 3 (2025) 772–778, https://doi.org/10.1021/acsaom.5c00029.
[117] D.-H. Chen, R. Haldar, C. Wöll, Stacking lanthanide-MOF thin films to yield highly sensitive optical thermometers, ACS Appl. Mater. Interfaces 15 (2023) 19665–19671, https://doi.org/10.1021/acsami.3c00860.
[118] W. Lai, C. Wu, X. Han, Facile synthesis of hyperbranched Eu-MOF structures for the construction of a $CsPbBr_3$ /Eu-MOF composite and its application as a ratiometric fluorescent probe, J. Mater. Chem. C 11 (2023) 2995–3002, https://doi.org/10.1039/D2TC04879E.
[119] L. Wu, L. Qu, C. Yang, Y. Xu, L. Zhang, S. Yang, Y. Gu, H. Pan, Advance in the application of MOF composites for breast cancer biomarkers sensing detection, Mater. Today Chem. 38 (2024) 102107, https://doi.org/10.1016/j.mtchem.2024.102107.
[120] X. Wang, G. Clavier, Y. Zhang, K. Batra, N. Xiao, G. Maurin, B. Ding, A. Tissot, C. Serre, A MOF/DNA luminescent sensing platform for detection of potential COVID-19 biomarkers and drugs, Chem. Sci. 14 (2023) 5386–5395, https://doi.org/10.1039/D3SC00106G.
[121] Y. Feng, Q. Xu, C. Ouyang, Y. Wei, Z. Gan, Y. Liu, L. Yu, Y. Xiao, Dual-enhanced lanthanide MOF-based fluorescent bio-barcode via conformational regulation for ultrasensitive detection of DNA epigenetic biomarker, Small 21 (2025) e04246, https://doi.org/10.1002/smll.202504246.
[122] P. Arul, C. Nandhini, S.-T. Huang, C.-H. Huang, N.S.K. Gowthaman, Ni-MOF embedded with carbon nanomaterials/polypyrrole/riboflavin oxidase biomimetic recognition for direct and ultrasensitive electrochemical detection of prostate cancer biomarker, Sens. Actuators B 444 (2025) 138410, https://doi.org/10.1016/j.snb.2025.138410.
[123] J. Cuan, D. Zhang, W. Xing, J. Han, H. Zhou, Y. Zhou, Confining $CsPbX_3$ perovskites in a hierarchically porous MOF as efficient and stable phosphors for white LED, Chem. Eng. J. 425 (2021) 131556, https://doi.org/10.1016/j.cej.2021.131556.
[124] X. Ma, X. Xu, F. Duan, W. Huang, Q. Chen, D. Wu, High-efficiency wideband excitable Mechanoluminescence from a yellow MOF phosphor as white LED and multicolor thin films, Adv. Opt. Mater. 10 (2022) 2101461, https://doi.org/10.1002/adom.202101461.
[125] H. Tsai, S. Shrestha, R.A. Vilá, W. Huang, C. Liu, C.-H. Hou, H.-H. Huang, X. Wen, M. Li, G. Wiederrecht, Y. Cui, M. Cotlet, X. Zhang, X. Ma, W. Nie, Bright and stable light-emitting diodes made with perovskite nanocrystals stabilized in metal–organic frameworks, Nat. Photonics 15 (2021) 843–849, https://doi.org/10.1038/s41566-021-00857-0.
[126] T. Yu, B. Wang, L. Yu, Dual-mode color-changing pH sensor based on fluorescent MOF embedded photonic crystal hydrogel, J. Chin. Chem. Soc. 69 (2022) 831–839, https://doi.org/10.1002/jccs.202200064.
[127] H. Li, Y. Li, L. Zhang, E. Hu, D. Zhao, H. Guo, G. Qian, A Thermo-responsive MOFs for X-ray scintillator, Adv. Mater. 36 (2024) 2405535, https://doi.org/10.1002/adma.202405535.
[128] H. Li, Q. Dong, Y. Li, E. Hu, Y. Cai, L. Zhang, D. Zhao, H. Guo, G. Qian, Thermal-adaptive photonic MOFs for high-performance X-ray scintillator, Adv. Funct. Mater. 35 (2025) 2500445, https://doi.org/10.1002/adfm.202500445.
[129] Y. Feng, J.-X. Wu, Y.-H. Mo, S. Liu, S.-L. Cai, W.-G. Zhang, J. Fan, S.-R. Zheng, Hierarchical porous amorphous metal–organic frameworks constructed from ZnO/MOF glass composites, Chem. Commun. 60 (2024) 6190–6193, https://doi.org/10.1039/D4CC01454E.
[130] O. Smirnova, R. Sajzew, S.J. Finkelmeyer, T. Asadov, S. Chattopadhyay, T. Wieduwilt, A. Reupert, M. Presselt, A. Knebel, L. Wondraczek, Micro-optical elements from optical-quality ZIF-62 hybrid glasses by hot imprinting, Nat. Commun. 15 (2024) 5079, https://doi.org/10.1038/s41467-024-49428-1.
[131] J.I. Deneff, L.E.S. Rohwer, K.S. Butler, B. Kaehr, D.J. Vogel, T.S. Luk, R.A. Reyes, A.A. Cruz-Cabrera, J.E. Martin, D.F. Sava Gallis, Orthogonal luminescence lifetime encoding by intermetallic energy transfer in heterometallic rare-earth MOFs, Nat. Commun. 14 (2023) 981, https://doi.org/10.1038/s41467-023-36576-z.
[132] M. Gupta, Z. Zhu, D. Kottilil, B.B. Rath, W. Tian, Z.-K. Tan, X. Liu, Q.-H. Xu, W. Ji, J.J. Vittal, Impact of the structural modification of Diamondoid cd(II) MOFs on the nonlinear optical properties, ACS Appl. Mater. Interfaces 13 (2021) 60163–60172, https://doi.org/10.1021/acsami.1c17327.
[133] A. Qiao, T.D. Bennett, H. Tao, A. Krajnc, G. Mali, C.M. Doherty, A.W. Thornton, J. C. Mauro, G.N. Greaves, Y. Yue, A metal-organic framework with ultrahigh glass-forming ability, Sci. Adv. 4 (2018) eaao6827, https://doi.org/10.1126/sciadv.aao6827.
[134] J. Zhang, L. Longley, H. Liu, C.W. Ashling, P.A. Chater, K.A. Beyer, K. W. Chapman, H. Tao, D.A. Keen, T.D. Bennett, Y. Yue, Structural evolution in a melt-quenched zeolitic imidazolate framework glass during heat-treatment, Chem. Commun. 55 (2019) 2521–2524, https://doi.org/10.1039/C8CC09574D.
[135] A.M. Chester, C. Castillo-Blas, L. Wondraczek, D.A. Keen, T.D. Bennett, Materials formed by combining inorganic glasses and metal-organic frameworks, Chem. Eur. J. 28 (2022) e202200345, https://doi.org/10.1002/chem.202200345.
[136] G.N. Greaves, F. Meneau, A. Sapelkin, L.M. Colyer, I. Ap Gwynn, S. Wade, G. Sankar, The rheology of collapsing zeolites amorphized by temperature and pressure, Nat. Mater. 2 (2003) 622–629, https://doi.org/10.1038/nmat963.
[137] K.S. Park, Z. Ni, A.P. Côté, J.Y. Choi, R. Huang, F.J. Uribe-Romo, H.K. Chae, M. O'Keeffe, O.M. Yaghi, Exceptional chemical and thermal stability of zeolitic imidazolate frameworks, Proc. Natl. Acad. Sci. USA 103 (2006) 10186–10191, https://doi.org/10.1073/pnas.0602439103.
[138] M. Stepniewska, K. Januchta, C. Zhou, A. Qiao, M.M. Smedskjaer, Y. Yue, Observation of indentation-induced shear bands in a metal−organic framework glass, Proc. Natl. Acad. Sci. USA 117 (2020) 10149–10154, https://doi.org/10.1073/pnas.2000916117.
[139] Z. Shi, A. Arramel, T.D. Bennett, Y. Yue, N. Li, The deformation of short-range order leading to rearrangement of topological network structure in zeolitic imidazolate framework glasses, iScience 25 (2022) 104351, https://doi.org/10.1016/j.isci.2022.104351.
[140] M. Gustafsson, X. Zou, Crystal formation and size control of zeolitic imidazolate frameworks with mixed imidazolate linkers, J. Porous. Mater. 20 (2013) 55–63, https://doi.org/10.1007/s10934-012-9574-1.
[141] S. Yu, H. Hu, Y. Lin, W. Yang, Z. Tian, Glass transition-induced luminescence in ZIF-62, Chem. Commun. 61 (2025) 13405–13408, https://doi.org/10.1039/D5CC01504A.
[142] J.W.P. Schmelzer, A.S. Abyzov, V.M. Fokin, C. Schick, E.D. Zanotto, Crystallization in glass-forming liquids: effects of decoupling of diffusion and viscosity on crystal growth, J. Non-Cryst. Solids 429 (2015) 45–53, https://doi.org/10.1016/j.jnoncrysol.2015.08.027.
[143] J.W.P. Schmelzer, A.S. Abyzov, V.M. Fokin, C. Schick, E.D. Zanotto, Crystallization of glass-forming liquids: maxima of nucleation, growth, and overall crystallization rates, J. Non-Cryst. Solids 429 (2015) 24–32, https://doi.org/10.1016/j.jnoncrysol.2015.08.023.
[144] Y. Zong, S.-M. Xu, W. Shi, C. Lu, Oriented arrangement of simple monomers enabled by confinement: towards living supramolecular polymerization, Nat. Commun. 12 (2021) 2596, https://doi.org/10.1038/s41467-021-22827-4.
[145] M. Wakeda, J. Saida, Temperature-dependent effect of cooling rate on the melt-quenching process of metallic glasses, Comput. Mater. Sci. 218 (2023) 111930, https://doi.org/10.1016/j.commatsci.2022.111930.
[146] P.W. Anderson, Through the glass lightly, Science 267 (1995) 1615–1616, https://doi.org/10.1126/science.267.5204.1615.f.
[147] J.-C. Guillemin, W. Nasraoui, H. Gazzeh, Synthesis of *N* -unsubstituted cycloalkylimines containing a 4 to 8-membered ring, Chem. Commun. 55 (2019) 5647–5650, https://doi.org/10.1039/C9CC01755K.
[148] D. Xu, Y. Liu, Y. Tian, L.-M. Wang, Communication: enthalpy relaxation in a metal-organic zeolite imidazole framework (ZIF-4) glass-former, J. Chem. Phys. 146 (2017) 121101, https://doi.org/10.1063/1.4979352.
[149] T.D. Bennett, A.L. Goodwin, M.T. Dove, D.A. Keen, M.G. Tucker, E.R. Barney, A. K. Soper, E.G. Bithell, J.-C. Tan, A.K. Cheetham, Structure and properties of an amorphous metal-organic framework, Phys. Rev. Lett. 104 (2010) 115503, https://doi.org/10.1103/PhysRevLett.104.115503.

[150] Y. Wang, G. Jiang, J. Li, A. Yang, B. An, F. Malchik, A. Galeyeva, F. Xu, H. Wang, Glassy metal–organic framework-based solid-state electrolytes: advance, challenge, and emerging opportunities, Small Methods (2025) e01131, https://doi.org/10.1002/smtd.202501131.
[151] T.D. Bennett, Y. Yue, P. Li, A. Qiao, H. Tao, N.G. Greaves, T. Richards, G. I. Lampronti, S.A.T. Redfern, F. Blanc, O.K. Farha, J.T. Hupp, A.K. Cheetham, D. A. Keen, Melt-quenched glasses of metal–organic frameworks, J. Am. Chem. Soc. 138 (2016) 3484–3492, https://doi.org/10.1021/jacs.5b13220.
[152] E. Méndez, R. Semino, Thermodynamic insights into the self-assembly of zeolitic imidazolate frameworks from computer simulations, Chem. Sci. 16 (2025) 11979–11988, https://doi.org/10.1039/D5SC00807G.
[153] S.S. Sørensen, M.B. Østergaard, M. Stepniewska, H. Johra, Y. Yue, M. M. Smedskjaer, Metal–organic framework glasses possess higher thermal conductivity than their crystalline counterparts, ACS Appl. Mater. Interfaces 12 (2020) 18893–18903, https://doi.org/10.1021/acsami.0c02310.
[154] W.-L. Xue, A. Klein, M. El Skafi, J.-B. Weiß, F. Egger, H. Ding, S.K. Vasa, C. Liebscher, M. Zobel, R. Linser, J.-C. Tan, S. Henke, Mechanochemical synthesis enables melting, glass formation and glass–ceramic conversion in a cadmium-based zeolitic imidazolate framework, J. Am. Chem. Soc. 147 (2025) 15625–15635, https://doi.org/10.1021/jacs.5c02767.
[155] S.-H. Chong, A.J. Moreno, F. Sciortino, W. Kob, Evidence for the weak steric hindrance scenario in the Supercooled-state Reorientational dynamics, Phys. Rev. Lett. 94 (2005) 215701, https://doi.org/10.1103/PhysRevLett.94.215701.
[156] J.R. Keith, N.J. Rebello, B.J. Cowen, V. Ganesan, Influence of Counterion structure on conductivity of polymerized ionic liquids, ACS Macro Lett. 8 (2019) 387–392, https://doi.org/10.1021/acsmacrolett.9b00070.
[157] M. Guo, C. Shao, Y. Zhang, J. Yu, Y. Jiao, M. Guzik, G. Boulon, J. Ren, L. Hu, Effect of B_2O_3 addition on structure and properties of Yb^{3+} /Al^{3+} /B^{3+} −co-doped silica glasses, J. Am. Ceram. Soc. 103 (2020) 4275–4285, https://doi.org/10.1111/jace.17155.
[158] M. Stepniewska, M.B. Østergaard, C. Zhou, Y. Yue, Towards large-size bulk ZIF-62 glasses via optimizing the melting conditions, J. Non-Cryst. Solids 530 (2020) 119806, https://doi.org/10.1016/j.jnoncrysol.2019.119806.
[159] J.R. Rajian, E.L. Quitevis, Translational diffusion in sucrose benzoate near the glass transition: probe size dependence in the breakdown of the stokes-Einstein equation, J. Chem. Phys. 126 (2007) 224506, https://doi.org/10.1063/1.2738474.
[160] L. Zhang, L. Shi, J. Xu, Hf–cu–Ni–Al bulk metallic glasses: optimization of glass-forming ability and plasticity, J. Non-Cryst. Solids 355 (2009) 1005–1007, https://doi.org/10.1016/j.jnoncrysol.2009.04.009.
[161] D. Li, Z. Yang, L. Yang, C. Ma, M. Ye, Y. Sun, Z. Qiao, A. Chen, Self-supported flux melted glass membranes fabricated by melt quenching for gas separation, J. Membr. Sci. 695 (2024) 122492, https://doi.org/10.1016/j.memsci.2024.122492.
[162] W.-L. Xue, P. Kolodzeiski, H. Aucharova, S. Vasa, A. Koutsianos, R. Pallach, J. Song, L. Frentzel-Beyme, R. Linser, S. Henke, Highly porous metal-organic framework liquids and glasses via a solvent-assisted linker exchange strategy of ZIF-8, Nat. Commun. 15 (2024) 4420, https://doi.org/10.1038/s41467-024-48703-5.
[163] L. Frentzel-Beyme, M. Kloß, R. Pallach, S. Salamon, H. Moldenhauer, J. Landers, H. Wende, J. Debus, S. Henke, Porous purple glass – a cobalt imidazolate glass with accessible porosity from a meltable cobalt imidazolate framework, J. Mater. Chem. A 7 (2019) 985–990, https://doi.org/10.1039/C8TA08016J.
[164] L. León-Alcaide, R.S. Christensen, D.A. Keen, J.L. Jordá, I. Brotons-Alcázar, A. Forment-Aliaga, G. Mínguez Espallargas, Meltable, glass-forming, iron zeolitic imidazolate frameworks, J. Am. Chem. Soc. 145 (2023) 11258–11264, https://doi.org/10.1021/jacs.3c01455.
[165] B. Peng, H. She, Z. Wei, Z. Sun, Z. Deng, Z. Sun, W. Chen, Sulfur-doping tunes p-d orbital coupling over asymmetric Zn-Sn dual-atom for boosting CO_2 electroreduction to formate, Nat. Commun. 16 (2025) 2217, https://doi.org/10.1038/s41467-025-57573-4.
[166] D. Xu, C. Pan, Glass formation, structure, relaxation, and property of metal-organic framework (MOF) glasses: a review, Prog. Nat. Sci.: Mater. Int. 35 (2025) 98–121, https://doi.org/10.1016/j.pnsc.2024.12.006.
[167] A. Ananthanarayanan, G. Tricot, G.P. Kothiyal, L. Montagne, A comparative overview of glass-ceramic characterization by MAS-NMR and XRD, Crit. Rev. Solid State Mater. Sci. 36 (2011) 229–241, https://doi.org/10.1080/10408436.2011.593643.
[168] X. Zhang, H. Luan, H. Lou, T. Liang, S. Chen, D. Xu, Z. Yin, L. Wang, J. Zeng, Y. Ren, Z. Zeng, Y. Shao, K.-F. Yao, Q. Zeng, Highly variable chemical short-range order in a high-entropy metallic glass, Mater. Today Phys. 27 (2022) 100799, https://doi.org/10.1016/j.mtphys.2022.100799.
[169] X. Li, Z. Jin, H. Lu, Y. Li, X. Chen, S. Zhu, Z. Jia, H. Tan, Y. Yang, L. Hou, Amorphization strategy for constructing metal-Triazole framework glass foams with multistage pore structure for selective removal of mercury, Adv. Funct. Mater. 35 (2025) 2501311, https://doi.org/10.1002/adfm.202501311.
[170] A.S. Abyzov, V.M. Fokin, E.D. Zanotto, Predicting homogeneous nucleation rates in silicate glass-formers, J. Non-Cryst. Solids 500 (2018) 231–234, https://doi.org/10.1016/j.jnoncrysol.2018.08.002.
[171] W.-L. Xue, G.-Q. Li, H. Chen, Y.-C. Han, L. Feng, L. Wang, X.-L. Gu, S.-Y. Hu, Y.-H. Deng, L. Tan, M.T. Dove, W. Li, J. Zhang, H. Dong, Z. Chen, W.-H. Deng, G. Xu, G. Wang, C.-Q. Wan, Melt-quenched glass formation of a family of metal-carboxylate frameworks, Nat. Commun. 15 (2024) 2040, https://doi.org/10.1038/s41467-024-46311-x.
[172] R. Gaillac, P. Pullumbi, K.A. Beyer, K.W. Chapman, D.A. Keen, T.D. Bennett, F.-X. Coudert, Liquid metal–organic frameworks, Nat. Mater. 16 (2017) 1149–1154, https://doi.org/10.1038/nmat4998.
[173] R. Gaillac, P. Pullumbi, F.-X. Coudert, Melting of Zeolitic Imidazolate frameworks with different topologies: insight from first-principles molecular dynamics, J. Phys. Chem. C 122 (2018) 6730–6736, https://doi.org/10.1021/acs.jpcc.8b00385.
[174] T.D. Bennett, A.K. Cheetham, A.H. Fuchs, F.-X. Coudert, Interplay between defects, disorder and flexibility in metal-organic frameworks, Nat. Chem. 9 (2017) 11–16, https://doi.org/10.1038/nchem.2691.
[175] Y. Fang, P. Cui, Z. Ding, J.-X. Zhu, Properties of a magnesium phosphate cement-based fire-retardant coating containing glass fiber or glass fiber powder, Constr. Build. Mater. 162 (2018) 553–560, https://doi.org/10.1016/j.conbuildmat.2017.12.059.
[176] G.N. Greaves, S. Sen, Inorganic glasses, glass-forming liquids and amorphizing solids, Adv. Phys. 56 (2007) 1–166, https://doi.org/10.1080/00018730601147426.
[177] B. Dong, S. Zhou, D. Li, C. Lu, F. Guo, X. Ni, Z. Lu, A new criterion for predicting glass forming ability of bulk metallic glasses and some critical discussions, Prog. Nat. Sci.: Mater. Int. 21 (2011) 164–172, https://doi.org/10.1016/S1002-0071(12)60051-3.
[178] X. Wu, S. Lan, Z. Wu, X. Wei, Y. Ren, H.Y. Tsang, X. Wang, Multiscale structures of Zr-based binary metallic glasses and the correlation with glass forming ability, Prog. Nat. Sci.: Mater. Int. 27 (2017) 482–486, https://doi.org/10.1016/j.pnsc.2017.08.008.
[179] M. Wang, H. Zhao, B. Du, X. Lu, S. Ding, X. Hu, Functions and applications of emerging metal–organic-framework liquids and glasses, Chem. Commun. 59 (2023) 7126–7140, https://doi.org/10.1039/D3CC00834G.
[180] B. Dong, S. Zhou, J. Qin, S. Pan, Z. Li, The influence of clusters in the melt of Fe80Si10B10 alloy on the subsequent glass-formation, Prog. Nat. Sci.: Mater. Int. 23 (2013) 216–219, https://doi.org/10.1016/j.pnsc.2013.02.002.
[181] A.M. Bumstead, M.F. Thorne, T.D. Bennett, Identifying the liquid and glassy states of coordination polymers and metal–organic frameworks, Faraday Discuss. 225 (2021) 210–225, https://doi.org/10.1039/D0FD00011F.
[182] H. Tao, T.D. Bennett, Y. Yue, Melt-quenched hybrid glasses from metal–organic frameworks, Adv. Mater. 29 (2017) 1601705, https://doi.org/10.1002/adma.201601705.
[183] Y. Zhao, L. Wu, K. Wu, R.-J. Wei, H. Zeng, H. Pang, W. Lu, D. Li, Host-guest interactions in the confined spaces of metal–organic frameworks: design principles, characterizations, and applications, Coord. Chem. Rev. 524 (2025) 216302, https://doi.org/10.1016/j.ccr.2024.216302.
[184] V. Nozari, C. Calahoo, J.M. Tuffnell, D.A. Keen, T.D. Bennett, L. Wondraczek, Ionic liquid facilitated melting of the metal-organic framework ZIF-8, Nat. Commun. 12 (2021) 5703, https://doi.org/10.1038/s41467-021-25970-0.
[185] V. Nozari, O. Smirnova, J.M. Tuffnell, A. Knebel, T.D. Bennett, L. Wondraczek, Low-temperature melting and glass formation of the Zeolitic Imidazolate frameworks ZIF-62 and ZIF-76 through ionic liquid incorporation, Adv. Mater. Technol. 7 (2022) 2200343, https://doi.org/10.1002/admt.202200343.
[186] C. Bi, Q. Wang, Y. Shao, Y. Yuan, Z. Xiao, J. Huang, Non-wetting surface-driven high-aspect-ratio crystalline grain growth for efficient hybrid perovskite solar cells, Nat. Commun. 6 (2015) 7747, https://doi.org/10.1038/ncomms8747.
[187] W. Xue, C. Das, J. Weiß, S. Henke, Insights into the Mechanochemical glass formation of Zeolitic Imidazolate frameworks, Angew. Chem. Int. Ed. 63 (2024) e202405307, https://doi.org/10.1002/anie.202405307.
[188] S. Liu, Z.-R. Wang, X. Lin, B.-Y. Guo, S. Cai, W.-G. Zhang, J. Fan, S.-R. Zheng, Structural comparisons, fluorescence properties, and glass-to-crystal transformations of heat–cooled and melt-quenched zeolitic imidazolate framework glass, Inorg. Chem. 63 (2024) 18574–18580, https://doi.org/10.1021/acs.inorgchem.4c01886.
[189] T.D. Bennett, S. Cao, J.C. Tan, D.A. Keen, E.G. Bithell, P.J. Beldon, T. Friscic, A. K. Cheetham, Facile Mechanosynthesis of amorphous Zeolitic Imidazolate frameworks, J. Am. Chem. Soc. 133 (2011) 14546–14549, https://doi.org/10.1021/ja206082s.
[190] J.B.H. Strautmann, S. Dammers, T. Limpke, J. Parthier, T.P. Zimmermann, S. Walleck, G. Heinze-Brückner, A. Stammler, H. Bögge, T. Glaser, Design and synthesis of a dinucleating ligand system with varying terminal donor functions that provides no bridging donor and its application to the synthesis of a series of Fe^{III} –μ-O–Fe^{III} complexes, Dalton Trans. 45 (2016) 3340–3361, https://doi.org/10.1039/C5DT03711E.
[191] T.D. Bennett, P.J. Saines, D.A. Keen, J. Tan, A.K. Cheetham, Ball-milling-induced Amorphization of Zeolitic Imidazolate frameworks (ZIFs) for the irreversible trapping of iodine, Chem. Eur. J. 19 (2013) 7049–7055, https://doi.org/10.1002/chem.201300216.
[192] M.F. Thorne, M.L.R. Gómez, A.M. Bumstead, S. Li, T.D. Bennett, Mechanochemical synthesis of mixed metal, mixed linker, glass-forming metal–organic frameworks, Green Chem. 22 (2020) 2505–2512, https://doi.org/10.1039/D0GC00546K.
[193] A.M. Bumstead, M.F. Thorne, A.F. Sapnik, C. Castillo-Blas, G.I. Lampronti, T. D. Bennett, Investigating the chemical sensitivity of melting in zeolitic imidazolate frameworks, Dalton Trans. 51 (2022) 13636–13645, https://doi.org/10.1039/D2DT02142K.
[194] J.C. Tan, T.D. Bennett, A.K. Cheetham, Chemical structure, network topology, and porosity effects on the mechanical properties of Zeolitic Imidazolate frameworks, Proc. Natl. Acad. Sci. USA 107 (2010) 9938–9943, https://doi.org/10.1073/pnas.1003205107.

[195] M.I. Nandasiri, S.R. Jambovane, B.P. McGrail, H.T. Schaef, Satish K. Nune, Adsorption, separation, and catalytic properties of densified metal-organic frameworks, Coord. Chem. Rev. 311 (2016) 38–52, https://doi.org/10.1016/j.ccr.2015.12.004.
[196] J. Song, L. Frentzel-Beyme, R. Pallach, P. Kolodzeiski, A. Koutsianos, W.-L. Xue, R. Schmid, S. Henke, Modulating Liquid–Liquid Transitions and Glass Formation in Zeolitic Imidazolate Frameworks by Decoration with Electron-Withdrawing Cyano Groups, J. Am. Chem. Soc. 145 (2023) 9273–9284, https://doi.org/10.1021/jacs.3c01933.
[197] L. Frentzel-Beyme, P. Kolodzeiski, J.-B. Weiß, A. Schneemann, S. Henke, Quantification of gas-accessible microporosity in metal-organic framework glasses, Nat. Commun. 13 (2022) 7750, https://doi.org/10.1038/s41467-022-35372-5.
[198] S. Noro, X. Zheng, A. Wang, K. Suzuki, S. Kosasang, S. Horike, D. Padovan, K. Nakajima, H. Sato, K. Takahashi, T. Nakamura, Mechanical force induced formation of extrinsic micropores in coordination polymers, Inorg. Chem. 61 (2022) 3379–3386, https://doi.org/10.1021/acs.inorgchem.1c02762.
[199] N. Ma, R. Ohtani, H.M. Le, S.S. Sørensen, R. Ishikawa, S. Kawata, S. Bureekaew, S. Kosasang, Y. Kawazoe, K. Ohara, M.M. Smedskjaer, S. Horike, Exploration of glassy state in Prussian blue analogues, Nat. Commun. 13 (2022) 4023, https://doi.org/10.1038/s41467-022-31658-w.
[200] C. Castillo-Blas, A.M. Chester, R.P. Cosquer, A.F. Sapnik, L. Corti, R. Sajzew, B. Poletto-Rodrigues, G.P. Robertson, D.J.M. Irving, L.N. McHugh, L. Wondraczek, F. Blanc, D.A. Keen, T.D. Bennett, Interfacial Bonding between a Crystalline Metal–Organic Framework and an Inorganic Glass, J. Am. Chem. Soc. 145 (2023) 22913–22924, https://doi.org/10.1021/jacs.3c04248.
[201] I. Luz, F.X. Llabrés I Xamena, A. Corma, Bridging homogeneous and heterogeneous catalysis with MOFs: “click” reactions with cu-MOF catalysts, J. Catal. 276 (2010) 134–140, https://doi.org/10.1016/j.jcat.2010.09.010.
[202] Y. Ma, X. Han, S. Xu, Z. Wang, W. Li, I. Da Silva, S. Chansai, D. Lee, Y. Zou, M. Nikiel, P. Manuel, A.M. Sheveleva, F. Tuna, E.J.L. McInnes, Y. Cheng, S. Rudić, A.J. Ramirez-Cuesta, S.J. Haigh, C. Hardacre, M. Schröder, S. Yang, Atomically Dispersed Copper Sites in a Metal–Organic Framework for Reduction of Nitrogen Dioxide, J. Am. Chem. Soc. 143 (2021) 10977–10985, https://doi.org/10.1021/jacs.1c03036.
[203] J. Park, A.C. Hinckley, Z. Huang, D. Feng, A.A. Yakovenko, M. Lee, S. Chen, X. Zou, Z. Bao, Synthetic Routes for a 2D Semiconductive Copper Hexahydroxybenzene Metal–Organic Framework, J. Am. Chem. Soc. 140 (2018) 14533–14537, https://doi.org/10.1021/jacs.8b06666.
[204] M. Kim, H.-S. Lee, D.-H. Seo, S.J. Cho, E. Jeon, H.R. Moon, Melt-quenched carboxylate metal–organic framework glasses, Nat. Commun. 15 (2024) 1174, https://doi.org/10.1038/s41467-024-45326-8.
[205] Y.-S. Wei, Z. Fan, C. Luo, S. Horike, Desolvation of metal complexes to construct metal–organic framework glasses, Nat. Synth. 3 (2023) 214–223, https://doi.org/10.1038/s44160-023-00412-5.
[206] W. Xu, N. Hanikel, K.A. Lomachenko, C. Atzori, A. Lund, H. Lyu, Z. Zhou, C. A. Angell, O.M. Yaghi, High-porosity metal-organic framework glasses, Angew. Chem. 135 (2023) e202300003, https://doi.org/10.1002/ange.202300003.
[207] Z. Yin, Y. Zhao, S. Wan, J. Yang, Z. Shi, S.-X. Peng, M.-Z. Chen, T.-Y. Xie, T.-W. Zeng, O. Yamamuro, M. Nirei, H. Akiba, Y.-B. Zhang, H.-B. Yu, M.-H. Zeng, Synergistic stimulation of metal–organic frameworks for stable super-cooled liquid and quenched glass, J. Am. Chem. Soc. 144 (2022) 13021–13025, https://doi.org/10.1021/jacs.2c04532.
[208] C.N. Dzesse T, E.N. Nfor, S.A. Bourne, Vapor sorption and solvatochromism in a metal–organic framework of an asymmetric pyridylcarboxylate, Cryst. Growth Des. 18 (2018) 416–423, https://doi.org/10.1021/acs.cgd.7b01417.
[209] T. Ogawa, K. Takahashi, S.S. Nagarkar, K. Ohara, Y. Hong, Y. Nishiyama, S. Horike, Coordination polymer glass from a protic ionic liquid: proton conductivity and mechanical properties as an electrolyte, Chem. Sci. 11 (2020) 5175–5181, https://doi.org/10.1039/D0SC01737J.
[210] Y. Feng, F.-C. Liang, Z.-Y. Huang, X.-X. Xie, S.-L. Cai, J. Fan, W.-G. Zhang, S.-R. Zheng, Regulating the porosity and iodine adsorption properties of metal-organic framework glass via an Ammonia-immersion approach, Inorg. Chem. (2022), https://doi.org/10.1021/acs.inorgchem.2c03035.
[211] Y. Wang, H. Jin, Q. Ma, K. Mo, H. Mao, A. Feldhoff, X. Cao, Y. Li, F. Pan, Z. Jiang, A MOF glass membrane for gas separation, Angew. Chem. Int. Ed. 59 (2020) 4365–4369, https://doi.org/10.1002/anie.201915807.
[212] Y. Zhao, S.-Y. Lee, N. Becknell, O.M. Yaghi, C.A. Angell, Nanoporous transparent MOF glasses with accessible internal surface, J. Am. Chem. Soc. 138 (2016) 10818–10821, https://doi.org/10.1021/jacs.6b07078.
[213] C. Zhou, L. Longley, A. Krajnc, G.J. Smales, A. Qiao, I. Erucar, C.M. Doherty, A. W. Thornton, A.J. Hill, C.W. Ashling, O.T. Qazvini, S.J. Lee, P.A. Chater, N. J. Terrill, A.J. Smith, Y. Yue, G. Mali, D.A. Keen, S.G. Telfer, T.D. Bennett, Metal-organic framework glasses with permanent accessible porosity, Nat. Commun. 9 (2018) 5042, https://doi.org/10.1038/s41467-018-07532-z.
[214] A.M. Bumstead, M.L. Ríos Gómez, M.F. Thorne, A.F. Sapnik, L. Longley, J. M. Tuffnell, D.S. Keeble, D.A. Keen, T.D. Bennett, Investigating the melting behaviour of polymorphic zeolitic imidazolate frameworks, CrystEngComm 22 (2020) 3627–3637, https://doi.org/10.1039/D0CE00408A.
[215] C. Das, S. Horike, Crystal melting and vitrification behaviors of a three-dimensional nitrile-based metal–organic framework, Faraday Discuss. 225 (2021) 403–413, https://doi.org/10.1039/D0FD00003E.
[216] M. Chen, J. Li, S. Liao, Y. Guo, T. Liu, R. Ma, T. Xie, W. Liu, S. Peng, X. Kuang, Z. Yin, Y. Zhao, M. Zeng, Multi-stage transformations of a cluster-based metal-organic framework: perturbing crystals to glass-forming liquids that re-crystallize at high temperature, Angew. Chem. Int. Ed. 62 (2023) e202305942, https://doi.org/10.1002/anie.202305942.
[217] M.A. Ali, X. Liu, J. Qiu, A review on the vitrification of metal coordination compounds and their photonic applications, J. Non-Cryst. Solids 597 (2022) 121936, https://doi.org/10.1016/j.jnoncrysol.2022.121936.
[218] A. Qiao, H. Tao, M.P. Carson, S.W. Aldrich, L.M. Thirion, T.D. Bennett, J. C. Mauro, Y. Yue, Optical properties of a melt-quenched metal–organic framework glass, Opt. Lett. 44 (2019) 1623, https://doi.org/10.1364/OL.44.001623.
[219] Mohamed A. Ali, X. Liu, H.-T. Sun, J. Ren, J. Qiu, Metal inorganic–organic complex glass and fiber for photonic applications, Chem. Mater. 34 (2022) 2476–2483, https://doi.org/10.1021/acs.chemmater.2c00240.
[220] S. Vaidya, O. Veselska, A. Zhadan, M. Diaz-Lopez, Y. Joly, P. Bordet, N. Guillou, C. Dujardin, G. Ledoux, F. Toche, R. Chiriac, A. Fateeva, S. Horike, A. Demessence, Transparent and luminescent glasses of gold thiolate coordination polymers, Chem. Sci. 11 (2020) 6815–6823, https://doi.org/10.1039/D0SC02258F.
[221] Z. Fan, C. Das, A. Demessence, R. Zheng, S. Tanabe, Y.-S. Wei, S. Horike, Photoluminescent coordination polymer bulk glasses and laser-induced crystallization, Chem. Sci. 13 (2022) 3281–3287, https://doi.org/10.1039/D1SC06751F.
[222] M.A. Ali, W.M.W. Winters, M.A. Mohamed, D. Tan, G. Zheng, R.S.K. Madsen, O. V. Magdysyuk, M. Diaz-Lopez, B. Cai, N. Gong, Y. Xu, I. Hung, Z. Gan, S. Sen, H. Sun, T.D. Bennett, X. Liu, Y. Yue, J. Qiu, Fabrication of super-sized metal inorganic-organic hybrid glass with supramolecular network via crystallization-suppressing approach, Angew. Chem. Int. Ed. 62 (2023) e202218094, https://doi.org/10.1002/anie.202218094.
[223] W. Zhao, Z. He, B.Z. Tang, Room-temperature phosphorescence from organic aggregates, Nat. Rev. Mater. 5 (2020) 869–885, https://doi.org/10.1038/s41578-020-0223-z.
[224] C. Chen, Z. Chi, K.C. Chong, A.S. Batsanov, Z. Yang, Z. Mao, Z. Yang, B. Liu, Carbazole isomers induce ultralong organic phosphorescence, Nat. Mater. 20 (2021) 175–180, https://doi.org/10.1038/s41563-020-0797-2.
[225] Y. Yang, K.-Z. Wang, D. Yan, Lanthanide doped coordination polymers with tunable afterglow based on phosphorescence energy transfer, Chem. Commun. 53 (2017) 7752–7755, https://doi.org/10.1039/C7CC04356B.
[226] X. Wang, H. Shi, H. Ma, W. Ye, L. Song, J. Zan, X. Yao, X. Ou, G. Yang, Z. Zhao, M. Singh, C. Lin, H. Wang, W. Jia, Q. Wang, J. Zhi, C. Dong, X. Jiang, Y. Tang, X. Xie, Y. (Michael) Yang, J. Wang, Q. Chen, Y. Wang, H. Yang, G. Zhang, Z. An, X. Liu, W. Huang, Organic phosphors with bright triplet excitons for efficient X-ray-excited luminescence, Nat. Photonics 15 (2021) 187–192, https://doi.org/10.1038/s41566-020-00744-0.
[227] Y. Zhang, L. Gao, X. Zheng, Z. Wang, C. Yang, H. Tang, L. Qu, Y. Li, Y. Zhao, Ultraviolet irradiation-responsive dynamic ultralong organic phosphorescence in polymeric systems, Nat. Commun. 12 (2021) 2297, https://doi.org/10.1038/s41467-021-22609-y.
[228] C. Chen, H. Gao, H. Ou, R.T.K. Kwok, Y. Tang, D. Zheng, D. Ding, Amplification of activated near-infrared afterglow luminescence by introducing twisted molecular geometry for understanding neutrophil-involved diseases, J. Am. Chem. Soc. 144 (2022) 3429–3441, https://doi.org/10.1021/jacs.1c11455.
[229] Y. Wang, J. Yang, M. Fang, Y. Yu, B. Zou, L. Wang, Y. Tian, J. Cheng, B.Z. Tang, Z. Li, Förster resonance energy transfer: an efficient way to develop stimulus-responsive room-temperature phosphorescence materials and their applications, Matter 3 (2020) 449–463, https://doi.org/10.1016/j.matt.2020.05.005.
[230] R. Gao, X. Mei, D. Yan, R. Liang, M. Wei, Nano-photosensitizer based on layered double hydroxide and isophthalic acid for singlet oxygenation and photodynamic therapy, Nat. Commun. 9 (2018) 2798, https://doi.org/10.1038/s41467-018-05223-3.
[231] P. Pattanayak, N. Modak, S. Guchhait, N. Ghosh, P. Purkayastha, Ultrasensitive Piezochromic molecular crystals: mechanical pressure-induced controlled regulation of TADF and RTP, Adv. Opt. Mater. 12 (2024) 2400404, https://doi.org/10.1002/adom.202400404.
[232] C. Ye, S. Mallick, M. Hertzog, M. Kowalewski, K. Börjesson, Direct transition from triplet excitons to hybrid light–matter states via triplet–triplet annihilation, J. Am. Chem. Soc. 143 (2021) 7501–7508, https://doi.org/10.1021/jacs.1c02306.
[233] B. Zhou, Z. Qi, D. Yan, Highly efficient and direct ultralong all-phosphorescence from metal–organic framework photonic glasses, Angew. Chem. 134 (2022) e202208735, https://doi.org/10.1002/ange.202208735.
[234] N.K. Kulachenkov, S. Bruyere, S.A. Sapchenko, Y.A. Mezenov, D. Sun, A. A. Krasilin, A. Nominé, J. Ghanbaja, T. Belmonte, V.P. Fedin, E.A. Pidko, V. A. Milichko, Ultrafast melting of metal–organic frameworks for advanced nanophotonics, Adv. Funct. Mater. 30 (2020) 1908292, https://doi.org/10.1002/adfm.201908292.
[235] H. Li, X. Li, D. Wang, J. Yan, S. Lv, A. Qiao, H. Zhang, Q. Yan, J. Qiu, S. Zhou, Hybrid photonic glass for optical sensing, Adv. Funct. Mater. 35 (2025) 2424218, https://doi.org/10.1002/adfm.202424218.
[236] T. Chiba, K. Hoshi, Y.-J. Pu, Y. Takeda, Y. Hayashi, S. Ohisa, S. Kawata, J. Kido, High-efficiency perovskite quantum-dot light-emitting devices by effective washing process and interfacial energy level alignment, ACS Appl. Mater. Interfaces 9 (2017) 18054–18060, https://doi.org/10.1021/acsami.7b03382.
[237] K. Zhang, D. Zhou, J. Qiu, Q. Wang, J. Lai, D. Wang, Z. Li, W. Shen, Effect of topological structure on photoluminescence of CsPbBr3 quantum dot doped glasses, J. Alloys Compd. 826 (2020) 154111, https://doi.org/10.1016/j.jallcom.2020.154111.

[238] M. Li, R. Liu, X. Wang, Y. Pu, F. Zheng, Z. Zhao, Z. Hu, Enhancing pure red perovskite LEDs via in-situ etching and pseudohalide passivation of mixed halide quantum dots, Appl. Mater. Today 46 (2025) 102896, https://doi.org/10.1016/j.apmt.2025.102896.
[239] M. Ghasemi, X. Li, C. Tang, Q. Li, J. Lu, A. Du, J. Lee, D. Appadoo, L.H.G. Tizei, S. T. Pham, L. Wang, S.M. Collins, J. Hou, B. Jia, X. Wen, Effective suppressing phase segregation of mixed-halide perovskite by glassy metal-organic frameworks, Small 19 (2023) 2304236, https://doi.org/10.1002/smll.202304236.
[240] W. Wang, M. Chai, W. Huang, Z. Xie, M. Ghasemi, P.D. Khanikar, F. Yuan, K. Xu, Y. Chen, X. Wen, P. Qi, J. Zhu, E.B. Namdas, V. Chen, A.K. Cheetham, L. Wang, J. Hou, Deep blue emitting Lead halide perovskite and metal-organic framework glass composites through Mechanochemistry, Small 21 (2025) 2411484, https://doi.org/10.1002/smll.202411484.
[241] R. Banerjee, A. Phan, B. Wang, C. Knobler, H. Furukawa, M. O'Keeffe, O.M. Yaghi, High-throughput synthesis of Zeolitic Imidazolate frameworks and application to CO_2 capture, Science 319 (2008) 939–943, https://doi.org/10.1126/science.1152516.
[242] J. Pang, Y. Liu, C. Zhao, J. Li, M. Ran, B. Zu, X. Dou, One-step coordinating POPD in H_3 BTB-sensitized EuMOF-enabled tunable antenna effects for fluorescence turn-on sensing of sarin analogue vapor, ACS Appl. Mater. Interfaces 17 (2025) 25722–25732, https://doi.org/10.1021/acsami.5c04451.
[243] D. Ye, R. Zhang, B. Xu, L. Zhu, B. Yue, Metal organic framework based on Photoactivated aggregation-induced emission molecule for achieving photoexcitation regulation, Chem. Asian J. 20 (2025) e202401512, https://doi.org/10.1002/asia.202401512.
[244] H. Wang, Y. Li, H. Zou, F. Liang, Z. Zhu, Smart lanthanide metal–organic frameworks with multicolor luminescence switching induced by the dynamic adaptive antenna effect of molecular rotors, Adv. Mater. 37 (2025) 2502742, https://doi.org/10.1002/adma.202502742.
[245] W. Cai, L. Yin, Y. Shi, H. Zhang, D. Wu, J. Li, L. Xu, Y. Kong, An ultrasensitive electrochemiluminescence sensor for dopamine based on dual-ligand Eu MOF with Cu2O nanocrystals as a co-reactant accelerator, Sensors Actuators B Chem. 443 (2025) 138278, https://doi.org/10.1016/j.snb.2025.138278.
[246] L.N. McHugh, T.D. Bennett, Introducing porosity into metal–organic framework glasses, J. Mater. Chem. A 10 (2022) 19552–19559, https://doi.org/10.1039/D2TA02560D.
[247] M. Dai, B. Zhou, D. Yan, Rare earth single-atomic hybrid glasses for near-infrared II optical waveguides, Angew. Chem. Int. Ed. 64 (2025) e202505322, https://doi.org/10.1002/anie.202505322.
[248] J. Wei, X. Zhang, X. Wang, Y. Liu, Y. Zhang, New transparent rare-earth-based hybrid glasses: synthesis, luminescence, and X-Ray imaging application, Aggregate 6 (2025) e70021, https://doi.org/10.1002/agt2.70021.
[249] M. Yu, Y. Zhang, B. Liu, D. Peng, Z. Hu, H. Wan, J. Liu, X. Sun, Enhancing upconversion luminescence of rare earth ions by the activation of the antenna effect in plasmonic cuprous sulfide nanoparticles, Opt. Mater. 144 (2023) 114358, https://doi.org/10.1016/j.optmat.2023.114358.
[250] L. Frentzel-Beyme, M. Kloß, P. Kolodzeiski, R. Pallach, S. Henke, Meltable mixed-linker Zeolitic Imidazolate frameworks and their microporous glasses: from melting point engineering to selective hydrocarbon sorption, J. Am. Chem. Soc. 141 (2019) 12362–12371, https://doi.org/10.1021/jacs.9b05558.
[251] Mohamed A. Ali, X. Liu, Y. Li, J. Ren, J. Qiu, Nonlinear-optical response in Zeolitic Imidazolate framework glass, Inorg. Chem. 59 (2020) 8380–8386, https://doi.org/10.1021/acs.inorgchem.0c00806.